ISSN 2701-939X

Communications in

Development and Assembling of Textile Products

Year 2020, Volume 1, Issue 1

Communications in Development and Assembling of Textile Products (CDATP)

ISSN 2701-939X is an international, ***peer reviewed, pure open access journal.***

www.cdatp.org

https://journals.qucosa.de/cdatp

Publisher

Chair of Development and Assembly of Textile Products
Technische Universität Dresden
Faculty of Mechanical Science and Engineering
Institute of Textile Machinery and High Performance Material Technology (ITM)
01062 Dresden

Tel.: +49 (0) 351 463-39313
Fax: +49 (0) 351 463-39301
E-Mail: yordan.kyosev@tu-dresden.de
http://tu-dresden.de/mw/itm/mt
http://tu-dresden.de/mw/itm
http://www.facebook.com/ITM.TUDresden

Besucheradresse:
Hohe Straße 6, Zi. 141
01069 Dresden

Principal Contact

Prof. Dr.-Ing. habil. Yordan **Kyosev**

Head of the Chair of Development and Assembly of Textile Products
yordan.kyosev@tu-dresden.de

Support Contact

Dr. Lutz **Kowalke**

journals@qucosa.de

Editorial Team

About the Journal

Aim

The journal **"Communications in Development and Assembling of Textile Products"** (CDATP) **ISSN 2701-939X** is an international, ***peer reviewed, pure open access journal.***

It has the mission to offer a forum for scientific exchange in the interdisciplinary area of the ***engineering development of textile based products and the technology of their assembling***.

Scope

Topic of interests are **new, not published** research results and materials related to:

- development of products of textiles
- textile materials, their production and parameter identification
- 2D and 3D pattern design
- optimisation and body shape fitting
- 3D/4D scanning, data processing
- cutting and investigations on preparatory processes
- assembling technologies – sewing, welding, gluing, thermoforming, folding, packing
- textile logistics
- recycling of textile products
- numerical modelling of all these processes
- interaction between clothing and human body with all its aspect related to mechanical, thermal, moisture, processes and human body comfort
- biomechanics related to textile product development
- other related topics.

Article types

The journal publishes communications in two types/parts:

A) **peer reviewed journal articles** (research papers, review of state-of-the art papers)
B) *not reviewed* ***communications*** in form of reports, data sets, technique reviews, conference papers, abstracts, discussions.

Language

The language of the **peer reviewed articles** is only **English**.

The non-reviewed communications have to be preferably in English, but can be published in German or other languages, too, if the editorial team is able to check the formal level and the quality of the material on this language. In this case title and abstract in English language has to be provided.

Review process for the review articles

Each submission is reviewed from at least four persons.

1. After the submission two of the Editors-in-Chief, or Editor-in-Chief and one Member of the Editorial Board (in case the other Editor-in-Chief is co-author or related to the authors of the manuscript) check the manuscript and decide about its potential for publication.

2. If the novelty and content is suitable two independent reviewers are invited to review the material. In case that their opinion is very different, additional reviewers can be invited.

The review process is **open and transparent for author and reviewers:**

- the reviewers can see the authors of the material
- the author receives the complete feedback of the reviewers, *without their personal data* (**single blind review process**).

Discussions on previous published results are welcome and will be published without review in form of short communication with DOI, too.

The length of the reviewed papers is not limited, but only well structured materials will be considered for publication.

Publication form

The journal is a **purely online journal**, without print issues. All published papers are available as **open access papers** in PDF format under Creative Commons Attribution-NonCommercial-NoDerivatives 4.0 International License.

Formally, all published manuscripts are structured in **two issues per year**.

References

The references have to be formatted following the **ACM reference stlye** https://www.acm.org/publications/authors/reference-formatting

This is available in Citavi, Zotero, Endnote and many other reference managers.

Submissions Template

Submission template in Word can be downloaded here www.cdatp.org

Publication charges / Article processing charges

CDATP journal do **not** charge any fees for publication of articles. The costs for DOI and web hosting are covered by the Saxonia State and University Library (SLUB), Dresden and TU Dresden. The work of all editors and production team is voluntary.

Copyright

Licensing

Plagiarism and self-plagiarism

The editorial team checks first the manuscripts on google.com. In cases of any suspicion using plagiarism or self-plagiarism detection software available at TU Dresden to check the submissions. If plagiarism is detected, the COPE guidelines on plagiarism will be followed.

Publication Ethics and Publication Malpractice Statement

The CDATP journal is committed to maintaining the highest level of integrity in the content published.

This journal follows the COPE *Code of Conduct and Best Practice Guidelines for Journal Editors* and the *Code of Conduct for Journal Publishers*.

Preprint servers

Posting a manuscript on a preprint server or an author personal or institutional webpage (without DOI, publisher) does not count as previous publication. Once the manuscript is accepted and published, the author is responsible to update the preprint record with a publication reference, including the DOI and URL link to the published version.

Repository policy

The authors are encouraged to deposit a copy of their accepted manuscripts papers in an institutional or other repository of their choice, as Accepted version (Author Accepted Manuscript) and as Published version (Version of Record). Authors should provide a link from the deposited version to the DOI and URL of the publication article. The only purpose of this link is to ensure, that the journal's website is clearly identified as the definitive version of record. There is no embargo period for self archiving.

The journal is listed in Romeo Service https://v2.sherpa.ac.uk/id/publication/39565

COMMUNICATIONS IN
DEVELOPMENT AND ASSEMBLING OF TEXTILE PRODUCTS

Editorial

Yordan Kyosev

Chair of Assembly Technology for Textile Products
Institute of Textile Machinery and High Performance Material Technology (ITM), TU Dresden
E-mail address: yordan.kyosev@tu-dresden.de

INFO

CDAPT, ISSN 2701-939X
Editorial
Year 2020, Vol. 1, Nr. 1, pp.1-2
DOI: 10.25367/cdatp.2020.1.p1-2

Dear Readers and Colleagues,

The development of textile products no longer takes place at a table with a ruler but has moved into the space of sophisticated 3D CAD systems. Hence, developers need deep engineering knowledge in order to satisfy customers' requirements. Even when creating daily clothing, designers want to be able to check pattern fits through virtual manikins and evaluate the draping behavior of different materials. Additionally, developers of functional clothing want to prove breathability, i.e. air permeability, water moisture permeability, compression at different body parts, and many other properties. Today, the development of products involving technical textiles does not depend on expert knowledge of experienced personnel alone, but is often a result of interdisciplinary work based on simulations of multiple physical processes, e.g. mechanics of textile materials and the human body, fluid mechanics, thermodynamics, etc.

The assembling procedure for state-of-the-art products has become an increasingly complex engineering task. The majority of manual work steps has been replaced by automated feeding devices supported by robots. Modern sewing machines are able to document every stitch and ensure constant sewing conditions for all safety products. Alternative assembling technologies, such as ultrasonic welding, high frequency welding, gluing, laser welding and hot air welding, are often integrated into the production process.

In the area of scientific publications, we are currently observing distinctly different publishing strategies. Well established and renowned peer reviewed journals have already adjusted their strategies to the modern electronic world, thus offering open access publications at extremely high processing costs. For most researchers, this financial barrier makes it impossible to submit publications to these journals. At this point, predatory journals have recognized a promising business opportunity and started sending regular advertising mails offering a quick publication process against comparatively small processing fees. Regular online "blogging" or publications in exclusively industrial journals do not provide the desired scientific value.

This is a particularly challenging situation for young researchers at the start of their career when scientific publishing becomes nearly impossible and they therefore often turn to journals with predatory practices in order to achieve some publication record.

Due to these observations combined with the desire to create an open access[1] initiative for the publication of scientific results, we, colleagues from leading research groups, decided to start the new fully open access journal "Communications in development and assembling of textile products". This journal has an exclusively academic editorial board and does not pursue commercial goals. Instead, it is hosted and supported by the Saxon State and University Library Dresden (SLUB) with the publication process being managed by a voluntary team of researchers at the Chair of Assembly Technology for Textile Products that is part of the ITM at TU Dresden. Under these conditions, the journal can act independently from the business strategies of commercial publishers and solely focus on the publication of scientific results.

The journal accepts two types of articles, i.e. "peer reviewed" material and "communications" articles. The peer reviewed papers undergo a rigorous check from at least three experts – the editor and two independent experts. The "communications" sector allows for the publishing of short case studies, valuable information, project reports, scientific data, abstracts and other content, which does not provide a sufficient amount of novel information, but is still valuable for industrials and researchers.

The journal welcomes manuscripts and communications in the field of development and assembling processes for textile products. Moreover, the journal gladly supports the 13th joint international conference CLOTECH 2020 [2], accommodating selected manuscripts which already passed or are currently going through the peer review process. All papers and communications will be available online for free and will be published with a unique DOI. After covering the requirements, the editorial team is eager to apply for registration in leading journal databases.

On behalf of the editorial team, I would like to invite you to contribute your scientific input for the purpose of good scientific communication by submitting your high quality manuscripts and supporting us with reviews. You are welcome to visit www.cdatp.org

Prof. Dr.-Ing. habil. Yordan Kyosev

Editor-in-Chief

References

[1] www.coalition-s.org
[2] www.clotech.eu

COMMUNICATIONS IN
DEVELOPMENT AND ASSEMBLING OF TEXTILE PRODUCTS

Structural compressibility in 3D printed abrasion protection structures

Sarah Lysann Zedler[1]*

[1]*Sächsisches Textilforschungsinstitut e. V., Chemnitz, Germany*
*Corresponding author *E-mail address:* sarah.lysann.zedler@stfi.de

INFO

CDAPT, ISSN: 2701-939X
Peer reviewed article
2020, Vol.1, Nr. 2, pp. 3-11
DOI:10.25367/cdatp.2020.1.p3-11
Received: 28 April 2020
Accepted: 10 June 2020
Available online: 22 September 2020

ABSTRACT

Abrasion protection in exposed areas is a common method of extending the life cycle of textile products. To achieve sufficient abrasion resistance, the textile products are usually coated or partially printed with hard products. But hard materials lead to stiffening and can have a negative effect on the haptics. The aim of this study is the application of abrasion-resistant and compressible print patterns directly to textile substrates by 3D printing. The compressibility is achieved by the inner structure, which, in contrast to conventional coatings and screen prints, is not 100 % filled. In the investigations, four thermoplastic materials were tested for their abrasion resistance and compressible properties. Fabrics made of cotton or polyester/cotton blends were used as textile substrates. Different approaches were taken to create the structures, some of which can only be realized using 3D printing technology. The abrasion resistance of the substrates could be increased from 50 abrasion cycles to over 8,000 cycles with the help of the 3D printed patterns. It was possible to print 3D structures that could be compressed in thickness by up to 53 %. The combination of both properties, abrasion resistance and compressibility, can be used for new types of individual products with good wearing comfort and functionality that meet the requirements, especially in the areas of functional, protective and sports clothing.

Keywords
textiles,
3D printing,
functionalization
abrasion resistance,
compressibility

1 Introduction

Textile products are additionally protected from abrasion and wear in exposed areas to increase the durability of the textile. For this purpose, durable raw materials or all-over coatings as well as partial print layers can be used. Abrasion protection by patches results in seams that are not always desired. With all-over coatings there is a risk that the flexibility and breathability of the textile will be reduced too much. Partial print layers or patterns reduce the flexibility of the textile less. However, hard materials are often used which reduce the wearing comfort under pressure/stress on the structures.

Currently, screen printing is mainly used for the application of partial, functional structures on textiles, as it allows the use of higher viscosity and filled printing materials [1-4]. The disadvantage of screen printing is that separate printing stencils must be produced for each design. This requirement increases both the set-up times and the costs for the production and storage of the stencils. With digital printing processes, the disadvantage of stencil production does not exist, but inkjet printing is used for color printing and conductive structures and not yet for commercial functional printing on textiles because low-viscosity inks are required [3, 5, 6].

3D printing combines the advantages of digital technologies and screen printing. The production process of stencils is no longer necessary. Design changes are therefore possible without long set-up times. In addition to the initial development of using different 3D printing processes for textile and clothing production [7, 8], there are increasing ambitions to functionalize textile substrates using 3D printing.

Fused Layer Modelling (FLM) is used for this purpose, in which thermoplastic materials are fed as a filament to a heated nozzle, melted in it and then deposited in layers with the correct contours [9]. In previous studies, the focus was on adhesion forces between printed material and textile substrates, because sufficient adhesion is required for a successful functionalization [10-14].

Furthermore, 3D printed structures have been used to influence physical properties of textiles, such as flexural strength [14], fabric draping [15] or abrasion resistance against wool fabric [16-20].

So far, no studies have been published on the production of very high abrasion resistance in combination with compressible structures on textiles. The aim of this study is the production of abrasion-resistant and compressible print patterns. The abrasion resistance should be effective against sandpaper instead of wool fabric. The compressibility is to be created by different structures inside.

2 Materials and methods

2.1 Materials

Fabrics from the sector of work and protective clothing made of cotton (CO) or polyester/cotton (PES/CO) blends with twill weave were used as textile substrates. Their properties, like basis weight (DIN EN 12127), number of threads (DIN EN 1049-2) and thickness (DIN EN ISO 5084), were tested according to international standards and are listed in Table 1.

Table 1. Textile properties.

Textile properties	T1	T2	T3
material composition	100 % CO	100 % CO	65 % PES / 35 % CO
description of finishing	finished, shrunk	flame retardant impregnated, shrunk	finished
basis weight (g/m²)	302.67 ± 2.50	294.99 ± 2.18	297.88 ± 0.98
number of warp threads (1/cm)	36.97 ± 0.217	29.70 ± 0.075	41.70 ± 0.274
number of weft threads (1/cm)	24.36 ± 0.06	19.20 ± 0.00	22.74 ± 0.06
thickness (mm)	0.55 ± 0.01	0.53 ± 0.01	0.52 ± 0.01

Four different 3D printing filaments with a Shore hardness of ≤ 95 A were used as printing materials which parameters are listed in Table 2.

Table 2. Parameters of printing material.

Print polymer	Chemical basis	Shore Hardness	Printing Temperature (°C)
P1	polylactic acid (PLA)	92 A	210
P2	co-polyester (Co-PES)	95 A	220
P3	thermoplastic elastomer (TPE)	92 A	170
P4	thermoplastic polyurethane (TPU)	85 A	235

The system used for the project was the 3D material application system of CVM GmbH (Neukirchen, Germany), which is installed at the Saxon Textile Research Institute (Chemnitz, Germany). The integrated

FLM module was used with a nozzle diameter of 0.4 mm. The textile substrate was clamped with the clamping possibilities available on the system (Fig. 1).

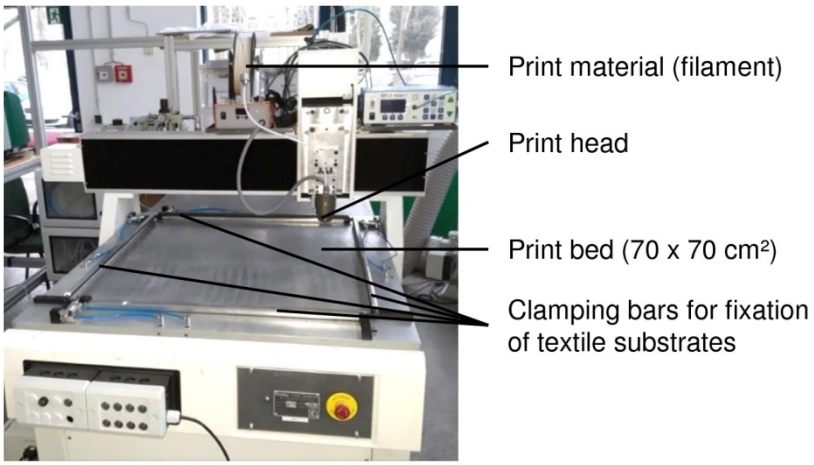

Fig. 1 3D material application system with clamping bars for fixation of textile substrates.

2.2 Methods

For the printing tests, 3D structures were created using Rhinoceros 6 and included Grasshopper (McNeel Europe S.L., Barcelona, Spain) as CAD software and then converted into machine-specific data for printing using Repetier-Host (Hot-world GmbH & Co. KG, Willich, Germany) as slicer software.

The study is divided into three parts: Part 1 is the development of the abrasion resistant structures which include data generation, printing and testing. The raw materials, pure printed layers and the printed specimens were tested for their resistance to abrasion in accordance to the standard DIN EN 388, 6.1. Two specimens each with a diameter of 38 mm were clamped in specimen holders and rubbed against sandpaper (Klingspor PL31B, grit 180). The minimum number of abrasion cycles at breakthrough, i. e. when holes are formed, is relevant for the evaluation of the material according to the performance levels 1 to 4 specified in the standard. The best possible rating is performance level 4, which is achieved when no breakthrough has occurred after 8,000 cycles. The lower value from the abrasion test was used for the evaluation.

Part 2 is the investigation of compressible properties which was performed parallel to abrasion tests. For testing the compressible properties, specimens with a square base area of 70 x 70 mm² were produced without a textile substrate. In accordance to DIN EN ISO 9863-1, the thicknesses t_{p_i} of the specimens were determined under the specified pressures of $p_1 = 2\,\mathrm{kPa},\ p_2 = 20\,\mathrm{kPa},\ p_3 = 200\,\mathrm{kPa}$. With these values the compressibility C according to equation (1) were calculated.

$$C = \frac{t_{p_i} - t_{p_1}}{t_{p_1}} \cdot 100\,\% \tag{1}$$

In addition, the thicknesses were measured after a recovery period of 3 min at the pressure of 2 kPa ($p_{1'}$) to get the regeneration R according to equation (2).

$$R = \frac{t_{p_{1'}}}{t_{p_1}} \cdot 100\,\% \tag{2}$$

Part 3 is the combination of the best results out of abrasion resistance and compressible properties which was performed after the two previous parts. The 3D printing parameters which were used in every part are listed in Table 3.

Table 3. 3D printing parameters.

Parameters	Part 1 (abrasion)	Part 2 (compressibility)
layer height (mm)	0.2	0.2
extrusion width (mm)	0.4	0.4
printing bed temperature (°C)	35	35
fill pattern	rectilinear	rectilinear
fill density (%)	100	100
exception: varying fill density FD (%)	-	$\mathrm{FD}_1 = 5,\ \mathrm{FD}_2 = 10,\ \mathrm{FD}_3 = 20$

3 Results

3.1 Abrasion resistance

The textile fabrics are destroyed after 50 (T1, T2) and 100 (T3) abrasion cycles which is less than performance level 1. For further abrasion tests T1 was used because it is the fabric with lowest abrasion resistance. The printing materials were tested individually as all-over print layers. A breakthrough in the printed layers were found after P1 = 4,400 cycles, P2 = 3,700 cycles and P3 = 5,500 cycles which is defined as performance level 3. P4 shows no perforation in the printed layer after 8,000 abrasion cycles (performance level 4). Because of their good abrasion resistance and printing properties, polymers P1 and P4 were used for the further abrasion tests. A total of 16 abrasion protection structures were constructed by factorial experimental design. The four factors with their levels are listed in Table 4.

Table 4. Factors and their levels for the generated abrasion resistant structures.

Factor	Level 1	Level 2
1) geometry	geometry A (diamonds)	geometry B (Voronoi structures)
2) geometry size	big geometries	small geometries
for geometry A: side length a (mm)	$\mathrm{a}_1 = 15$	$\mathrm{a}_2 = 10$
for geometry B: number of base points x	$\mathrm{x}_1 = 10$	$\mathrm{x}_2 = 20$
3) area coverage ratio CR (%)	$\mathrm{CR}_1 = 60$	$\mathrm{CR}_2 = 80$
4) print height H (mm)	$\mathrm{H}_{\mathrm{const}} = 0.4$	$\mathrm{H}_{\mathrm{var}} = \{0.4, 0.6, 0.8\}$

For the basic geometry two different approaches were followed. Geometry A consists of a uniform pattern based on rounded diamonds with a rounding radius $\mathrm{r} = 2.5\ \mathrm{mm}$. The diamond size was varied by the side length a. Geometry B consists of algorithm based Voronoi structures. Thereby a rectangle is provided with base points. The size of the Voronoi cells was determined by the number of base points x (Fig. 2a). The structures were created once with a constant print height $\mathrm{H}_{\mathrm{const}} = 0.4\ \mathrm{mm}$. In addition, an algorithm was used to set a variable print height of $\mathrm{H}_{\mathrm{var}} = \{0.4\ \mathrm{mm}, 0.6\ \mathrm{mm}, 0.8\ \mathrm{mm}\}$ depending on the center of the test surface. The centre point corresponds to the maximum height (Fig. 2b, c). A sample of the printed specimens out of P4 on T1 is shown in Figure 2d.

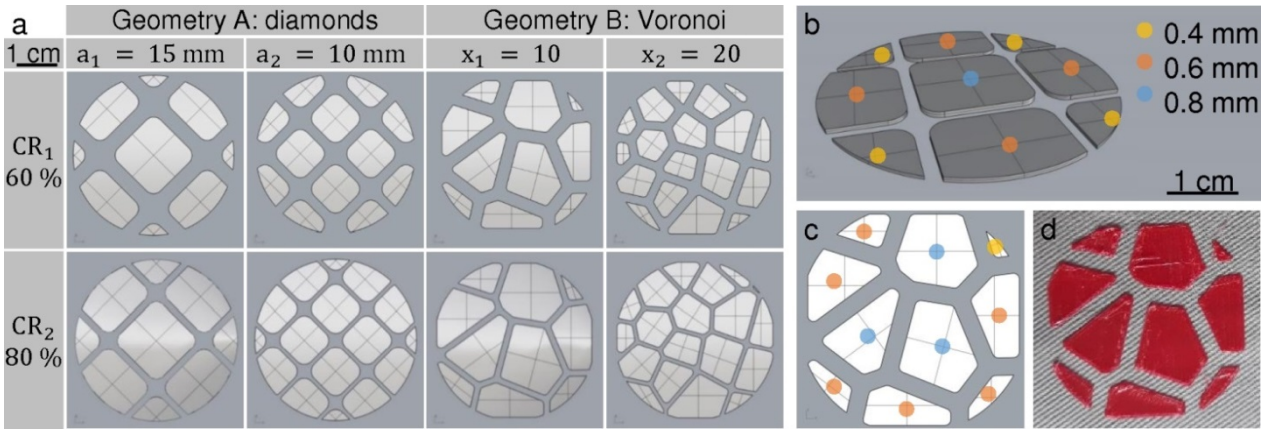

Fig. 2 Abrasion protection structures: (a) plan view of the test geometries; (b) perspective view of structure with variable height (color-coded); (c) plan view of structure with variable height (color-coded); (d) printed sample with Voronoi geometry.

Five parameter combinations have reached the maximum performance level 4 (Figure 3). These combinations were manufactured with P4 and variable print height. The print height is a very important parameter to improve abrasion resistance. It is not necessary to increase the print height uniformly over the entire surface. As the results show, it is sufficient to strengthen the center of abrasion protection structures. In this case, the 3D printing process can show its advantages when printing variable heights without the need for different stencils. The figure also shows that the area coverage ratio is another influential parameter. As expected, higher area coverage results in better abrasion resistance. In most cases, a variable print height leads to the same improvement as increasing area coverage ratio. These results mean that both parameters can be used for improvements depending on the printing time. In contrast, the geometry as well as geometry size has less influence on the abrasion resistance.

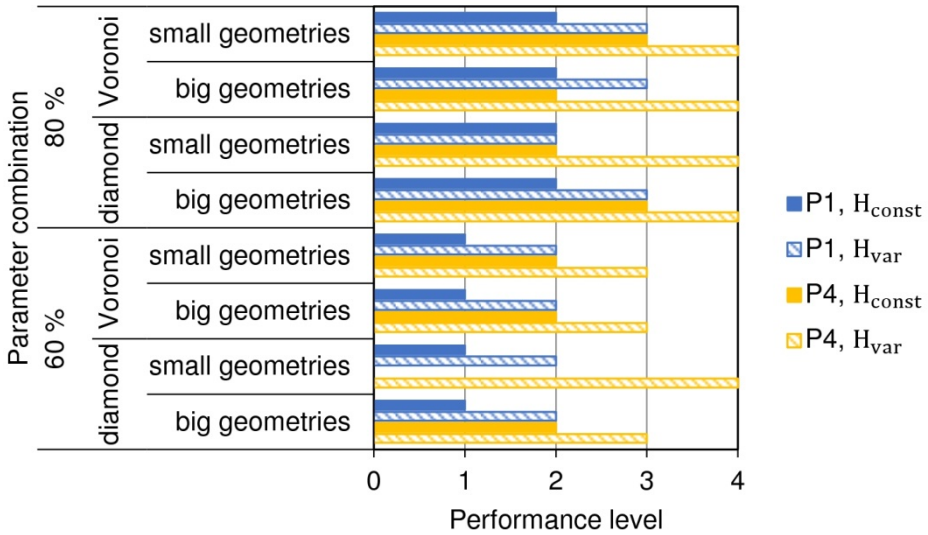

Fig. 3 Achieved performance levels of the different parameter combinations grouped by material and print height.

3.2 Compressible properties

The compressible structures were created using two different design approaches. On the one hand, the fill density FD of a cuboid was varied within the slicer software: $\mathrm{FD}_1 = 5\ \%$, $\mathrm{FD}_2 = 10\ \%$ and $\mathrm{FD}_3 = 20\ \%$. In each case nine layers with the corresponding fill density and additionally completely filled base and top layers were set. On the other hand, the closed base and top layers were connected in the second approach by constructed dampening bars. These bars were created in CAD software with an overhang angle of $\alpha = 45°$ and a varying number of turns n (Figure 4). A single bent bar (one zigzag) corresponds to one turn $(\mathrm{n} = 1)$.

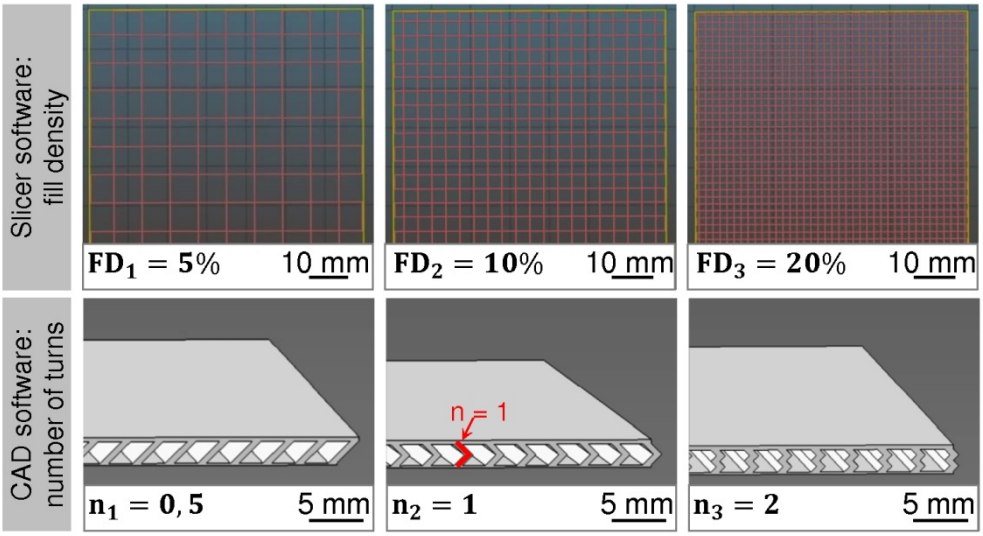

Fig. 4 Internal structures created by varying fill density in slicer software (top) and structures created in CAD software with dampening bars depending on the number of turns n (bottom).

The compressibility C depends on the printing material, the test pressure and the geometry of the inner structure (Figure 5). Polymer P4, which has the lowest Shore hardness, is more compressible. At a test pressure of 20 kPa, the compressibility hardly differs between the different geometries. For specimens printed with P1 and P2 compressibility is lower if the fill density is varied instead of the number of turns. For samples made of P4 it is the other way around. At a fill density of 5 %, the compressibility of specimens printed with P4 increases clearly up to 17 %. It was not possible to print samples out of P3 with fill density of 5 % because of printing process purposes. The printed strands fell into the cavities. That is why the top layers were too uneven to get tested. At a test pressure of 200 kPa the compressibility values are significantly higher. The variation of the fill density leads to differently strong rising values, while the compressibility is increased more evenly by changing the number of turns. The highest compressibility is 53 %, which is reached by P4 samples with $\mathrm{FD}_1 = 5\ \%$.

The quality and durability of the compressible structures were analyzed by regeneration R (Figure 6). The structures of all polymers except P1 have regenerated with values of $97.9\ \% \leq \mathrm{R} \leq 100.0\ \%$. The samples made of P1 contain regeneration values of $83.6\ \% \leq \mathrm{R} \leq 100.0\ \%$. The minimum regeneration occurred at $\mathrm{FD}_1 = 5\ \%$. This significantly less regeneration indicates a damage of the inner structure of the samples of P1 at this fill density. This conclusion is supported by crackling noises when the samples are compressed after the test.

Overall, both design approaches are suitable for creating cavities to achieve structural compressibility in addition to the material compressibility. The first design approach with the fill density has less engineering effort. Thus the fill density can be easily changed in slicer software. But this parameter cannot be varied within a single object. This means, for example, that the object has the same fill density in the middle as at the borders.

The second design approach using the number of turns or other designs generated in CAD software rather than slicer software is much more customizable. Therefore, the second approach can be used to create a variable internal structure depending on the required compressibility.

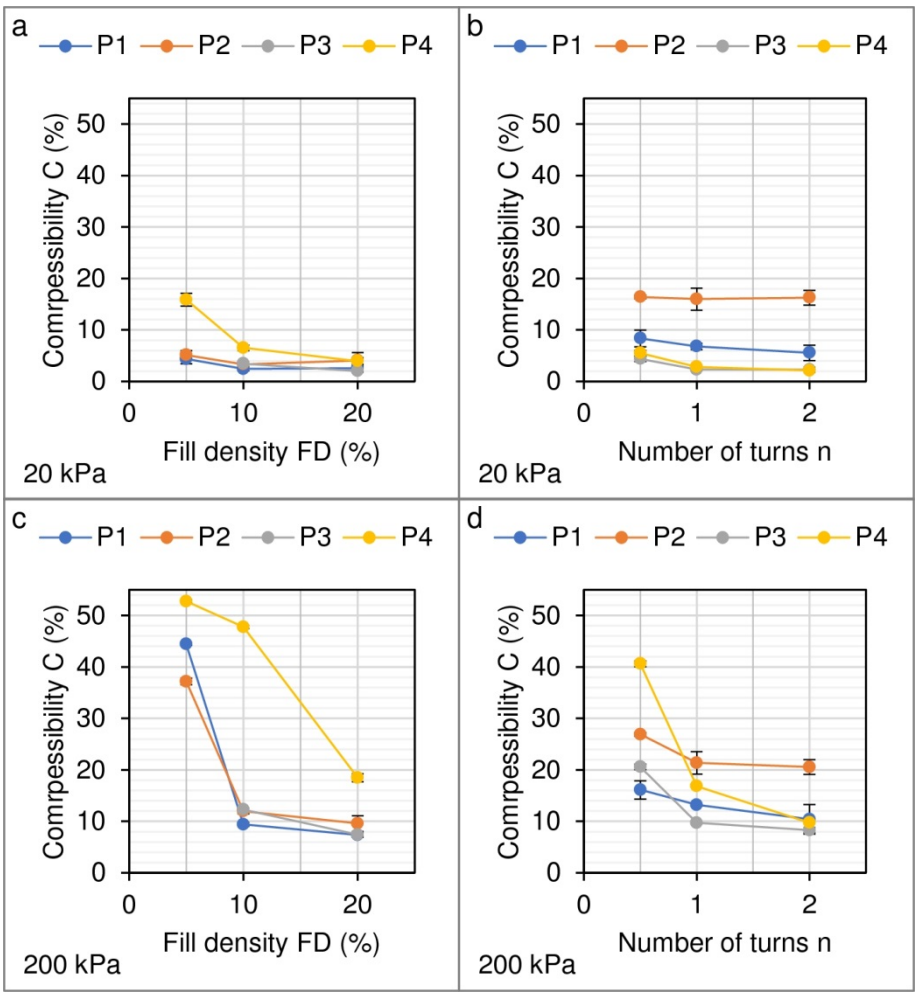

Fig. 5 Compressibility C depending on material with (a) test pressure of 20 kPa and varying fill density; (b) test pressure of 20 kPa and varying number of turns; (c) test pressure of 200 kPa and varying fill density; (d) test pressure of 200 kPa and varying number of turns.

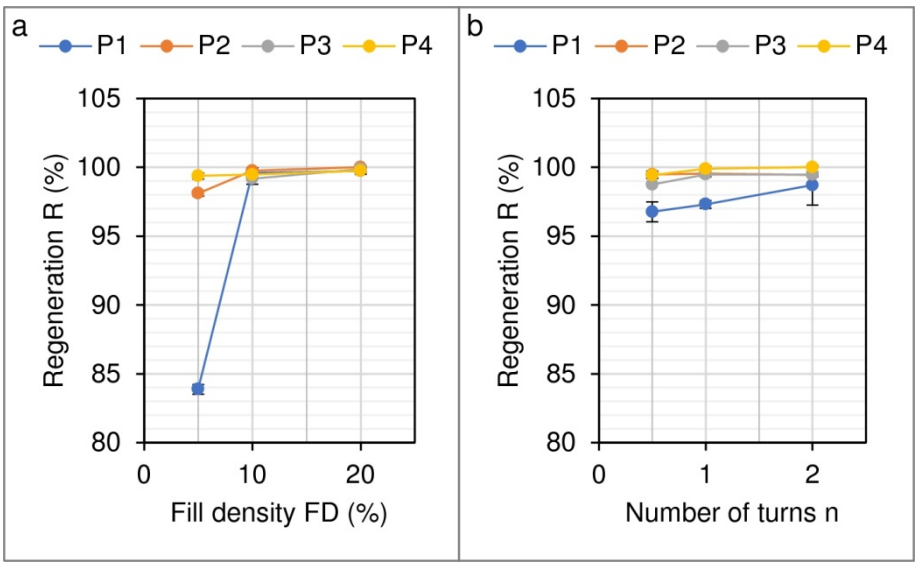

Fig. 6 Regeneration R depending on material and (a) fill density; (b) number of turns.

3.3 Combination of abrasion-resistant and compressible properties

Finally, the best results of the previous structures were selected to produce 3D prints with abrasion resistance and compressibility. The combination of both properties can be used to create novel individual products with good wearing comfort and functionality in line with requirements. Figure 7 shows a printed sample made of P4 on T1 with abrasion-resistant structure out of diamonds with an area coverage ratio of 80 % and variable print height of $\mathrm{h_{var}} = \{0.4\ \mathrm{mm}, 1.2\ \mathrm{mm}, 2.0\ \mathrm{mm}, 2.6\ \mathrm{mm}\}$. The print height is higher than in previous abrasion tests because the dampening bars with $\mathrm{n} = 0.5$ were included as internal structure for compressible properties. The combination of these properties can be used in protective structures in functional and sports clothing.

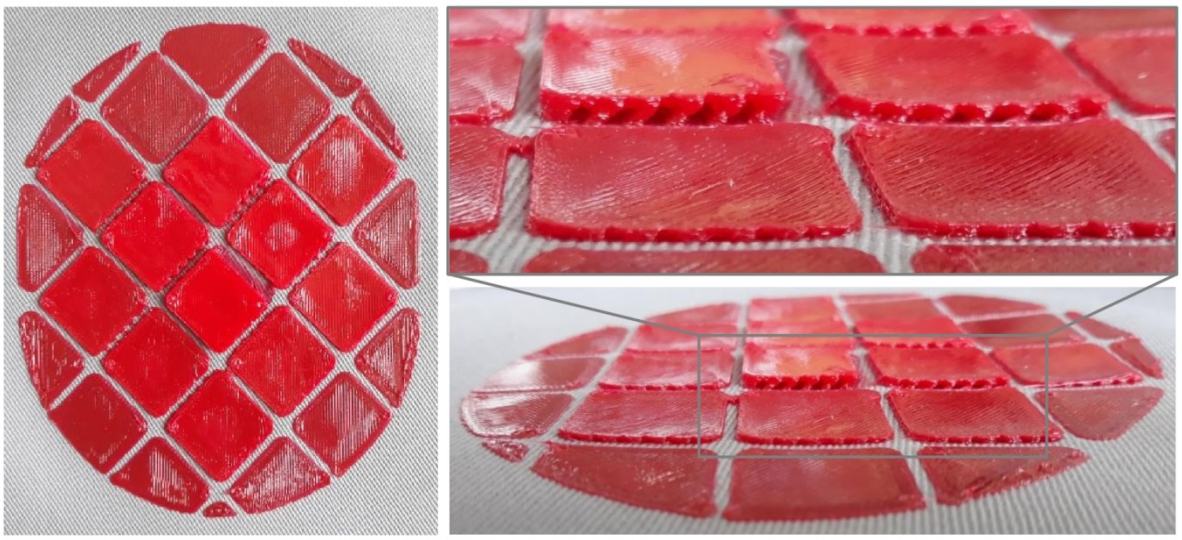

Fig. 7 Printed sample of diamond structures with variable print height for abrasion resistance combined with dampening bars for compressible properties.

4 Conclusions

Using 3D printing, structures were created that increase the abrasion resistance of the examined cotton fabric from 50 abrasion cycles to over 8,000 cycles. The printing material, the print height and the area coverage ratio are the most important parameters to improve the abrasion resistance. It is sufficient to increase the print height at the center of the abrasion protection structure. Both design parameters, print height and area coverage ratio, can be used for improvements depending on the printing time. The geometry as well as the geometry size has shown less influence on the abrasion resistance.

Materials with a Shore hardness of ≤ 95 A were used. By adapting the internal structure of the three-dimensional designs, it is possible to achieve a compressibility of up to 53 %. While varying the fill density has less engineering effort, generating specific inner structures in CAD software is much more customizable. Therefore, the second approach can be used to create a variable internal structure depending on the required compressibility. When selecting the appropriate structure, the ability to regenerate must also be taken into account because damages of the internal structure at $\mathrm{FD_1} = 5\ \%$ for P1 specimens were detected.

The results contribute to the extension of the application possibilities of 3D printing on textile substrates. The combination of both properties, abrasion resistance and compressibility, can be used for new types of individual products with good wearing comfort and functionality that meet the requirements. Thus, these results are relevant especially for the areas of functional, protective and sports clothing.

Acknowledgements

We acknowledge the support of the Federal Ministry of Economics and Energy for the funding of the project (Reg.-No. 49MF170026) within the funding programme “FuE-Förderung gemeinnütziger externer Industrieforschungseinrichtungen - Innovationskompetenz (INNO-KOM) - Modul: Marktorientierte Forschung und Entwicklung (MF).”

References

[1] Martinez I.; Mao, C.-X.; Vital, D.; Shahariar, H.; Werner, D. H.; Jur, J. S.; Bhardwaj, S. Compact, Low-Profile and Robust Textile Antennas With Improved Bandwidth for Easy Garment Integration. *IEEE Access*, 2020, 8, pp. 77490-77500. DOI: 10.1109/ACCESS.2020.2989260.

[2] Suikkola, J.; Björninen, T.; Mosallaei, M.; Kankkunen, T.; Iso-Ketola, P.; Ukkonen, L.; Vanhala, J.; Mäntysalo, M. Screen-Printing Fabrication and Characterization of Stretchable Electronics. *Sci. Rep.*, 2016, 6 (25784). DOI: 10.1038/srep25784.

[3] Zeng, W., Shu, L., Li, Q., Chen, S., Wang, F., Tao, X.-M. Fiber-Based Wearable Electronics: A Review of Materials, Fabrication, Devices, and Applications. *Adv. Mater*, 2014, 26 (31), pp. 5310–5336. DOI: 10.1002/adma.201400633.

[4] Stančić, M.; Kasikovic, N.; Novaković, D.; Dojcinovic, I.; Vladić, G.; Dragić, M. The influence of washing treatment on screen printed textile substrates. *TEKSTİL ve KONFEKSİYON*, 2014, 24 (1), pp. 96- 104.

[5] Tawiah, B.; Howard, E. K.; Asinyo, B. K. The Chemistry Of Inkjet Inks For Digital Textile Printing – Review. *BEST: IJMITE*, 2016, 4 (5), pp. 61-78.

[6] Chauraya, A.; Whittow, W. G.; Vardaxoglou, J. C.; Li, Y.; Torah, R.; Yang, K.; Beeby, S.; Tudor, J. Inkjet Printed Dipole Antennas on Textiles for Wearable Communications. *IET Microw. Antennas Propag.*, 2013, 7 (9), pp.760-767. DOI: 10.1049/iet-map.2013.0076.

[7] Beecroft, M. 3D printing of weft knitted textile based structures by selective laser sintering of nylon powder. Global Conference on Polymer and Composite Materials (PCM 2016), *IOP Conf. Ser.: Mater. Sci. Eng.*, 2016, 137, pp. 01-07. DOI: 10.1088/1757-899X/137/1/012017.

[8] Beecroft, M. Digital interlooping: 3D printing of weft-knitted textile based tubular structures using selective laser sintering of nylon powder. *Int. J. Fash. Des., Technol. Educ.*, 2019, 12 (2), pp. 218-224. DOI: 10.1080/17543266.2019.1573269.

[9] VDI-Gesellschaft Produktion und Logistik. VDI 3405:2014-12 - Additive manufacturing processes, rapid manufacturing - Basics, definitions, processes. Beuth Verlag: Berlin, Germany, 2014; pp. 12-13.

[10] Deleersnyder, K. 3D Printing on textiles – new tool for customized fabrics. 3F-Talks: Functional Fibres and Films, Aachen, Germany, 29.04.2016.

[11] Korger, M.; Bergschneider, J.; Lutz, M.; Mahltig, B.; Finsterbusch, K.; Rabe, M. Possible Applications of 3D Printing Technology on Textile Substrates. 48th Conference of the International Federation of Knitting Technologists (IFKT), *IOP Conf. Ser.: Mater. Sci. Eng.*, 2016, 141. DOI:10.1088/1757-899X/141/1/012011

[12] Döpke, C., Grimmelsmann, N., Ehrmann, A. 3D-Druck auf Gestricken. Melliand Textilberichte, 2016, 97 (4), pp. 195-196.

[13] Hashemi Sanatgar, R.; Campagne, C.; Nierstrasz, V. Investigation of the adhesion properties of direct 3D printing of polymers and nanocomposites on textiles: Effect of FDM printing process parameters. *Appl. Surf. Sci.*, 2017, 403, pp. 551–563. DOI: 10.1016/j.apsusc.2017.01.112.

[14] Göbel, S. L.; Siegel, F. Changing Physical Properties of Textiles by 3D Printing. Proceedings of the Printing Future Days 2017, Chemnitz, Germany, 04.-06.10.2017; Verlag für Wissenschaft und Bildung: Berlin, Germany, 2017; pp. 171-175.

[15] Ehrmann, A.; Fafenrot, S.; Grimmelsmann, N. Beeinflussung des Warenfalls durch 3D-Aufdruck. TEXTILplus, 2017, 1-2; pp. 21-23.

[16] Sabantina, L.; Kinzel, F.; Ehrmann, A.; Finsterbusch, K. Combining 3D printed forms with textile structures – mechanical and geometrical properties of multi-material systems. *IOP Conf. Ser.: Mater. Sci. Eng.*, 2015, 87. DOI:10.1088/1757-899X/87/1/012005

[17] Korger, M.; Bergschneider, J.; Neuss, J.; Mahltig, B.; Rabe, M. Additive Manufacturing for Textile Surface Modification. 3F-Talks: Functional Fibres and Films, Aachen, Germany, 29.04.2016.

[18] Bergschneider, J.; Korger, M.; Kyosev, Y.; Lutz, M.; Rabe, M.; Mahltig, B. Textilfunktionalisierung mit 3D-Druck - Echtheiten und Schichtadhäsion. Melliand Textilberichte, 2016, 97 (4), pp. 197-199.

[19] Kreikebaum, E.; Lutz, M.; Doerfel, M.; Finsterbusch, K.; Ehrmann, A.; 3D-Druck von Blindenschrift auf Textil. Technische Textilien, 2017, 60 (2), pp. 92-93.

[20] Sanduloff, S., Korger, M., Glogowsky, A., Meyer, J., Steinem, C., Huysman, S., Ernst, M., Rabe, M. Body contour compatible protectors using 3D printing technology / Körperkonturgerechte Protektoren mittels 3D-Drucktechnologie. 58th DORNBIRN-GFC, Dornbirn, Austria,12.09.2019.

COMMUNICATIONS IN
DEVELOPMENT AND ASSEMBLING OF TEXTILE PRODUCTS

Modeling of electro-conductive properties of woven structure based on mixing model

Magdalena Tokarska[1,*]

[1]*Institute of Architecture of Textiles, Lodz University of Technology, Poland*
*Corresponding author *E-mail address:* magdalena.tokarska@p.lodz.pl

INFO

CDAPT, ISSN: 2701-939X
Peer reviewed article
2020, Vol.1, Nr. 3, pp. 12-19
DOI:10.25367/cdatp.2020.1.p12-19
Received: 29 April 2020
Accepted: 21 Mai 2020
Available online: 22 September 2020

ABSTRACT

The main purpose of the research is to model the electro-conductive properties of the woven structure based on the mixing model. The generalized Archie's law for analysis of the woven structure and its conductivity was chosen. The generalized Archie's law can be applied to objects containing pores filled with phases. The phases are pathways enabling conduction. The remaining part is a non-conducting matrix. The model of the composite was transferred to a woven structure. Electro-conductive components of woven structure i.e. strips and contacts of strips were treated as conducting phases in the structure. The remaining part is pore space corresponds to the matrix. Based on generalized Archie's law, the connectivity as being a measure of how the components of the whole structure are arranged, and the connectedness of a given phase as being a measure of the availability of pathways for conduction through that phase was determined for all structures. It was found that the connectivity of the strips phase is higher than the connectivity of the contacts of strips phase. It means that the strips phase (in terms of their quantity) has a greater effect on the conductivity of the woven structure than the contacts of strips phase. A decrease of the connectedness of strips and contacts of strips phases (in terms of their quality) can be obtained by adding another component to the woven structure which will reduce the conductivity of the structure.

Keywords
woven structure,
electrical conductivity,
composite,
mixing model,
generalized Archie's law,
connectivity,
connectedness

1 Introduction

Textile materials are fundamental components of our everyday lives. Nowadays, consumers are becoming more and more demanding. Especially, they expect clothing to contain many functionalities. By combining traditional textiles and new fabrication technologies, we can achieve new functionalities [1-3]. As a result, the area of applications of textiles has been expanded. Created smart textiles can be used in every-day clothing integrated with electronic elements such as displays, controls, and keyboards enabling e.g. the monitoring of physiological signals [2]. Smart textiles contain e-textiles which due to their electro-conductive properties have wide possibilities of applications. They include electrical circuits, transmission lines, antennas, heating elements, electrodes, sensors, EMI shielding materials [2,4-6,7].

The e-textiles are in particular woven fabrics-based. Modeling of the electro-conductive properties of a woven structure is important for designing new textile elements integrated with clothing. Simulation tools make it possible to predict their electro-conductive properties. To determine resistivity, models based on equivalent resistance schemes are used for regular fabrics with yarns being ideal resistors of known resistance [8,9].

The resistivity of woven fabric which is much more complex and shows anisotropy of electrical properties is modeled using the McLachlan equation [10,11]. The McLachlan equation was derived for the conductivity of binary mixtures with anisotropic grain structures [12]. The dependence also works for woven fabrics treated as metal-dielectric composites where conductive linear components (yarns) create a system of empty spaces filled with dielectric air. A prediction level was in the range of 83-88% for fabrics with surface percentage cover above 96% [11]. This may be because the contact resistance resulting from the interlaced yarns [7,9] was not taken into account in the study. In the article a new approach to modeling the electro-conductive properties of woven structure was proposed based on a mixing model. The generalized Archie's law developed by Glover [13,14] was chosen. The conductivity of contacts was taken into account in assessing the electro-conductive properties of the woven structure based on the model.

2 Materials and Methods

2.1 Woven structures

The generalized Archie's law can be applied to objects containing pores filled with phases. The phases are pathways enabling conduction. The remaining part is a non-conducting matrix. The model of the composite was transferred to a woven structure composed of interlaced conductive narrow strips. In the woven structure, the conducting phases are strips and contacts of strips. Due to different conductivities of components, electrical conductivity takes place to varying degrees. The remaining part is pore space filled with dielectric air. It should be emphasized that in the proposed model, the pore space of the woven fabric are not identical with the pores of the model described by generalized law, but oppositely with the non-conducting matrix.

Three woven structures were designed from the same kind of strips. The same dimension (9 cm $\times$ 13 cm) of each structure is assumed. It was assumed that the number of weft and warp stripes is the same i.e. 3$\times$3, 4$\times$4, and 5$\times$5. The different number of stripes constituting the weft and warp of the woven structure enabled obtaining structures of different densities.

Nine different woven structures were created using strips of 1 cm wide cut from three different textile materials (woven fabrics). Characteristics of the materials which are important from the point of view of electrical conductivity are given in Table 1.

The linear resistance of 1 cm wide strips was determined based on the four-electrode method according to EN 16812:2016 standard [15]. The thickness was determined based on EN ISO 5084:1996 standard [16]. Measurements of strip resistance were repeated 10 times, while woven fabric thickness 5 times. The coefficient of variation *CV* was given in parentheses.

Table 1. Characteristics of textile materials used for strips.

Woven fabric	Raw material composition	Manufacturer	Linear resistance (Ω/cm)	Thickness (mm)
A	100% polyamide woven fabric; nickel and copper metalized	Laird PLC, GB	0.035 (4%)	0.124 (4%)
B	100% polyester woven fabric; nickel metalized	Soliani EMC, Italy	0.180 (6%)	0.078 (6%)
C	100% polyester woven fabric; nickel metalized	Soliani EMC, Italy	0.246 (9%)	0.270 (4%)

Summarizing, each woven structure was composed of two conducting phases (strips and contacts of strips) and one non-conducting phase (pore space).

2.2 Mixing model

Many types of mixing models are used to determine the electrical properties of porous materials. One of them is Archie's law [17] extended for n phases and known as the generalized Archie's law [13]. The Archie's law is empirical quantitative relationship between porosity, electrical conductivity, and brine saturation of rocks [17]. It describes a relationship of the conductivity σ of a clean reservoir rock to its porosity ϕ and the conductivity of phase σ_f (e.g. fluid) that completely saturates the pore space. There is also cementation exponent *m* related to the degree of cementation of the rock fabric. Archie's law can be expressed as follows [13]:

$$\sigma = \sigma_f \phi^m \quad (1)$$

where: σ – the bulk effective conductivity of the rock; σ_f – the conductivity of the fluid occupying the pores; ϕ – the volume fraction of the fluid phase; *m* – the cementation exponent.

Small exponent (m<2) occurs for high connectivity phases. Pores that are well connected provide an efficient pathway for the fluid flow. Large exponent *m* (m≥2) occurs for low connectivity phases. The cementation exponent *m* dependents on the shapes and type of the sedimentary rocks grains, shape and types of pores, specific surface area, tortuosity, anisotropy, and compaction.

Archie's object can be compared to a woven structure composed of two conducting phases (strips and contacts of strips) and one non-conducting phase (pore space). The generalized Archie's law applied to the woven structure can be given as follows [13]:

$$\sigma_{str} = \sigma_{th}\phi_{th}^{m_{th}} + \sigma_{cont}\phi_{cont}^{m_{cont}} \quad (2)$$

where: σ_{str} – the woven structure conductivity in Ωcm^{-1}; σ_{th}, σ_{cont} – the strips and the contacts of strips phases conductivity in Ωcm^{-1}, respectively; ϕ_{th}, ϕ_{cont} – the strips and the contacts of strips phases volume fraction, respectively; m_{th}, m_{cont} – the exponents of strips and the contacts of strips phases, respectively.

Each of the exponents the generalized law share the same physical meaning as those in the classical Archie's law.

To find the exponents of strips and the contacts of strips phases additional dependence is needed [13]:

$$\left(-\frac{\phi_{th}^2}{2}\right) m_{cont}^2 + \left(\phi_{th} - \frac{\phi_{th}^2}{2}\right) m_{cont} - \phi_{th}^{m_{th}} = 0 \quad (3)$$

It was stated that the sum of the volume fractions of all of the phases in porous material must equal unity. The same assumption was adopted for the sum of the connectedness of all of the phases in the porous material.

Based on Eq. 2 and Eq. 3 the exponents of phases can be determined unequivocally.

The woven structure can be described using two parameters: the connectedness and the connectivity defined by Glover [13] and Glover and Walker [14]. The connectedness *G* of each phase is given by:

$$G_i = \frac{\sigma_{str}}{\sigma_i} \quad (4)$$

where: σ_{str} – the woven structure conductivity in Ωcm^{-1}; σ_i – the *i*-th phase conductivity in Ωcm^{-1}.

The connectedness of a given phase is a measure of the availability of pathways for conduction through that phase.

The connectivity χ for each phase is defined as:

$$\chi_i = \phi_i^{m_i - 1} \quad (5)$$

where: ϕ_i – the *i*-th phase volume fraction; m_i – the *i*-th phase exponent.

The connectivity is a measure of how the components and therefore the pore space is arranged.

2.3 Measurement methods

To determine the exponents of strips and the contacts of strips phases, the conductivity of strips, the conductivity of contacts of strips, and the conductivity of woven structure are needed to be identified. The resistance of strip can be determined based on the four-electrode method (Fig. 1a) according to EN 16812:2016 standard [15].

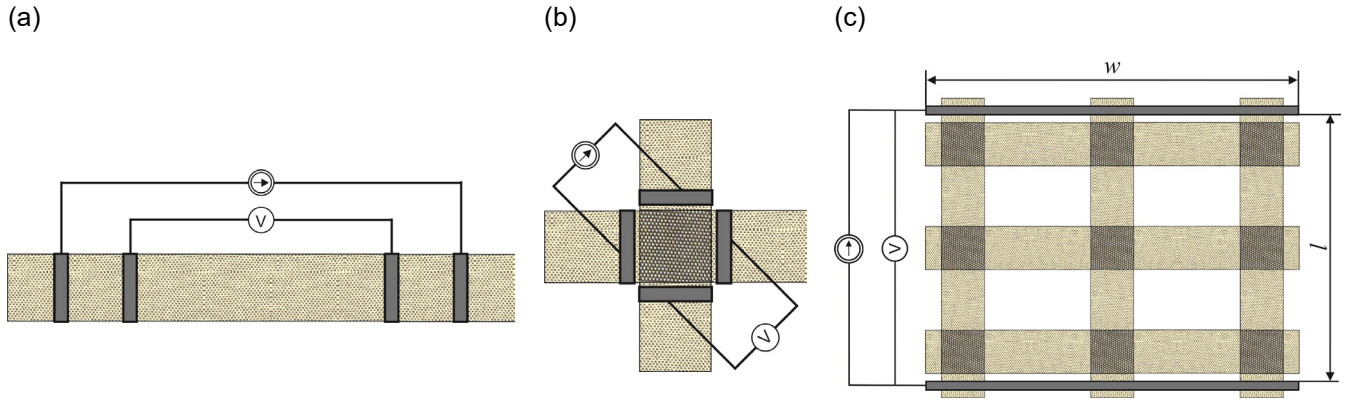

Fig. 1 Resistance measurement (a) Strip; (b) Contact of strips; (c) Woven structure.

The conductivity of strip σ_{th} can be determined based on its linear resistance (Table 1). Therefore the dependence is as follows:

$$\sigma_{th} = \frac{1}{dhR_L} \quad (6)$$

where: R_L – the linear resistance of strip; *d* – the strip width (*d* = 1 cm); *h* – the strip thickness.

The resistance of strips contact can be determined using the four-electrode method (Fig. 1b) described in detail [18]. The conductivity of strips contact σ_{cont} can be calculated from the following dependence:

$$\sigma_{cont} = \frac{1}{2Rh} \quad (7)$$

where: *R* – the resistance of strips contact; *h* – the strip thickness.

The resistance of woven structure can be performed using two electrodes, four wires method (Fig. 1c) according to AATCC 76-2018 standard [19]. The conductivity of woven structure σ_{str} can be determined using the following formula:

$$\sigma_{str} = \frac{l}{wh'R} \quad (8)$$

wherein

$$h' = 2h \cdot C_{cont} + h \cdot C_{th} \quad (9)$$

where: R – the resistance of woven structure; l – the electrodes spacing (l = 9 cm); w – the structure width (w = 13 cm); h' – the averaged fabric thickness; C_{cont} – the fraction of contacts of strips in whole woven structure; C_{th} – the fraction of strips in the whole woven structure.

3 Results and Discussion

Analysis of designed structures was conducted. The fraction C_{th} and C_{cont} of strips and contacts of strips, respectively, in the whole structure was determined (Table 2). Remaining part is pores, from which the porosity of the woven structure results.

Table 2. Fraction of strips and contacts of strips in woven structure.

Woven structure density (strips×strips)	**Fraction of strips C_{th} (-)**	**Fraction of contacts of strips C_{cont} (-)**
3×3	0.410	0.077
4×4	0.479	0.137
5×5	0.513	0.214

Based on measurement results and Eq. 6 and Eq. 7, conductivities σ_{th} and σ_{cont} were determined respectively. Based on the values of parameters C_{th} and C_{cont} (Table 2) and fabric thickness h (Table 1), the averaged fabric thickness h' was calculated (Eq. 9) for each designed structure. Next, according to Eq. 8, conductivity σ_{str} was determined for each woven structure. Moreover, two phases volume fractions ϕ_{th} and ϕ_{cont} were determined based on the spacing of strips, the width of strips, and the assumed dimension of the whole woven structure. The sum of the two volume fractions (conductive phases in woven structure) is equal to unity. Solving simultaneous equations (Eq. 2 and Eq. 3), the exponents of phases m_{th} and m_{cont} were determined. The received results are juxtaposed in Table 3. The coefficient of variation was given in parentheses for parameters determined based on measurement results.

Table 3. Parameters of woven structures and their components based on the generalized Archie's law.

Woven structure	**σ_{th} (Ωcm^{-1})**	**σ_{cont} (Ωcm^{-1})**	**σ_{str} (Ωcm^{-1})**	**ϕ_{th} (-)**	**ϕ_{cont} (-)**	**m_{th} (-)**	**m_{cont} (-)**
3×3 A	2291 (4%)	3200 (17%)	1032 (7%)	0.84	0.16	4.7	3.0
3×3 B	712 (6%)	3339 (13%)	302 (2%)	0.84	0.16	5.2	3.0
3×3 C	150 (9%)	146 (11%)	69 (1%)	0.84	0.16	4.5	2.9
4×4 A	2291 (4%)	3200 (17%)	967 (4%)	0.78	0.22	3.6	3.1
4×4 B	712 (6%)	3339 (13%)	286 (7%)	0.78	0.22	4.0	3.2
4×4 C	150 (9%)	146 (11%)	70 (9%)	0.78	0.22	3.1	3.1
5×5 A	2291 (4%)	3200 (17%)	911 (5%)	0.71	0.29	2.8	3.4
5×5 B	712 (6%)	3339 (13%)	286 (7%)	0.71	0.29	3.2	3.4
5×5 C	150 (9%)	146 (11%)	68 (4%)	0.71	0.29	2.4	3.3

Pearson's correlation coefficient R_P was used in statistics to measure how strong a relationship is between the conductivity of strips, contacts of strips, and whole woven structure. The significance level equals 0.10 was assumed. It was noticed that for couples σ_{th}, σ_{cont}, and σ_{cont}, σ_{str}, a strong uphill (positive) linear relationship is observed; R_P = 0.675 and R_P = 0.661 were received respectively. For a couple of σ_{th}, σ_{str}, an almost perfect uphill (positive) linear relationship was noticed (R_P = 0.997). This is due to the fact that the strips phase volume fraction ϕ_{th} this greater than the contacts of strips phase volume fraction ϕ_{cont}.

Relatively small values of ϕ_{cont} and low level of diversity of woven structures were reflected in the comparable values of phase exponent m_{cont}. For all woven structures the average value of the parameter equals 3.16, whereas *CV* is equal to 6%. Values of m_{th} were considered in groups divided by structure density. Therefore following results were obtained for structures: 3×3, m_{th} = 4.84, *CV* = 8%; 4×4, m_{th} = 3.58, *CV* = 12%; 5×5, m_{th} = 2.79, *CV* = 14%. In addition to structure features, the exponents also depend indirectly on the conductivity of individual components. This is due to the mixing model (Eq. 2). It can be generally stated that the even woven structure (see Fig. 1c), where identical pores in the shape of rectangles and conductive phases are evenly distributed throughout the structure, characterizes large values of phase exponent (above 2). Therefore the low connectivity of conductive phases occurs. The smaller the woven structure density, the larger the phase exponent m_{th}.

Next, the connectedness *G* (Eq. 4) and the connectivity χ (Eq. 5) for each phase were calculated and given in Table 4.

Table 4. Parameters describing electro-conductive woven structure.

Woven structure	G_{th} (-)	G_{cont} (-)	χ_{th} (-)	χ_{cont} (-)
3×3 A	0.45	0.32	0.53	0.03
3×3 B	0.42	0.09	0.48	0.02
3×3 C	0.46	0.48	0.54	0.03
4×4 A	0.42	0.30	0.53	0.04
4×4 B	0.40	0.09	0.47	0.04
4×4 C	0.46	0.48	0.58	0.04
5×5 A	0.40	0.28	0.53	0.05
5×5 B	0.40	0.09	0.47	0.05
5×5 C	0.45	0.47	0.62	0.06

The connectedness of the strips phase and the contacts of strips phase indicates the availability of the pathways for conduction through this phase. Therefore it is a qualitative feature. The conductivity of each phase was higher than the conductivity of the woven structure therefore values of *G* are in the range of (0,1). It was noticed, that adding another component to the woven structure can reduce the conductivity of the structure, which results in a decrease of parameter *G* (Table 4).

It was found, that the connectedness of both phases slightly increases with decreasing woven structure density. It is particularly visible for both phases of woven structures designed using strips of the woven fabric denoted as A (Fig. 2a). The extent to which the strips phase and the contacts of strips phase affect (in terms of their quality) the conductivity of the woven structure depends on woven fabric. In most cases, the impact of the strips phase is greater than the contacts of strips phase as shown in Fig. 2a.

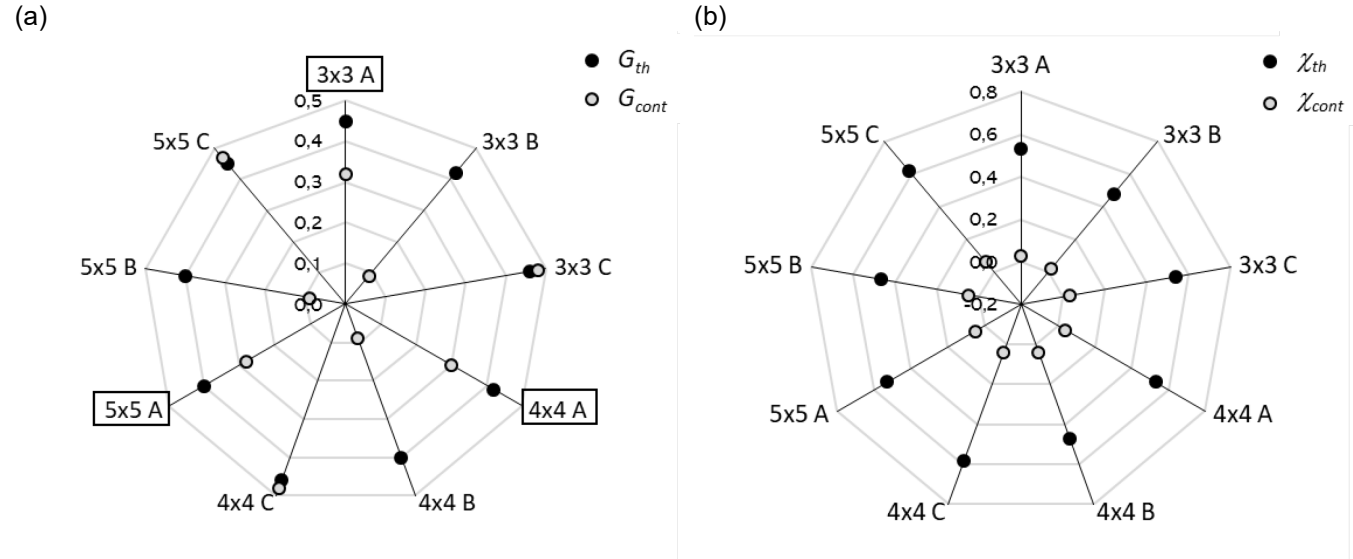

Fig. 2 Parameters of strips and contacts of strips phases (a) Connectedness; (b) Connectivity.

The connectivity indicates how components are arranged in a woven structure. The values of connectivity χ are greater than 0. The effect of strips phase and contacts of strips phase on the woven structure conductivity are presented in Fig. 2b.

The larger values of χ_{th} compared to χ_{cont} mean that the strips phase (in terms of their quantity) has a greater effect on the conductivity of the woven structure than the contacts of strips phase. It was observed for all woven structures. However, it should be noted, this parameter is related to phase exponent which indirectly implies the impact of the components' conductivity on the connectivity value.

4 Conclusions

It was found, that the chosen mixing model can be used to modeling the electro-conductive properties of woven structure which consists of electro-conductive components i.e. strips and contacts of strips treated as conducting phases in the whole structure.

A strong uphill linear relationship was observed for conductivities of strips and contacts of strips phases, and also for conductivities of contacts of strips and woven structure. An almost perfect uphill linear relationship was observed for conductivities of strips and woven structure.

A decrease of the connectedness of strips and contacts of strips phases (in terms of their quality) can be obtained by adding another component to the woven structure which will reduce the conductivity of the whole structure.

The larger values of connectivity χ_{th} compared to χ_{cont} mean that the strips phase (in terms of their quantity) has a greater effect on the conductivity of the woven structure than the contacts of strips phase. However, contacts of strips must be taken into account in assessing the electro-conductive properties of the woven structure. The generalized Archie's law enables such analysis and from this point of view, it is better than the McLachlan model.

By designing the same structure but from other components, you can predict the conductivity of the new structure based on parameters determined from the mixing model. It was found that the phase exponent m_{cont} equals 3.16 for all woven structures and the exponent m_{th} equals 2.79, 3.58, and 4.84 for structures 5×5, 4×4, and 3×3, respectively. The smaller the woven structure density, the larger the phase exponent m_{th}. Having a well-defined electrical conductivity, volume fraction, and exponent for all phases, the electrical conductivity of the whole composite can be calculated and compared to the experimental result.

References

[1] Cherenack, K.; van Pieterson, L. Smart textiles: Challenges and opportunities. *J Appl Phys*, 2012, 112(9), 091301-1–091301-14. DOI: 10.1063/1.4742728.

[2] Gonçalves, C.; Ferreira da Silva, A.; Gomes, J.; Simoes, R. Wearable e-textile technologies: A review on sensors, actuators and control elements. *Inventions*, 2018, 3(1), 1–13. DOI: 10.3390/inventions3010014.

[3] Castano, L.M.; Flatau, A.B. Smart fabric sensors and e-textile technologies: A review. *Smart Mater Struct*, 2014, 23, 053001–053027. DOI: 10.1088/0964-1726/23/5/053001.

[4] Acar, G.; Ozturk, O.; Golparvar, A.J.; Elboshra, T.A.; Böhringer, K.; Yapici, M.K. Wearable and flexible textile electrodes for biopotential signal monitoring: A review. *Electronics*, 2019, 8(5), 1–25. DOI: 10.3390/electronics8050479.

[5] Gil, I.; Fernández-García, R.; Tornero, J.A. Embroidery manufacturing techniques for textile dipole antenna applied to wireless body area network. *Text Res J*, 2019, 89(8), 1573–1581. DOI: 10.1177/0040517518770682.

[6] Shaw, V.P.; Jagatheesan, K.; Ramasamy, A. Mechanical and electromagnetic shielding behaviours of thermoplastic conductive composite: Influence of yarn structure and process variables. *J Text I*, 2019. DOI: 10.1080/00405000.2019.1688903.

[7] Zeng, W.; Shu, L.; Li, Q.; Chen, S.; Wang, F.; Tao, X-M. Fiber-based wearable electronics: A review of materials, fabrication, devices, and applications. *Adv Mater*, 2014, 26, 5310–5336. DOI: 10.1002/adma.201400633.

[8] Liu, S.; Tong, J.; Yang, C.; Li, L. Smart e-textile: Resistance properties of conductive knitted fabric - Single pique. *Text Res J*, 2017, 87(14), 1669–1684. DOI: 10.1177/0040517516658509.

[9] Gunnarsson, E.; Karlsteen, M; Berglin, L; Stray, J. A novel technique for direct measurements of contact resistance between interlaced conductive yarns in a plain weave. *Text Res J*, 2015, 85(5), 499–511. DOI: 10.1177/0040517514532158.

[10] Tokarska, M. New concept in assessing compactness of woven structure in terms of its resistivity. *J Mater Sci-Mater El*, 2016, 27(7), 7335–7341. DOI: 10.1007/s10854-016-4703-2.
[11] Tokarska M., Mathematical model for predicting the resistivity of an electroconductive woven structure. *J Electron Mater*, 2017, 46(3), 1497–1503. DOI: 10.1007/s11664-016-5186-x.
[12] McLachlan, D.S. Equations for the conductivity of macroscopic mixtures. *J Phys C Solid State*, 1986, 19(9), 1339–1354. DOI: 10.1088/0022-3719/19/9/007.
[13] Glover, P.W.J. A generalized Archie's law for n phases. *Geophysics*, 2010, 75(6), E247–E265. DOI: 10.1190/1.3509781.
[14] Glover, P.W.J.; Walker, E. Grain-size to effective pore-size transformation derived from an electrokinetic theory. *Geophysics*, 2009, 74(1), E17–E29. DOI: 10.1190/1.3033217.
[15] EN 16812:2016. *Textiles and textile products. Electrically conductive textiles. Determination of the linear electrical resistance of conductive tracks*. 2016.
[16] EN ISO 5084:1996. *Textiles. Determination of thickness of textiles and textile products*. 1996.
[17] Archie, G.E. Electrical resistivity log as an aid in determining some reservoir characteristics. *T Metall Soc AIME*, 1942, 146(1), 54–62. DOI: 10.2118/942054-G.
[18] Vasile, S.; Deruck, F.; Hertleer, C.; De Raeve, A.; Ellegiers, T.; De Mey, G. Study of the contact resistance of interlaced stainless steel yarns embedded in hybrid woven fabrics. *Autex Res J*, 2017, 17(2), 170–176. DOI: 10.1515/aut-2016-0024.
[19] AATCC 76-2018. *Electrical resistivity of fabrics*. 2018.

COMMUNICATIONS IN
DEVELOPMENT AND ASSEMBLING OF TEXTILE PRODUCTS

Data mining-based optimal assignment of apparel size for mass customization

Zhu-Jun Wang[1,2], Cheng Chi[3], Meng-Yun Zhang[3], Xian-Yi Zeng[3], Pascal Bruniaux[3], Jian-Ping Wang[1,*], Ying-Mei Xing[2], Shuo Xu[1]

[1]*College of Fashion and Design, Donghua University, Shanghai, China*
[2]*School of Textile and Garment, Anhui Polytechnic University, Wuhu, China*
[3]*GEMTEX Laboratory, Ecole Nationale Superieure des Arts et Industries Textiles, Roubaix, France*
*Corresponding author *E-mail address:* wangjp@dhu.edu.cn

INFO

CDAPT, ISSN: 2701-939X
Peer reviewed article
2020, Vol.1, Nr. 4, pp. 20-29
DOI:10.25367/cdatp.2020.1.p20-29
Received: 04 May 2020
Accepted: 23 June 2020
Available online: 22 September 2020

ABSTRACT

In this study, we have explored and discussed the data mining-based solutions to apparel size assignment using an approach principle, K-means clustering, and support vector machine, respectively. A case of mass customization for men's pants in China with 200 adult males were employed to validate and evaluate the solutions. After anthropometric data acquisition and preprocessing, three key body dimensions were identified based on hierarchical clustering as well as their ranges and fit models. Sequentially, we calculated all the possible values of the distance between the target population and fit models by the enumeration algorithm. Afterward, we assigned the garment sizes for the target population using the above mentioned data mining approaches. Finally, the solution based on the support machine was considered as the optimal solution for the pant mass customization after being comprehensively assessed by the aggregate loss of fit, the number of poor fit, accommodation rate of ideal fit, and the number of garment size employed, since it employed only 48 sizes to reach the accommodation rate of target population up to 82%. The experimental results demonstrate that the present solution is a low-cost method for the size assignment by exploiting the potentials of existing sizing system, instead of creating new sizing systems, and also easy to be flexibly extended to any types of garments.

Keywords
garment size assignment,
mass customization,
data mining,
hierarchical clustering algorithm,
K-means clustering,
support vector machine

1 Introduction

Among all facets associated with the purchase decisions of consumers, wearing comfort represents a fundamental and central concern, which is linked inextricably with a garment fit, which largely relies on the garment design and the relative size between body and clothing [1]. Appropriate garment fit can not only provide the adequate space allowance for body movements, but also give consumers a rewarding experience of self-expression and self-image [2]. Most recently, with the rapid development of mobile e-commerce, along with the convenient shopping way, the personalized demands for garments such as styles, colors, and fit have been dramatically enhanced. Enterprises have paid attention to mass customization (MC) in the clothing industry [3]. MC means enterprises are driven by personalized orders, offering individualized products by the industrial manufacturing process. Contributing to the advanced manufacturing technologies, i.e., 3D whole-body scanning, virtual reality, and apparel CAD/CAM, the garment enterprises can realize the customization using the full automation systems preliminarily. However, such a manner could not be made available and flexible under the circumstances of MC, i.e., small series production. Furthermore, the high costs of expensive systems with advanced technologies also hinder their applications in the garment MC. Therefore, it is a paramount issue of how to meet the needs of individual consumers, while getting the benefits of economy of scale should be concerned comprehensively [4].

Ordinarily, in the context of MC, garments are manufactured following the process illustrated in Fig. 1. First of all, the anthropometric data of target consumers are acquired after the personalized garment order is placed and signed. Before drafting the garment patterns for the target population, the body sizes and garment sizes are identified and determined based on the sizing system and the returned merchandising reports. Afterward, the products are produced by the industrial manufacturing process. In this way, the garment sizing system is the inextricable linkage of the development of personalized garments and the industrial manufacturing process. With the help of sizing system, the manufacturers could only utilize a limited number of patterns, while simultaneously catering to the fit requirements of the individual consumer in the industry. Besides, the correct assignment for apparel sizes is said to have the advantage of predicting sales of diverse sizes and determine production quantities, resulting in the accurate material cost control and manufacturing planning. However, the size assignment is still a challenging issue to resolve in the garment MC. Much of research have examined the utilization of advanced technologies, such as traditional step-wise methods, multivariable approaches, and optimization techniques, concerning the assignment of apparel sizes [5-11]. Nevertheless, plenty of the studies concentrated on establishing a new sizing system only, instead of exploiting the potentials of the existing sizing system. The effectiveness and feasibility of the new sizing system still need to be further verified. In practice, improving the existing one is more economical than developing an alternative. Moreover, the improved one can be more easily implemented by the operators in the enterprises.

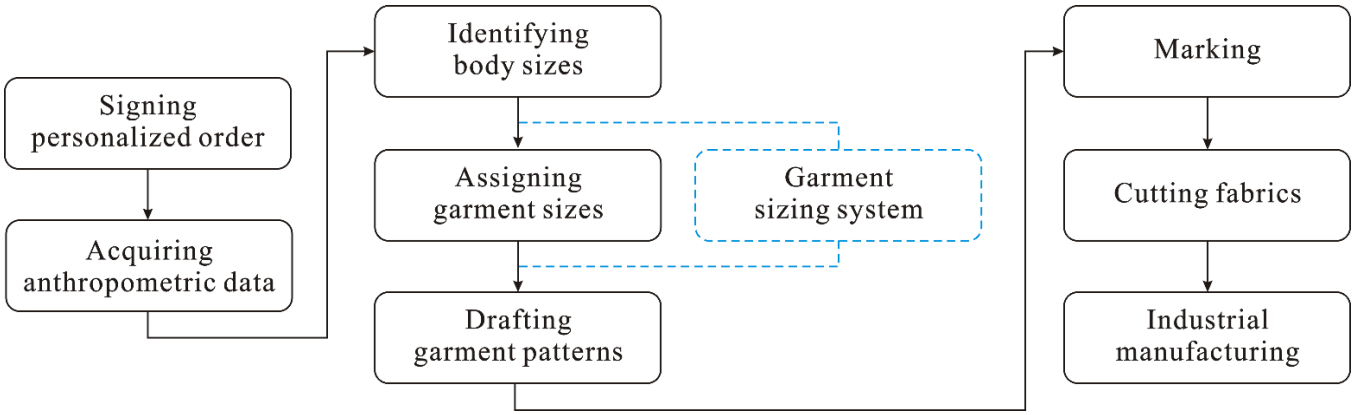

Fig. 1 Flowchart of garment mass customization

Data Mining (DM) is an interdisciplinary technique focusing on exploiting useful knowledge from a large dataset, involving the application of algorithms that explore the data, develop models and discover the useful knowledge that supports decision making, which has been viewed as an efficient tool of solving

complicated engineering problems [12]. Therefore, an approach of optimizing sizing assignment toward MC was proposed based on the DM technique in this study, to fulfill the individualized fit requirement for consumers with few quantities of sizes.

2 Method

2.1 Research scheme

Fig.2 presents the research process in this study. Research work can be split into five sequential procedures, i.e., an anthropometric data acquisition, data preprocessing, body size identification, apparel size assignment, and evaluation. We mainly took into account the following factors affecting the size assignment: the target population, garment, standard sizing system, manufacturer as well as the market feedback.

Step 1: The anthropometric data of the target population were measured according to the desired garment style. Both the manual and automatic machine measurement are available.

Step 2: The data noises are inevitable during the process of data acquisition. To minimize the impact of data noises, we preprocessed the original data obtained in the previous step using the detection of outliers, descriptive analysis, and test of normality.

Step 3: The hierarchical algorithm identified key body dimensions of the target population.

Step 4: According to the target population and the relevant standard sizing system, we determined the intervals, fit models, and size range. The assignment of apparel sizes was executed using approaching principle, *K*-means clustering, and support vector machine, respectively.

Step 5: The optimal solution to size assignment was found by evaluating the experimental results eventually.

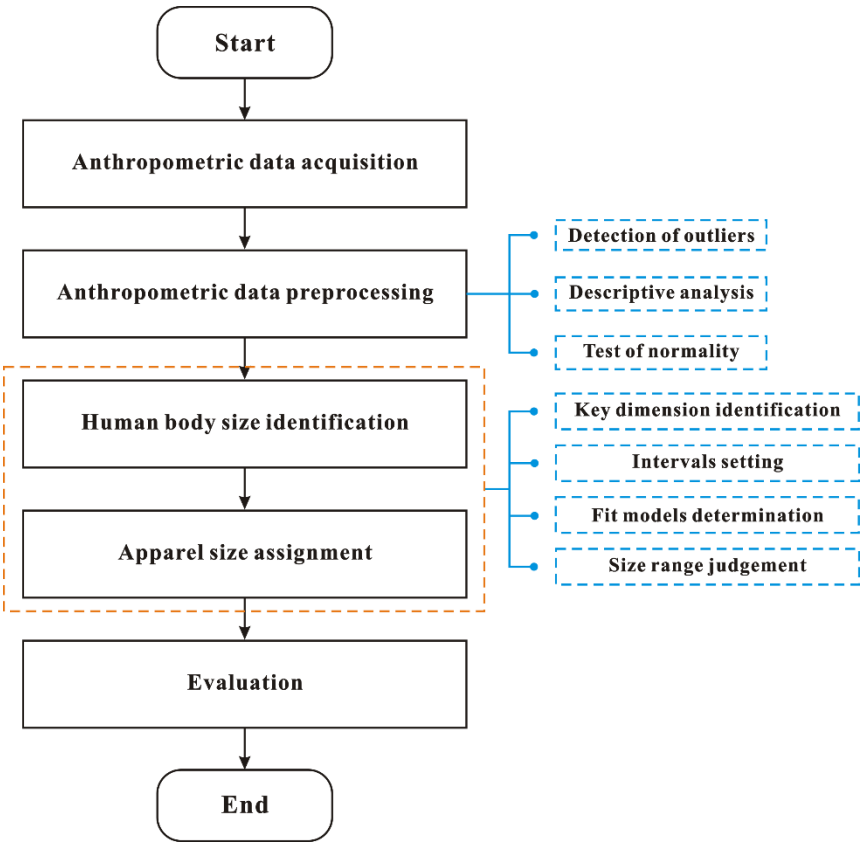

Fig. 2 Research scheme

2.2 Applied algorithms

2.2.1 Hierarchical clustering algorithm

To reflect how the body dimensions are merged or divided evidently, the hierarchical clustering algorithm was employed to identify the key body dimensions after anthropometric data of the target population were captured and preprocessed.

2.2.2 Enumeration algorithm

Enumeration algorithm was utilized by listing all the possible values while computing the distance between the body dimensions of target population and the dimensions of the fit models.

2.2.3 K-means clustering algorithm

K-means algorithm is a popular partitioning approach. The classic clustering procedure was as follows: (a) Choose K as the number of clusters; (b) Initialize the cluster centroid vector $\{c_1,c_2,\ldots,c_k\}$; (c) For each new object vector, calculate the distance between the new object vector and cluster centroid vector; (d) Assign the new object to its closest cluster centroid, and re-compute the centroid of the closest cluster with the new object; (e) If the position of any cluster centroid changed, return to (c), otherwise, stop.

2.2.4 Support vector machine method

Due to the distinct advantages, i.e., an excellent generation performance, fast convergence, and robustness for noise, support vector machine (SVM) have been diffusely applied in solving nonlinear, high-dimensional pattern recognition, classification, and regression problems. SVM was introduced to assign garment size in this work.

3 Test

In this section, we adopt a case of men's pants to interpret the implementation of the present solution to the garment size assignment.

3.1 Data acquisition

Owing to the advantages of taking automatic body measurements in a manner of non-contact precisely and expeditiously, we procured the anthropometric data of 200 adult males aged from 18 to 55 using the Vitus Bodyscan shown in Fig. 3.

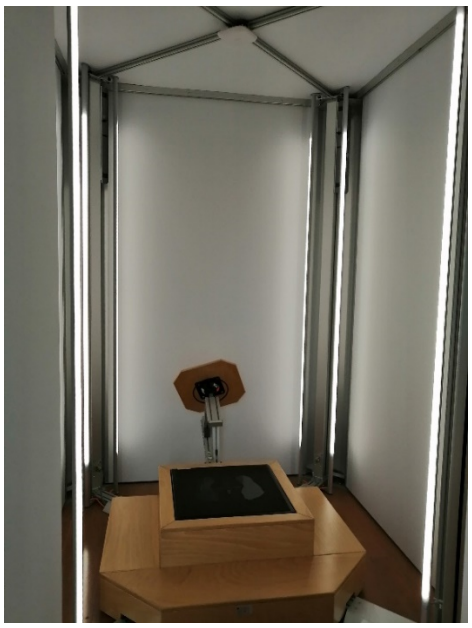

Fig. 3 Vitus Bodyscan

According to the characteristics of the garment type and the relationship with garment pattern blocks, we extracted nineteen lower body measurements from the whole body datasets. They were: stature, waist height, abdomen height, hip height, knee height, inseam length, waist girth, abdomen girth, hip girth, thigh root girth, mid-thigh girth, crotch length, knee girth, waist width, hip width, waist depth, abdomen depth, mid-hip depth, and hip depth. Fig. 4 demonstrated, how the body dimensions were measured.

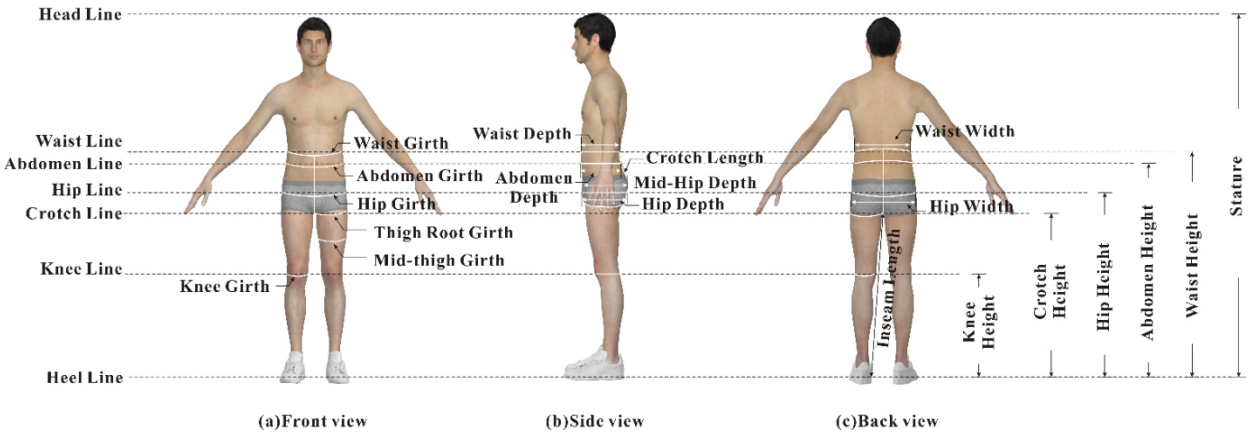

Fig. 4 Diagram of lower body measurements

3.2 Data preprocessing

3.2.1 Detection of outliers

In the statistical analysis, the outliers are a set of data to be an observation or subset of data that appears to be inconsistent with the remainder of that set of data. Outliers in a set of data will influence the modeling precision. Thus, the original data were conduct outlier analysis by the method of 3σ-rule. Once the outliers were detected, the data will be re-measured and executed outlier analysis again. If they were still outliers, it could be inferred that they were particular dimensions. We maintained all the particular dimensions in this study.

3.2.2 Descriptive analysis

Descriptive analysis is a simple, straightforward, and practical approach to mirroring the data features. The features of the experimental data were presented in Table 1.

Table 1. Description of the anthropometric dimensions

Measurements [cm]	Sample number	Minimum [cm]	Maximum [cm]	Mean [cm]	Standard deviation [cm]
Stature	200	150.85	183.21	166.04	5.32
Waist height	200	93.42	116.41	102.89	4.09
Abdomen height	200	83.50	102.76	92.28	4.13
Hip height	200	72.30	88.12	80.06	3.40
Knee height	200	39.28	49.72	44.34	2.16
Inseam length	200	64.45	83.34	74.55	3.79
Waist girth	200	61.21	101.90	79.75	8.87
Abdomen girth	200	63.10	101.95	82.41	7.50
Hip girth	200	76.57	105.25	90.69	5.04
Mid-thigh girth	200	40.10	58.00	49.03	3.48
Crotch length	200	65.50	90.30	77.50	4.67
Knee girth	200	31.80	41.50	36.17	1.92
Thigh root girth	200	42.20	62.90	51.67	3.87
Waist width	200	21.25	32.46	26.64	2.37
Hip width	200	28.00	35.70	31.81	1.55
Waist depth	200	14.10	29.35	20.73	3.11
Abdomen depth	200	14.70	27.90	20.84	2.77
Hip depth	200	15.40	26.35	20.63	2.28
Mid-hip depth	200	15.82	25.87	20.95	2.08

3.2.3 Test of normality

The normality test was utilized to check if the data sample deviates from the Gaussian distribution. In this study, all the measurements were tested for the normality. From Fig. 5, the data of waist girth agreed with the normal distribution. After being tested, all the measurements used in this study were following the normal distribution.

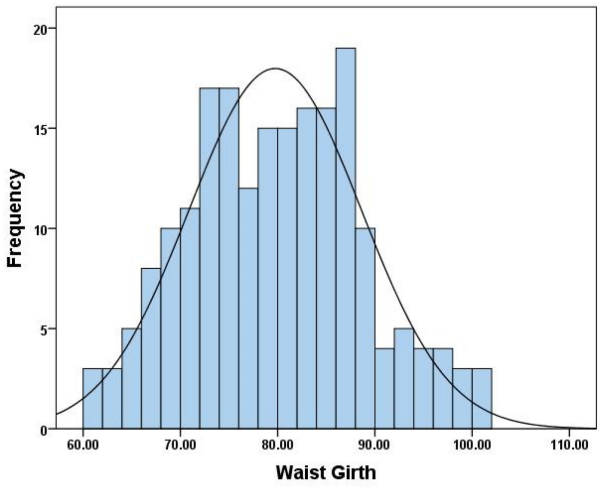

Fig. 5 Histogram of waist girth

3.3 Preparation for garment size assignment

3.3.1 Key body dimension identification

Key body dimension (KBD) denotes the essential dimensions influencing the garment fit [13]. Since the hierarchical clustering algorithm has the advantages of ease of handling any attributes type and interpreting the consequence, we applied it to identify the KBD in this study. The dendrogram (see Fig. 6)

presented the clustering results and order for each anthropometric measurements. All of dimensions could be split into three blocks. Stature, waist girth, and hip girth were the first dimension clustered in each block. Therefore, they were selected for the KBD in this study.

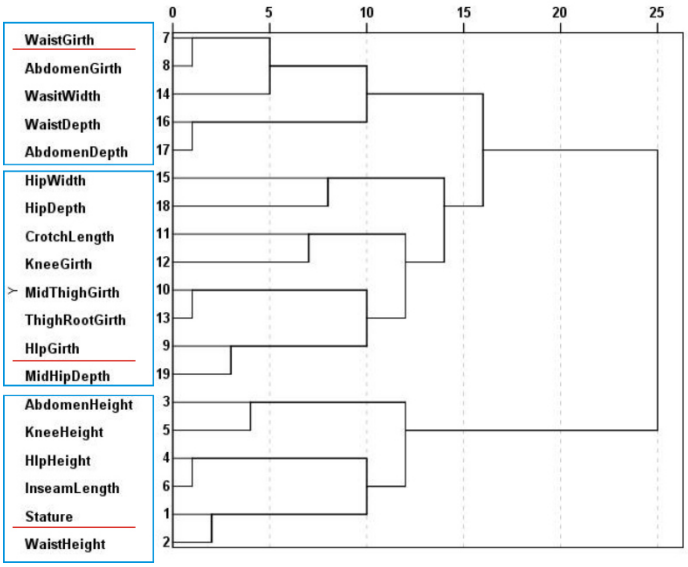

Fig. 6 Dendrogram of hierarchical clustering

3.3.2 Intervals setting

Considering the specific target population, characterized by its region, age, and gender, and the required garment represented, represented by its style and type, the standard sizing systems for garments - Men (GB/T 1335.1-2008) in China was taken into account. According to this sizing system, the intervals for the statue, waist girth, and hip girth were set to 5 cm, 2 cm, and 1.6 cm, respectively.

3.3.3 Fit models determination

Fit models refer to the basic sizes, which are selected by the companies to cover their whole target market [11]. According to the range and the intervals of KBD, we determined the fit models by the sequential steps:

1) Setting the grade of each KBD

Stature: 155, 160, 165, 170, 175, 180, and 185;

Waist girth: 62, 64, 66, 68, 70, 72, 74, 76, 78, 80, 82, 84, 86, 88, 90, 92, 94, 96, 98, 100, and 102;

Hip girth: 77.2, 78.8, 80.4, 82, 83.6, 85.2, 86.8, 88.4, 90, 91.6, 93.2, 94.8, 96.4, 98, 99.6, 101.2, 102.8, 104.4, and 106.

2) Assigning the fit models

Since there were 7, 21, and 19 grades in the stature, waist girth, and hip girth, respectively, 2793 fit models were determined in total.

3.4 Garment size assignment

In this section, we assigned the garment sizes in the light of approaching principle, *K*-Means clustering, and support vector machine method, respectively.

3.4.1 Application of approaching principle

The enumeration algorithm was introduced to calculate the distances between the target population and fit models. Moreover, the distance was computed by the formula (1). For each instance, the closest fit model filtered out according to the distances was chosen as the optimal garment size. In this phase, we arranged 159 sizes for the target population.

$$D_{ij}^{Euclidean} = \left\| p_i - f_j^{model} \right\|, i = 1,2,\cdots,200, j = 1,2,\cdots,2793 \quad (1)$$

3.4.2 Application of K-means clustering

Before clustering, the initial centroids should be determined. We set the initial centroids following the distribution of key body dimensions in the standard sizing system. For instance, in the standard sizing system GB/T 1335-2009, if the statue equals to 155 cm, the range of waist girth (WG) is from 62 cm to 74 cm. Since the interval of WG is 2 cm, there are six grades for WG except for 68 cm. For hip girth (HG), the range is set in [77.2, 85.2], and the interval is 1.6 cm. It could be inferred that there are six grades for HG. Consequentially, there exist 36 sizes for the statue of 155 cm. For other grades of stature, the number of sizes was computed through the same process. In total, we chose 669 sizes as the initial centroids. Afterward, the target population was classified using *K*-means clustering with the fixed initial centroids. Finally, 112 sizes were assigned.

3.4.3 Application of support vector machine

Based on the result of section 3.4.2, we classified the garment sizes by the support vector machine (SVM). The parameters of penalty factor *C* and spread factor *q* have a significant impact on the performance of SVM for class. We searched the optimal combination of *C* and *q* using the grim search technique. Finally, we employed 48 sizes, when the parameters of *C* and *q* equaled to 4.351 and 0.023.

4 Results

4.1.1 Indexes for evaluating the effects of size assignment

(1) The aggregate loss of fit

The aggregate loss of fit stands for the averaged distance between the body dimensions of instances and dimensions of the selected garment size, calculated by the formula (2), which has been considered as a general criterion for evaluating the sizing selection [14]. Hence, the aggregate loss was employed in this work. A lower aggregate loss indicates that the shorter distance between the body and the selected size, in which case the garment is considered to have better fit. An optimal solution for garment size selection would have the lowest value of aggregate loss.

$$D_{ave} = \frac{\sum \|d_i - c_i\|}{n} \quad (2)$$

where: d_i represents the body dimensions of the instance, c_i stands for the dimensions of the selected garment size; *n* refers to the number of instances.

(2) Number of poor fit and the accommodation rate of ideal fit

The ideal aggregate loss was about 3.58 cm presented by Gupta [13]. Based on this criterion, the case, in which the distance between the body and the selected size exceeded 3.58 was regarded to have a poor fit. Otherwise, the case, in which the distance did not exceed 3.58 was viewed as the one, which has an ideal fit. The accommodation rate of the ideal fit was calculated by the formula (3).

$$R_{Acc} = \frac{n_{ideal}}{N} \quad (3)$$

where: n_{ideal} represents the number of individuals with the ideal fit; N refers to the total amount of the individuals.

4.1.2 Evaluation of apparel size assignment

Table 2 demonstrates the results of apparel size assignment based on the approaching principle, *K*-means clustering, and support vector machine, respectively. Among the three methods, the aggregate loss of fit and the poor fit number of the solution using approaching principle was the lowest, while the accommodate rate of ideal fit was the highest reaching 100%. All of these indicated that the method using approaching principle could reach the optimal garment fit comprehensively. However, this method required the largest

number of garment sizes, meaning that the cost of the method was the highest. From the aggregate loss of fit and accommodation rate of ideal fit, SVM was inferior to approaching principle slightly. Nevertheless, SVM only employed approximately one-third of the sizes used by the approaching principle to obtain the accommodate rate up to 82%. Therefore, it could draw to the conclusion that the method based on SVM was the optimal solution for the garment size assignment, compromising the comprehensive garment fit and cost.

Table 2. Performance comparison of apparel size assignment using different approaches.

Methods	**Aggregate loss of fit [cm]**	**Accommodation rate of ideal fit [%]**	**Number of poor fit**	**Number of size employed**
Approaching principle	1.58	100	0	159
K-means clustering	4.08	56	88	112
Support vector machine	3.07	82	32	48

5 Conclusions

In this study, solutions for the apparel size assignment toward the mass customization have been discussed and probed based on differing data mining techniques, involving approaching principle, *K*-means, and support vector machine (SVM). The solutions were assessed by the same case of men's pants in China with 200 adult males. Before assigning the garment size, key body dimensions (KBD) were determined using the hierarchical clustering algorithm as well as the distribution features of the KBD, after anthropometric data acquisition and preprocessing. Hereafter, the fit models were identified under the standard sizing system. Two thousand seven hundred ninety-three fit models were determined concerning the standard sizing system initially. Afterward, the garment sizes of the target population were assigned using the approaching principle, *K*-means, and SVM methods, respectively. And then, the solutions were evaluated by the aggregate loss of fit, the number of poor fit, accommodation rate of ideal fit, and the number of garment size employed. Ultimately, the solution based on SVM was justified as the optimal one, which could cover more populations with fewer sizes compared with another solutions. The SVM-based solution for garment sizes has the merits as follows: (1) a low-cost solution for the size assignment by exploiting the potentials of existing sizing system, without creating new sizing systems; (2) Easy of understanding and handling by the operators in the company, based on their existing experience and expertise; (3) Flexible feasibility to other types of garments. Besides, the solution proposed could be improved and extended in the future. For the customers, a sizing selection approach can be developed to support their buying decisions. For the enterprises, a garment pattern recommendation system can be put forth to promote the accuracy and efficiency of patternmaking in the context of MC. Indeed, as the advent of the big data era, it is significant to apply artificial intelligence techniques to improve the accuracy and efficiency due to the complicated relationship between human body types and size combinations in the future work.

Acknowledgements

The authors wish to acknowledge the financial support of the Special Excellent Ph.D. International Visit Program of DHU, the Fundamental Research Funds for the Central Universities (CUSF-DH-D-2020091), the Key Research Project of Humanities and Social Sciences in Anhui Province College (No. SK2016A0116 and SK2017A0119), the Open Project Program of Anhui Province College Key Laboratory of Textile Fabrics, Anhui Engineering and Technology Research Center of Textile, the Social Science Planning Project in Anhui (No. AHSKQ2019D085), and the National Key Research and Development Program of China (No. 2019YFF0302100).

References

[1] Kilinc-Balci F.S. 4 - How consumers perceive comfort in apparel. In Improving Comfort in Clothing; G. Song, Editor; Woodhead Publishing: Oxford, Great Britain, 2011; pp. 97-113.

[2] Tangchaiburana, S.; KW. Techametheekul. Development model of web design element for clothing e-commerce based on the concept of mass customization. *KJSS*, 2017, 38(3), pp. 242-250. DOI:10.1016/j.kjss.2016.07.007

[3] Jost, P.-J.; T. Süsser. Company-customer interaction in mass customization. *IJPE*, 2020, 220: pp. 107454. DOI:10.1016/j.ijpe.2019.07.027.

[4] Song, X.; L. Tang. Customization-Massing-New Angle of View to Implement C2B Development in China. AJIBM, 2017, 7(6): pp. 735-740. DOI: 10.4236/ajibm.2017.76052.

[5] Salusso-Deonier, C.J., et al., A Multivariate Method of Classif in Bod Form Variation for Sizing Women's Apparel. CTRJ, 1985, 4(1): pp. 38-45. DOI: 10.1177/0887302X8500400106.

[6] Hsu, C.-H.; M.-J.J. Wang. Using decision tree-based data mining to establish a sizing system for the manufacture of garments. IJAM, 2005. 26(5): pp. 669-674. DOI: 10.1007/s00170-003-2032-0.

[7] Zheng, R.; W. Yu; J. Fan. Development of a new chinese bra sizing system based on breast anthropometric measurements. IJIE, 2007, 37(8): pp. 697-705. DOI: 10.1016/j.ergon.2007.05.008.

[8] Hsu, C.-H., Developing Accurate Industrial Standards to Facilitate Production in Apparel Manufacturing Based on Anthropometric Data. HFM, 2009, 19(3): pp. 199-211. DOI:10.1002/hfm.v19:3.

[9] Bagherzadeh, R.; M. Latifi; A.-R. Faramarzi. Employing a Three-Stage Data Mining Procedure to Develop Sizing System. WASJ, 2010, 8(8): pp. 923-929.

[10] Esfandarani, S. M.; Shahrabi J. Developing a new suit sizing system using data optimization techniques. *IJCST*, 2012, 24(1): pp. 27-35. DOI: 10.1108/09556221211194327.

[11] Vinué, G., et al. Looking for representative fit models for apparel sizing. *DSS*, 2014, 57: pp. 22-33. DOI: 10.1016/j.dss.2013.07.007.

[12] Maimon, O.; L. Rokach, Eds. *Data Mining and Knowledge Discovery Handbook*, 2nd ed. 2010.

[13] Zakaria, N. 4-Body shape analysis and identification of key dimensions for apparel sizing systems, In *Anthropometry, Apparel Sizing and Design*, D. Gupta, N. Zakaria, Editors; Woodhead Publishing: Oxford, Great Britain, 2014; pp. 95-119.

[14] Gupta, D. A statistical model for developing body size charts for garments. *IJCST*, 2004, 16(5): pp. 458-469. DOI: 10.1108/09556220410555641.

COMMUNICATIONS IN
DEVELOPMENT AND ASSEMBLING OF TEXTILE PRODUCTS

4D scanning - The dynamic view on body measurements

Anke Klepser[1,*], Simone Morlock[1]

[1]*Hohenstein Institut fuer Textilinnovation gGmbH, Boennigheim, Germany*
*Corresponding author *E-mail address:* a.klepser@hohenstein.de

INFO

CDAPT, ISSN: 2701-939X
Peer reviewed article
2020, Vol.1, Nr. 1, pp.30-38
DOI:10.25367/cdatp.2020.1.p30-38
Received: 6 May 2020
Accepted: 7 June 2020
Available online: 22 September 2020

Keywords
anthropometry,
4D scanning,
measurements,
photogrammetry,
3D analysis

ABSTRACT

Fitting test in movement are an important issue not only in work and sports wear since garment should not restrict the range of motion. Therefore, dynamic anthropometry is a major research topic. Until now, only static position could be captured. Still, it is not known how body geometry changes in dynamic movement. In IGF project "Mobilityrestrictions" photogrammetry scanner "Little Alice" was investigated regarding 4D. It enables serial recording in seconds. The aim of the research project was beside other to identify differences between static and dynamic body measurements.

Scanner "Little Alice" has never been utilized for body form analysis. Therefore, a basic research was performed. Several parameters were examined by iterative tests before scan procedure was defined. Three work or sport related movements were defined and compared to standard position: Biceps curl, leg flex and squat. The changes in scan surface were investigated by a three-step analysis: body measurements, cross sections and a 3D analysis. Scan procedure was performed by six test subjects German sizes 50 and 58, age group 25 – 55 years.

The results show that photogrammetry can be utilized to investigate body geometry changes due to movement. Body surface deviations have been investigated. Thus, not in all cases there were differences between static and dynamic scans. Yet, body geometry alters. 4D scanning enables comprehensive analysis of body geometry changes due to movement. Body measurement and surface alterations can be visualized and quantified. Scans of motions may be used to validate 3D simulation avatars.

1 Introduction

Dynamic anthropometry became one of the most important research topics in clothing technology in the last years [1,2]. To understand if and how the human body alters while it is moved is the foundation of ergonomic fit of personal protective equipment, work wear, sportswear and other functional garments [3]. In the past the assessment of body measurement alteration was only possible with measurement tape. This was time consuming and could only be realized with great effort [4]. With the development of 3D scanning systems an appropriate analysis was feasible [5]. Though, 3D body scanner technology enables only the capturing of static postures. Therefore, the scan shows the muscular system working to hold the position and not the interaction between agonist and antagonist in dynamic movement. It can be assumed that body proportion differs between dynamic and static status especially when performed by sporty subjects. The technological evolution from 3D to 4D scanning systems enables scanning in motion [6-8].

Garments are still developed on the basis of the anthropometric standard position defined in standards and sizing charts as: standing upright, legs hip wide spread, arms slightly abducted [9,10]. Although, the garment user is only seldom in exact this position. Mostly people are moving during the day. Especially in functional clothing like work or sportswear constant movement is performed. Therefore, it is of importance to analyze the body in motion, to extract significant measurement alterations and transfer the results into the garment development process. Kirk et al. (1966) were the first to develop a method to assess the enlargement and reduction of the body surface in connection with position changes. They applied measurement lines on the knee. Schmid et al. (1981) assumed that seam damages were caused by body geometry changes. Girth alterations at the waist-hip area in standing, sitting and squat posture were investigated by Yu et al. (2000). The research group of Ashdown analyzed dimensional changes on the basis of 3D data for the upper and the lower body half [5,13,14,19]. According to the state-of-the-art approach the modification of the body surface was investigated by static postures. Yet, so far there are just a few studies on measurement alteration due to movement [9,10]. Dynamic anthropometry was successfully applied mostly for the development of high performance sportswear. The goals were reduction of muscle fatigue, increase of physical comfort, reduction of resistance and performance increase [20,21]. Morlock et al. (2018) investigated for the first time body measurement differences between work and sports related positions over an entire size range of men and women [10].

So far, body movement is mostly captured with Motion Capture Technology. Defined landmarks on the body are tracked and transferred in digital data. Goals are e.g. video game design, computer animated movies or biomechanical analyzes in medicine and sports science. The output is an abstract skeleton for the assessment of range of motion. The acquisition of 3D surfaces with motion capturing has been investigated [22-26]. A large amount of markers are attached on the human body and tracked by the systems. In the beginning, 4D technology was utilized in medical research with computer tomography, magnetic resonance imaging and ultrasound. In the past years systems were developed to capture the body surface in a fast and precise way [6,7]. Mostly based on structural light and depth sensor technology. Where a defined pattern is projected on the object and captured by multiple cameras. Using algorithms and measurement principles e.g. triangulation or light section technique the surfaces are calculated. These high performance systems provide up to 180 frames per second in high resolution quality. Yet, they are very expansive and therefore mostly used by research institutes or big companies.

Photogrammetry seems to be a low cost alternative for small and medium enterprises to capture human bodies three- and four-dimensionally. Hereby, pictures are taken with digital reflex cameras from multiple angles. On the base of these picture sets a specific software calculates 3D models. The utilization of digital reflex cameras enables serial captures. Therefore, picture sets of the moving body can be taken. Each set represents one position of the movement. So far, three frames per second can be captured. If it is possible to take pictures of the most significant positions, most movements can be analyzed and body surface alterations identified. Until now, body measurements from scans can only be taken automatically from the so called a-pose. Taking measurements form the 3D-data of the moved body can only be realized interactive. From this point, the reduced data of photogrammetry systems is more of an advantage. Thus, photogrammetry full body scanners, so far not been utilized in this research field, should be investigated in regard of their operational capability in dynamic anthropometry focusing clothing technology

applications. Like all 3D technologies they are only capable of the calculation of objects' surface that is visible to the sensors or cameras. Acquisition settings (area, light, camera set up) as well as the defined movement (reproducibility, feasibility) have a major impact on the visibility of the captured body. Capturing methods need to be developed with the aim to provide valid 3D data on which body surface changes due to movement can be examined.

2 Method

To investigate the operational capability in dynamic anthropometry focusing clothing technology applications 3D photogrammetry full body scanner "Little Alice" from 3Dcopysystems was utilized. The basic configuration is for three-dimensional scanning of human bodies. Objects are captured by 38 digital reflex cameras from multiple angles. Four computers are controlling the process, each one responsible for 9-10 cameras shooting synchronically. Three shots or frames per second can be performed. The pictures are transferred to a main computer on which photogrammetry software RealityCapture is utilized to calculate 3D-models. It is of importance that pictures of the captured object are overlapping. 38 cameras are the minimum amount to create full body scans. The overlapping areas enable automatic alignment of the pictures. The calculated 3D data consist of a solid mesh and texture information. Scanner "Little Alice" has never been utilized for body form analysis. Therefore, a basic research was performed. Six parameters were examined by iterative tests before scan procedure was defined: Shadowing of body areas, maximum of frames to be processed, acquisition area, movement speed, color and pattern of captured objects, data export and size accuracy. The aim of these tests was to generate 3D data with a minimum of shadowing and a maximum of accuracy on the one hand. On the other hand it was important to generate files that could be ease and fast imported in state of the art software of clothing technology research and development. These are programs to postprocess 3D data, to take automatically body measurements and 3D simulation applications.

As stated above, body measurements are undergoing changes while the body moves. To develop garments with optimal ergonomic fit the knowledge of the alterations is crucial. On the foundation of the basic research work in regard of the system's capabilities, three work or sport related movements were defined. The aim was to describe sequences that are typical for many working or sporting situations. In addition, the defined movements should lead to extreme changes in body proportions. The focus was the upper arm and thigh area. Reference to identify body surface alterations was the standard position (relaxed): standing upright, legs hip wide spread, arms slightly abducted. The defined body movements were: Biceps curl, leg flex and squat. All definitions are structured in a starting posture, a motion sequence and an ending posture. The scan procedure was performed by six test subjects in the German sizes 50 and 58, age group 25 – 55 years. Every participant wore tight fitting underwear. Anthropometric landmarks were highlighted by polystyrene balls of 2cm diameter. The definition of the landmarks was performed according to Morlock et al. (2018) [10]. The following measurements were taken: body height, chest girth, waist girth, hip girth, across back, arm length, upper arm length, leg length, upper arm girth, thigh girth, knee girth and calf girth.

The changes in scan surface were investigated by a three-step analysis: body measurements, cross sections and a 3D analysis. Body measurements were taken from standard position and from the relevant position of de 4D scans. Software AnthroScan was utilized to take measurements automatically according to ISO 8559. To understand and quantify the difference in arm and leg length due to movement, the measurement definitions had to be adapted in those case. Arm length was taken from mid armfold to wrist. Leg length was taken from crotch height over knee to the floor. In a second step, cross sections of the upper arm and the thigh were taken in 1cm distances. The assessment of the cross sections was performed in software Geomagic studio 2012 (curve generation) and Rhinoceros 6 (measurement). The value of each measurement position of upper arm and thigh at each scan was collected, respectively. Differences were identified and described. The last step were 3D analyzes utilizing Geomagic studio 2012. Scans of the standard position and the ending posture were postprocessed to generate smooth wraps. The full body scans were segmented and the right upper arm and the right thigh of the standard and the defined 4D posture were extracted. Then, segments were merged and a 3D analysis describing the differences in geometry was performed. The results are so called heat maps that visualize the distance

between the reference and the compared segment. With this method the interaction between agonist and antagonist (e.g. biceps and triceps) and the geometry alterations can be illustrated.

3 Results

The results of the basic research in regard of the operational capability showed that the scanner system “Little Alice” can be utilized for 3D and 4D scanning processes. Measurement and geometric differences between the scanned movement positions could be examined. In the first section of this chapter the results of the general assessment of the system are presented. In the second section the findings of the three-step analysis are shown.

With iterative tests the quality factors shadowing of body areas, maximum of frames to be processed, acquisition area, movement speed, color and pattern of captured objects, data export and size accuracy were assessed. As the 38 cameras stand for the minimum set up some quality reductions must be accepted. Areas between arms and torso or between legs at the crotch area demonstrate shadowing similar to other scanner systems. Yet, the multiple angels of the cameras reduce enable good capturing of most areas of the body. And the shadowing compared to full body scanners like e.g. laser scanners is significantly less in positions divergent to the standard posture. The vertical setting with the horizontal laser line of these systems lead to less data on horizontal body parts and obviously larger shadowing between limps and torso especially when arms or legs are positioned between column and torso.

The maximum amount of frames to take in a row was seven. Capturing more frame sets overstrained the computer system and pictures got mixed up on the transfer to the main computer. Therefore, movements have to be performed within three seconds. The acquisition area is determined by the systems structure. The base plate is ellipse shaped with a width of 230cm and a depth of 168cm. The case is in an egg form with dimensions of 330 x 320 x 260 cm (length, width, height). The maximum area to capture objects measures 75 x 75cm. The movement speed was no critical point for clothing technology applications. Fig. 1 shows jumping tests to investigate motion speed acceptance which underline the finding.

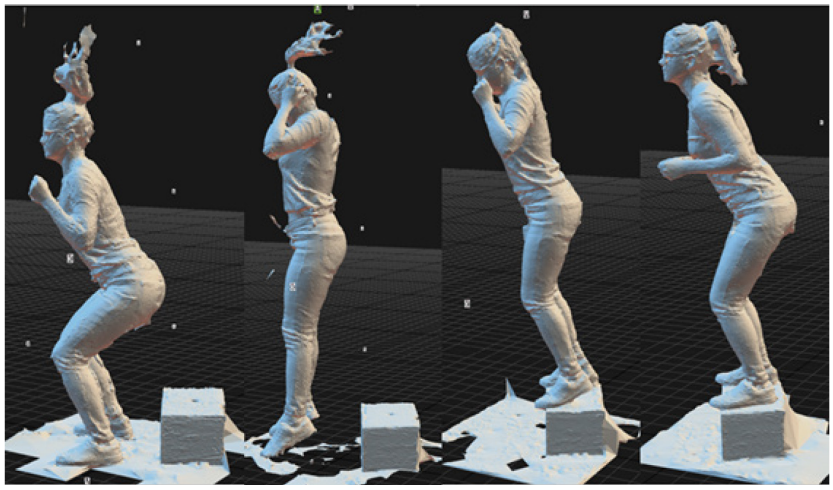

Fig. 1 Investigation motion speed acceptance.

To achieve optimal scan data quality the photogrammetry system can be supported by surfaces with pattern. Test showed that single-colored garment lead to decrease of geometry precision. Skin could be captured well, there was no difference in color. In a next step, the data export was examined. The mesh can be exported in different qualities in regard of resolution. Yet, quality affects file sizes and this has an impact on import and calculating times. Therefore, scans in three resolutions five million triangles, two million triangles and 500,000 triangles were exported in four different data formats (obj, ply, xyz and dxf). All were imported in standard utilized 3D postprocessing and 3D simulation software (Antroscan, Geomagic Studio, Rhinocerus, CLO 3D and Browzwear). Import time, usability and visualization was assessed and rated from 1 to 4, were 1 stands for very good and 4 for insufficient. It was shown, that obj-files provided the highest flexibility to be imported in other programs. In the lowest resolution (500,000 triangles) all the tested software were able to calculate and process the data.

The last step of the basic investigation was the assessment of size accuracy. Since, the 3D / 4D data is generated to analyze body measurements and surface alterations this was the essential test. Three tailor dummies in the German sizes 50, 54 and 58 (bust girth 100, 108 and 116cm) were scanned in Vitus Smart XXL and with “Little Alice”. All scans were measured in Anthroscan. The percentage variance was 1.5cm in all primary measurements (bust girth, waist girth, hip girth and inseam length). This was rated as insufficient for the field of clothing technology. Therefore, the calibration process was optimized with the support of 3D copysystems. Afterwards, the percentage variance was < 0.3cm in the defined measurements.

On the foundation of the basic research work three work or sport related movements were defined with a starting posture, sequence and ending posture (see Table 1).

Table 1. Defined body movements.

Designation	Starting posture	Sequence	Ending posture
Biceps curl	Legs hip wide spread, arms on shoulder level stretch in front of the body, hand to fists, back of the hand to the floor, extra load with 1kg dumbbells	Elbow flexion up to 90° degree in elbow joint	Legs hip wide spread, arms on shoulder level, 90° degree in elbow joint, back of the hand to front
Leg flex	Legs hip wide spread, arms in 0° position	Right leg lift up to hip and knee flexion of 90° degrees, natural arm movement, right foot is positioned on platform, left foot follows	Legs hip wide spread, arms in 0° position
squat	Legs hip wide spread, arms in 0° position	hip and knee flexion up to of 90° degrees, arms moved stretched on the side	Squat with hip and knee flexion up to of 90° degrees

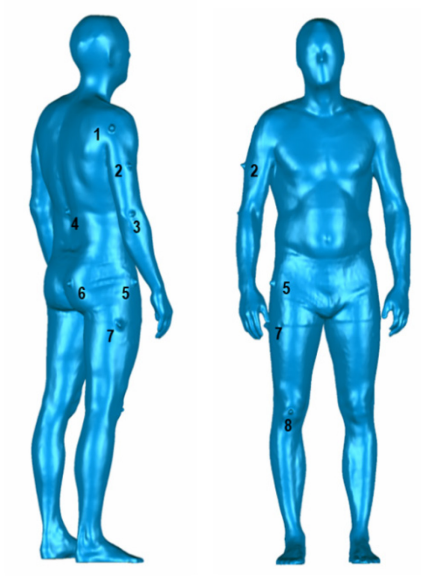

Fig. 2 Defined landmarks on standard position.

To enable valid measurement anthropometric landmarks were highlighted by polystyrene balls of 2cm diameter. Fig. 2 shows the defined landmarks: 1. Mid armfold, 2. Position of largest girth upper arm, 3. Elbow, 4. Waist point at back, 5. Hip height at side, 6. Hip height at back, 7. Crotch height and 8. Mid of knee. Measurements were taken according to ISO 8559 standard: body height, chest girth, waist girth, hip girth, across back, upper arm length, upper arm girth, thigh girth, knee girth and calf girth. Yet, motion postures made adjustment necessary. For example, arm length was taken from mid armfold to wrist. This enables the identification of the maximal length. Leg length was taken in an adjusted method, too. It was

measured not on the side but on the front of the leg, from crotch height over the knee and ankle to floor level.

The changes in scan surface were investigated by a three-step analysis: body measurements, cross sections and a 3D analysis. Therefore, the scans were segmented. The upper arm and the thigh area were cut at the joints (shoulder-elbow; hip-knee). The two upper arm segments and the three thigh segments were merged. The girths at the upper arm were measured from shoulder to elbow in stretched and flexed arm position (see Fig. 3). Girths were positioned in 1cm distance to another. Depending on the upper arm lengths up to 21 measurements were taken. The differences in girth between stretched and flexed arms were investigated. The analysis showed differences between -1.3cm and +2.8cm. The average deviation was 3.61%. To illustrate the measurement differences due to movement the upper arm was segmented in three sections: close to shoulder, middle and close to elbow. The largest differences were identified in the section close to elbow.

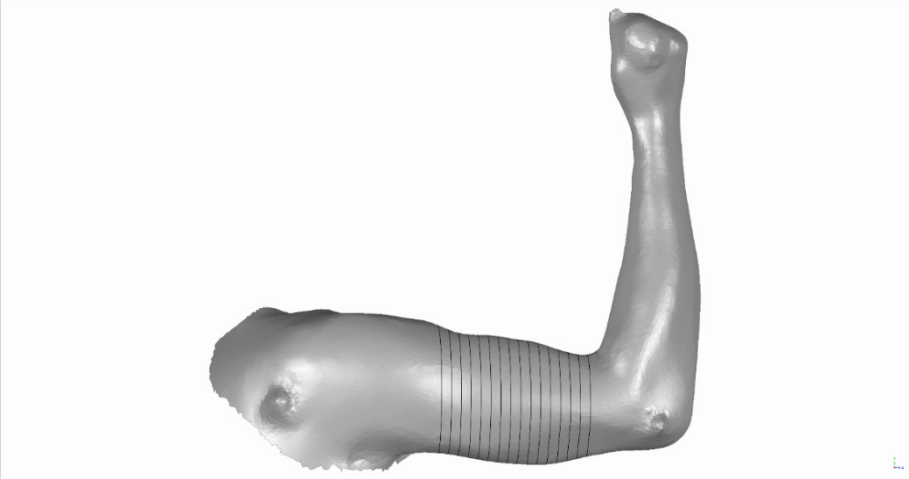

Fig. 3 Flexed arm with measurement positions.

The process to assess the thigh was similar to the upper arm analysis. Girths were measured from positions relaxed, leg flex and squat. For the leg flex movement it was assumed that the major muscle work would happen when the body weight is shifted to the foot on the platform. For the squat movement the end position was chosen. Starting from near crotch girths were positioned 1cm distance from another. Depending on thigh lengths up to 33 measurements were taken. The analysis of the leg flex position showed differences between -4.1cm and +1.8cm. The average deviation was -2.7%. The analysis of the squat position showed differences between -9.5cm and +6.5cm. The average deviation was 0%. The results from the test subjects varied extremely. To illustrate the measurement differences due to movement the thigh was segmented in three sections: close to hip, middle and close to knee. The largest differences were identified in the middle section in both assessed positions.

With the cross sections the middle of the upper arm and the thigh were assessed. The results indicate, that even when the girths show no significant value differences, the body form changes due to movement. Obviously width and depths of the body parts alter (see Fig. 4).

Finally, 3D analysis was performed to investigate the changes in geometry in regard of whole areas (upper arm and thigh). The generated heat maps show reductions in blue and increase in yellow/orange/red. Each color is correlated with a defined distance. The more intense the color the larger is the distance. Fig. 5 displays one result of a 3D analysis of the thigh in size 58 comparing the relaxed with leg flex position. From left to right the pictures show the front, side medial and the back view. There are reductions on the side and an increase of geometry in front and back.

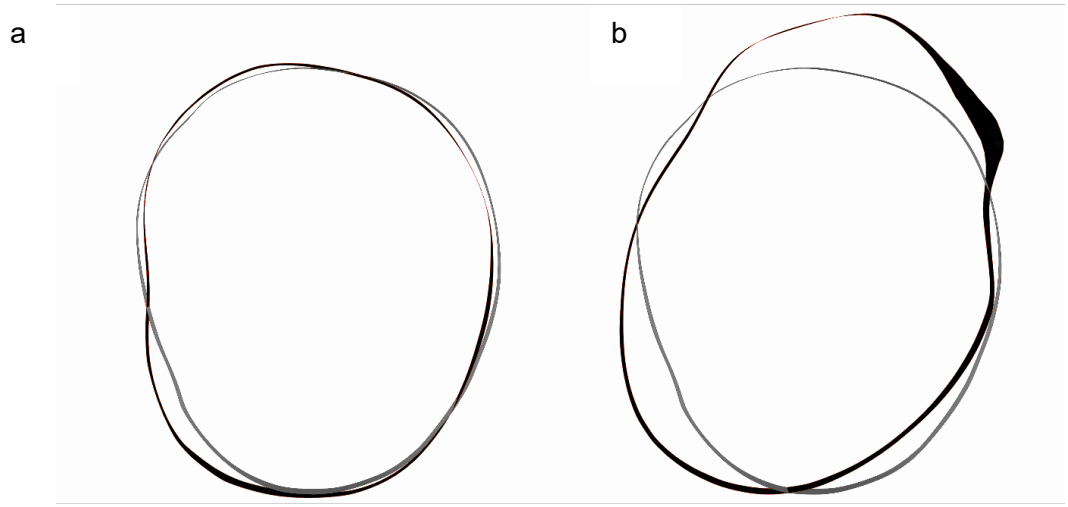

Fig. 4 (a) comparing cross section thigh relaxed (grey) with leg flex position (black); (b) comparing cross section thigh relaxed (grey) with squat position (black).

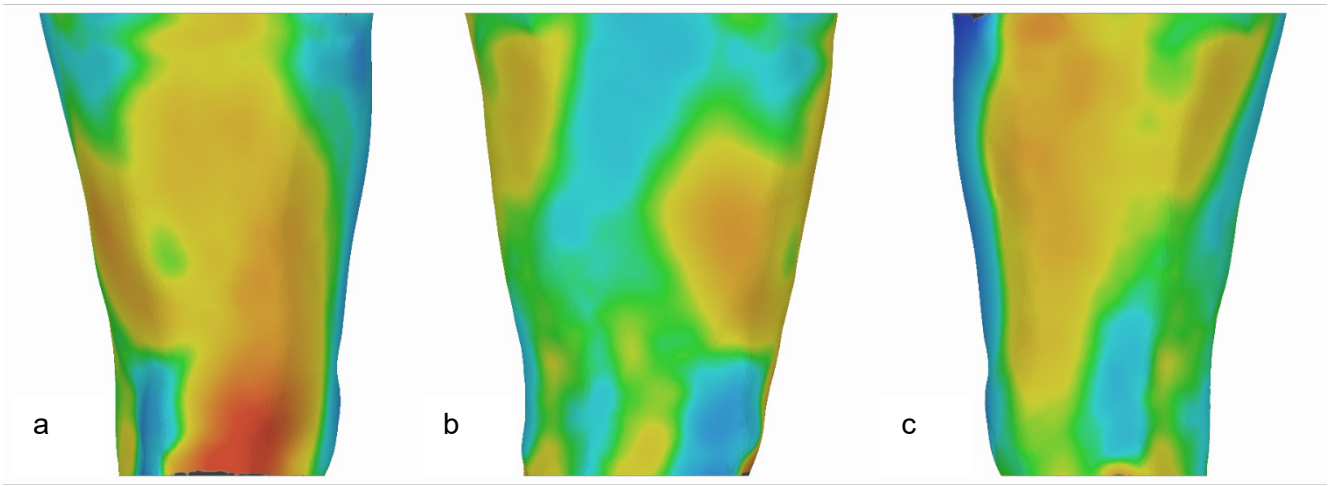

Fig. 5 Heat map comparison thigh relaxed with leg flex positon: (a) front view; (b) side view medial; (c) back view.

4 Conclusion

Garment fit in movement is a crucial for work and sportswear. Therefore, comprehensive dynamic anthropometric data is needed to develop garment with optimal ergonomic fit. To investigate the operational capability focusing clothing technology applications 3D photogrammetry full body scanner “Little Alice” from 3Dcopysystems was utilized to capture movements. A basic research was performed. Six parameters were examined by iterative tests: Shadowing of body areas, maximum of frames to be processed, acquisition area, movement speed, color and pattern of captured objects, data export and size accuracy. The results showed that 3D scan data shows appropriate accuracy to be used to analyze body measurements and geometry changes. Since, the low cost setup with 38 cameras represents the minimum amount to generate scans, limitations in quality were investigated. There was shadowing between arms and torso as well as between legs. Yet, compared to laser scanner systems there was less interference especially in movement. The acquisition area is rather small. Therefore, the range of motion must be considered when movements are defined. Though, three meaningful work and sports related movements were defined to assess body geometry alteration. It was found, that the dumbbell with 1kg was not enough weight to lead to major muscle changes. Therefore, further tests with a larger workload should be performed. This is recommended with special view on the bigger sizes where the muscle form is less obvious due to the subcutaneous fat. The girth alteration at the upper arm in the section close to elbow were unexpected. These results need to be transferred in pattern development and further analyzed. The investigation of changes at thigh area were more difficult. There was shadowing between the legs

especially in squat position. Here, the limitations of the system are more than obvious. Depending on the application it needs to be evaluated if an increase of cameras is reasonable. In addition, it seems of importance to enlarge the test sample and compare different target groups e.g. sporty and non-sporty as well as further sizes.

Acknowledgements

The IGF project 20121 N by the research association Forschungskuratorium Textil e.V., Reinhardtstraße 12-14, 10117 Berlin, was sponsored via the AIF as part of the program to support "Industrial Community Research and Development" (IGF), with funds from the Federal Ministry of Economics and Energy (BMWi) following an Order by the German Federal Parliament.

References

[1] Boorady, M.; Rucker, M.; Haise, C.; Ashdown, S. P. Protective Clothing for Pesticide Applicators: A Multimethod Needs Assessment, *Journal of Textile And Apparel, Technology and Management,* 2009, 6 (2), pp. 1-17.
[2] Bye, E.; Labat, K. L.; Delong, M. R. Analysis of Body Measurement Systems for Apparel, *Clothing and Textiles Research Journal*, 2006, 24 (2), pp. 66-79.
[3] Boorady, L. M. Functional clothing - Principles of fit, *Indian Journal of Fibre & Textile Research,* 2011, 36, pp.344-347.
[4] Schmid, U.; Mecheels, J. Kräfte an Textilien und Nähten der Kleidung in Abhängigkeit von Körperbewegungen und Kleidungsschnitt, *Bekleidung & Wäsche,* 1981, 2, 77-82.
[5] Choi, S.; Ashdown, S. P. 3D body scan analysis of dimensional change in lower body measurements for active body positions, *Textile Research Journal*, 2011, 81(1), pp. 81-93.
[6] Temporal-3dMD Systems (4D). Available online: http://www.3dmd.com/static-3dmd_systems/dynamic-surface-motion-capture-4d/ (accessed on 21.04.2020).
[7] 3D body shape movement. Available online: https://antropometria.ibv.org/en/laboratory/ (accessed on 21.04.2020).
[8] 4D Dynamic Scanner. Available online: https://ps.is.tuebingen.mpg.de/pages/4d-capture (accessed on 21.04.2020).
[9] Ashdown, S. P. Improving body movement comfort in apparel. In *Improving comfort in clothing*, Song, G., Woodhead Publishing, Cambridge, Great Britain, 2011, pp. 278-302.
[10] Morlock, S.; Lörcher, C.; Schenk, A. *Entwicklung eines ergonomisch- und bewegungsorientierten Größensystems für Funktionsmaße zur optimierten Gestaltung von Berufs- und Schutzbekleidung / IGF 18993N*, Hohenstein Institut fuer Textilinnovation gGmbH, Boennigheim, Germany, 2018.
[11] Bougourd, J. P.; Dekker, L. ; Ross, P. G.; Ward, J. P. A Comparison of Women's Sizing by 3D Electronic Scanning and Traditional Anthropometry, *The Journal of The Textile Institute,* 2000, 91(2), pp. 163-173.
[12] Brunsman, M. A.; Daanen, H. M.; Robinette, K. M. Optimal postures and positioning for human body scanning, Proceedings of the International Conference on Recent Advances in 3-D Digital Imaging and Modeling Ottawa, Ontario, Canada, 1997.
[13] Choi, S.-Y.; Ashdown, S. P. Application of Lower Body Girth Change Analysis Using 3D Body Scanning to Pants Patterns, *Journal of the Korean Society of Clothing and Textiles,* 2010, 34(6), pp. 955-968.
[14] Lee, J.; Ashdown, S. P. Upper Body Surface Change Analysis using 3-D Body Scanner, *Journal of Korean Society of Clothing and Textiles*, 2005, 29(12), pp. 1595-1607.
[15] Baytar, F.; Aultman, J.; Han, J. 3D Body Scanning for Examining Active Body Positions: An Exploratory Study for Re-Designing Scrubs, Proceedings of the 3rd International Conference on 3D Body Scanning Technologies, Lugano, Swiss, 2012.
[16] Nam, J.; Barnson, D. H.; Asdown, S. P. et al. Fit Analysis of Liquid Cooled Vest Prototypes Using 3D Body Scanning Technology, *Journal of Textile and Apparel, Technology and Management,* 2005, 4(3), pp. 1-15.
[17] Nawaz, N.; Troynikov, O.; Kennedy, K. Investigation into Fit, Distribution and Size of Air Gaps in Fire-Fighter Jackets to Female Body Form, Proceedings of the 3rd International Conference on 3D Body Scanning Technologies, Lugano, Swiss, 2012.
[18] Morlock, S.; Schenk, A. et al. *3D-basierte Entwicklung eines innovativen Verfahrens zur Passformdiagnose von Bekleidung / IGF 17763N*, Hohenstein Institut für Textilinnovation gGmbH, Boennigheim, 2016.
[19] Choi, J.; Hong, K. 3D skin length deformation of lower body during knee joint flexion for the practical application of functional sportswear, *Applied Ergonomics*, 2015, 48, pp. 186-201.
[20] Gupta, D.; Zakaria, N. *Anthropometry, apparel sizing and design*, Woodhead Publishing Cambridge, Great Britain, 2014.
[21] Ebert, C. Neuentwickelter Stretchindex, *Sport+Mode*, 2015, 2, pp. 63.
[22] Park, S. I.; Hodgins, J. K. Capturing and Animating Skin Deformation in Human Motio, Proceedings of the SIGGRAPH 2006, Bosten, USA, 2006, pp. 881-889.

[23] Aguiar, E. Performance Capture Methods, Proceedings of the European Conference on Computer Vision (ECCV), Zürich, Swiss, 2014.
[24] Wu, C.; Varanasi, K.; Liu, Y. et al. Shading-based Dynamic Shape Refinement from Multi-view Video under General Illumination, Proceedings of the IEEE International Conference on Computer Vision. Barcelona, Spain, 2011.
[25] Rose, B.; Murphy, M. *Mapping wearer mobility for clothing design*, European Publication Server, Cambridge, Great Britain, 2015.
[26] Fit to Deformation. Available online: http://www.drematrix.de/projects/fit-to-deformation/ (accessed on 23.04.2020).

COMMUNICATIONS IN
DEVELOPMENT AND ASSEMBLING OF TEXTILE PRODUCTS

Characterization of the thermophysiological comfort of duvets in consideration of the bed cave

Dr. Bianca-Michaela Wölfling[1]*, Dr. Edith Classen[1], Dr. Anja Gerhardts[1]

[1]*Hohenstein Institut für Textilinnovation GmbH, Bönnigheim, Germany*
*Corresponding author *E-mail address:* b.woelfling@hohenstein.de

INFO

CDAPT, ISSN: 2701-939X
peer reviewed article
2020, Vol.1, Nr. 1, pp. 39-47
DOI:10.25367/cdatp.2020.1.p39-47
Received: 06 May 2020
Accepted: 10 August 2020
Available online: 22 September 2020

Keywords
duvets,
bed cave,
sweating, thermal manikin,
thermophysiological comfort,

ABSTRACT

Sleep is a fundamental need for humans. On average 1/3 of the lifetime is spent in bed. Important for a healthy sleep is the duvet. This should have sufficient heat insulation and should ensure a dry bed climate at the same time. The thermophysiological comfort of classic duvets can be rated via skin model and thermal manikin. The simultaneous detection of dry and moist heat flux of duvets is now not possible.

The lecture presents results of the German funded project AiF 19522 N "Bed Cave and Comfort". Within the project the interaction of thermophysiological comfort during sleeping and the bed cave was investigated. Duvets with different filling materials (down and feathers, polyester, animal hair as well as new developments) were examined according the classical, thermophysiological evaluation method for sleep comfort. Furthermore, a new evaluation method for duvets with the sweating, thermal manikin Sherlock (Newton type, Thermetrics) was developed. During the measurement, a realistic sleep situation can be reconstructed with the sweating, thermal manikin. All measured data were validated by monitored sleep test within a climatic chamber.

1 Introduction

Sleep is a fundamental an underestimated basic need of humans. On average 1/3 of the lifetime is spent in bed. After 48 hours without sleep the concentration for simplest tasks is lost [1]. Restful sleep is very important for human regeneration and health maintenance [2].

During sleep a comfortable warm bed climate, night movements and a lowering of body temperature of 0.5 °C with subsequent rise should be possible. Therefore, produced body heat is dissipated by the skin by radiation, conduction, and convection. Further sweating can occur to cool down the human body. To avoid moisture in the bed system sweat should be transported through the system during sleep [1]. Studies show that about one fifth of the produced heat and moisture produced during sleep is released to the mattress. The majority of 80 % is released to the duvet [3]. Other components like mattress, linen or nightwear play a tangential role. So, the duvet should be able to transport the produced sweat to the ambient. Further the human body should not cool down during sleeping. Duvets must therefore have adequate thermal insulation.

Nowadays there are traditional filling of duvets like down and feathers, animal hair (e. g. sheep, camel) and nonwovens. In addition, new filling and insulation materials are used for duvets, e. g. nonwovens made from hemp fibers, microfine fiber structures, 3D knitted fabrics, polyester fiber balls, mixtures of different materials as well as new assemblies like zoned duvets with higher filling levels on the feed zone or open ventilation zones.

In the 1990s a method and model to characterize the comfort of duvets was invented at Hohenstein, which is still used today [4]. This evaluation system is based on two methods: dry heat insulation of ready-made duvets measured with the thermal manikin and the material-specific characteristics of heat and moisture transport determined with the Hohenstein skin model. The measurement of dry and wet heat flow of ready-made duvets in consideration of the bed cave is until now not possible.

Further, the insulation of the duvet depends on the draping of the duvet and the so formed bed cave between human and duvet. This draping ability of the blanket depends on the material, the rigidity, the filling quantity, and the packaging. However, so far there are no scientific studies dealing with the ideal bed cavity for thermal insulation. With the 3D scanner technology, a powerful tool is available, with which a quantitative, exact 3D measurement of the bed cavity and draping of the duvet is possible.

Within a German funded research project AiF 19522 N a new measuring and evaluation method for traditional and new ready-made duvets in consideration of the bed cave was investigated. In addition, the bed cavity geometry is measured using 3D scanner technology and the influence of the bed cave and the enclosed air layer on the thermal insulation and sleeping comfort was researched.

2 Materials and Methods

Within the project more than 40 duvets with different cover materials and fillings e. g. polyester (PES), down and feathers, wool (WO), camel hair, cotton (CO) were investigated. Screening tests showed that 18 duvets represent state of the art of German duvets. These duvets were used for further investigation. Table 1 shows these duvets with the available product information.

Table 1. Duvet materials.

Sample	Cover material	Filling	Stitching	Size [m²]	Weight [kg]	Thickness [mm]
M3	100% CO	100% PES	lengthwise	2,91	1,282	28
M4	100% CO	100% PES	lengthwise	2,68	1,662	51
M5	100% CO	90% down, 10% feather	square	2,75	1,176	22/13
M6	100% CO	100% down	lengthwise	2,77	1,774	25/14
M7	-	100% down	square	2,90	1,746	19/14
M8	100% Lyocell	60% Lyocell, 40% PES	square	2,77	1,894	41/24
M11	50% CO, 50% Lyocell	100% PES-hollow fiber	dots	2,73	1,775	53/40
M12	100% PES	100% PES-hollow fiber	flower shaped	2,75	0,804	15
M13	100% CO	100% Polylactide	body fit	2,80	1,855	42/26
M14	100% CO	100% PES	body fit	2,82	1,315	29/20
M17	100% CO	100% PES-nonwoven	lengthwise	2,63	1,197	21/14
M18	100% CO	100% PES	lengthwise	2,7	1,286	19/14
M20	-	100% WO	lengthwise	2,68	1,843	27/25
M21	100% CO	100% WO	square	2,68	1,288	15/9
M25	80% micromodal, 20% CO	100% camel hair	body fit	2,74	1,982	42
M28	100% CO	60% linen, 40% CO	lengthwise with circles	2,90	1,142	9/8
M29	70% micromodal, 30% CO	100% PES	Beads stitching with ventilation system	2,76	1,715	41/36
M32	100% CO, climate zone: 100% PES	100% down	cross with air chambers	2,91	1,121	-

2.1 Sweating, thermal manikin

The Hohenstein evaluation system for duvets is based on two methods: dry heat insulation of ready-made duvets measured with the thermal manikin and the material-specific characteristics of heat and moisture transport determined with the Hohenstein skin model. The measurement of dry and wet heat flow of ready-made duvets in consideration of the bed cave is until now not possible. Therefore, a new method was invented to characterize the thermophysiological comfort of duvets in consideration of surface coverage, snugness and the microclimate within the bed cave using the sweating, thermal manikin Sherlock (type Newton, Thermetrics).

The sweating, thermal manikin Sherlock has the anatomical shape of a human standard man (height 1.75 m, body surface 1.85 m², clothing size 50). The skin surface of the manikin was regulated to a constant temperature T_s of 31 ° C. The required electrical heating power H_c for the constant surface temperature was the measured value, for the determination of the thermal resistance R_c of duvets. The measurement was set in a climate chamber at temperature of T_a = 15 ° C and relative humidity of RH_a = 50% rh.

To create a realistic sleeping condition, the measurement took place with the sweating, thermal manikin Sherlock lying down, wearing a two-piece pajamas (CO). The head rest on a pillow. The duvet itself was measured without a cover. To record the microclimate of the bed cave, ten additional temperature and humidity sensors were attached to the sweating, thermal Manikin Sherlock, and the duvet (figure 1, middle). The duvet was draped uniformly around the manikin, which was covered up to the neck. Care was taken to ensure that the duvet lies loosely so that there is enough air volume in the bed cave". A standard bed construction consisting of a tubular steel bed frame with a one-piece foam mattress (180

mm thick), which is covered with a cotton sheet, was chosen for the investigation. Figure 1 shows the measurement setup for evaluating duvets with the sweating, thermal Manikin Sherlock.

Fig. 1 Measurement setup to characterize the thermophysiological parameters of duvets with the sweating, thermal manikin Sherlock (type Newton, Thermetrics); left: dressed Sherlock equipped with temperature and humidity sensors lying on mattress and bed frame, right: complete measurement setup.

In addition to these investigations of the thermal resistance R_c, realistic sweating during sleep was simulated with Sherlock to determine the water vapor resistance R_e of duvets. The same measurement setup was used for this. Sweating is achieved with the help of a tight sweat suit and sweat nozzles, which are distributed over the body. The sweat suit has the function of distributing the sweat (water) from the sweat nozzles evenly over the body. The sweat nozzles can be controlled individually, so different sweating rates can be set. Table 2 shows the used sweating rate, which are based on Park et al. [5]. The sweating nozzles on the back side were switched off because the measurements focus on the duvet and the microclimate within the bed cave. These sweating rates reproduce a realistic sleeping situation and leads to reproducible measurement results for duvets.

Table 2. Sweating rates during measurement of duvets with the sweating, thermal manikin Sherlock (type Newton, Thermetrics).

Manikin zone	**Sweating rate [ml/hr m²]**	**Manikin zone**	**Sweating rate [ml/hr m²]**
face	0	lower back	0
head	0	right upper thigh front	15
right upper arm front	58	right upper thigh guard	0
right upper arm back	0	right upper thigh back	0
left upper arm front	58	left upper thigh front	15
left upper arm back	0	left upper thigh guard	0
right forearm front	18	left upper thigh back	0
right forearm back	10	right lower thigh front	18
left forearm front	18	right lower thigh back	0
left forearm back	10	left lower thigh front	18
right hand	72	left lower thigh back	0
left hand	72	right calf front	17
upper chest	16	right calf back	0
shoulders	0	left calf front	17
stomach	17	left calf back	0
mid back	0	right foot	65
waist	15	left foot	65

2.2 Subject trial

To validate the results with the thermal, sweating manikin subject trials with selected duvets M5, M14 and M32 were done. Five male subjects (table 2) performed monitored sleep experiments in the climate chamber. The subjects were healthy men. Before the study, the participating subjects were given detailed information about the schedule of the test series after a medical check, were informed about possible risks, gave their consent to the tests, and confirmed their voluntary participation.

Table 3. Sample of subjects.

Subject	Age [years]	Height [cm]	Weight [kg]	BMI [ ]	Body Surface DuBois [cm²]
TP1	28	184	79	23	2,02
TP2	33	186	82	24	2,06
TP3	30	172	65	22	1,77
TP4	24	170	73	25	1,84
TP5	29	182	81	24	2,02
MW	28,8	178,8	76	23,6	1,94
Stdev	3,2	7,3	7,1	1,1	0,1

The monitored sleeping experiments were performed at 20 °C, 50% RH in a climatic chamber with air movement 0.3 m / s. To create comparable conditions to the experiments with the sweating, thermal manikin Sherlock the subjects slept in the climatic chamber for at least 6 hours, wearing a pair of cotton underpants and a two-piece pajama out of cotton. The head rested on a pillow. The duvet itself was tested without a cover, using five temperature and humidity sensors to record the microclimate of the bed cave. The test bed was draped loosely by the test subjects, so that they formed a “sleeping cave”. A "standard bed construction" was chosen for the present study. It consists of a tubular steel bed frame with a one-piece foam mattress (180 mm thick), which is covered with a cotton sheet. Figure 2 shows the experimental test setup during the monitored sleeping experiment with subjects.

Fig. 2 Measurement setup “Sleeping trial” in climatic chamber with subject (left), position of temperature and humidity sensors (right, duvet turned for visualization).

The objective body data were recorded using various sensors. The heart rate was recorded using a chest strap (Polar WearLink). Temperature sensors (T) for the skin temperature as well as combined temperature-humidity sensors (T, RH; MSR Electronics GmbH) for recording the microclimate were distributed on the body surface in accordance with ISO 9886. To create a distance to the skin and thus to record the moisture in the microclimate between textile and skin, the sensor was attached to a spacer (thickness 3 mm). In addition to the objectively recorded measured values, the subject's subjective sensations after the sleep were queried and recorded using a questionnaire.

Before sleeping experiments, the test subjects were equipped with the sensors and get dressed. This process took at least 30 minutes to also acclimatize the subjects. The individual experiments each lasted at least 6 hours, during which the test subjects slept in a bed under the respective duvet.

Furthermore, the change in weight of the test subjects and the sweat absorption of the individual items of clothing and the duvet were determined by weighing before and after the sleep experiment. For this purpose, the test subjects and the clothing were weighed before and after the experiment.

3 Results and Discussion

3.1 Sweating, thermal manikin

The investigations with the sweating, thermal manikin Sherlock indicate that it is possible to determine the thermal resistance R_c and water vapor permeability R_e of duvets. Table 4 shows the results of these characterizations. Regarding the thermal resistance R_c the values are in the rage 0.56 – 1.00 m²K/W. M28 shows the lowest thermal resistance with 0.56 m²K/W (table 4). Therefore, this duvet is less insulating and should be used as summer duvet. Duvets M5, M8, M17, M18, M20 and M32 have R_c-values in the middle range between 0.61 – 0.72 m²K/W. The residual duvets M3, M4, M6, M7, M11, M12, M13, M14, M21, M25, M29 show high thermal resistance values in the range 0.75 – 1.00 m²K/W (table 4). So, the thermal insulation of these duvets can be rated as high and they should be used in winter when the ambient temperature in bedrooms is low.

Table 4. Thermal resistance R_c and water vapor resistance R_e of different duvets measured with sweating, thermal manikin Sherlock.

Sample	Thermal resistance R_c [m²K/W]	Water vapor resistance R_e [m²Pa/W]
M3	0.77	98.78
M4	0.76	82.93
M5	0.61	64.86
M6	0.96	104.84
M7	1.00	102.54
M8	0.72	73.98
M11	0.87	100.09
M12	-	54.09
M13	0.77	83.13
M14	0.75	73.33
M17	0.65	66.85
M18	0.69	68.23
M20	0.71	84.74
M21	-	61.54
M25	0.95	92.48
M28	0.56	51.89
M29	0.87	84.69
M32	0.62	60.15

The results of water vapor resistance R_e are in the range 51.89 – 104.84 m²Pa/W. Especially duvet M28 and M12 has low R_e-values, which means these duvets have a good breathability and during sleep produced sweat can be transported through the duvet to the ambient. The highest water vapor permeabilities have the duvets M6 and M7 with values in the range 102.54 – 104.84 m²Pa/W. This can be explained, among other things, by the high thickness of the duvet. The by human produced sweat (water vapor) must pass through more material before it can be released into the ambient. The results show no correlation between the R_e-value and the filling or stitching design of the duvets.

In addition, the microclimate in the bed cave was determined during the measurements of the water vapor resistance by ten temperature and humidity sensors. Figure 4 shows the average temperature (orange, left) and relative humidity (blue, right) in the bed cave during the measurements of the water vapor resistance R_e using the sweating, thermal manikin Sherlock. There are slight differences in the microclimate of the bed cave for different duvets. The temperature is between 25.67 - 28.89 °C. The lowest temperatures in the bed cave were achieved for duvet M3 and M28, for duvets M11, 21 the highest. In the case of relative humidity in the bed cave, the values are in the range of 54.43 - 67.43% RH. From a clothing physiological point of view, the relative humidity should be below 60% RH, because at higher relative humidity's no differentiation can be made by humans and it is sensed as unpleasant wet. The duvets M14

and M28 have the lowest relative humidity in the bed cave during the determination of the water vapor resistance. The duvets M7 and M11 the highest relative air humidity in the bed cave.

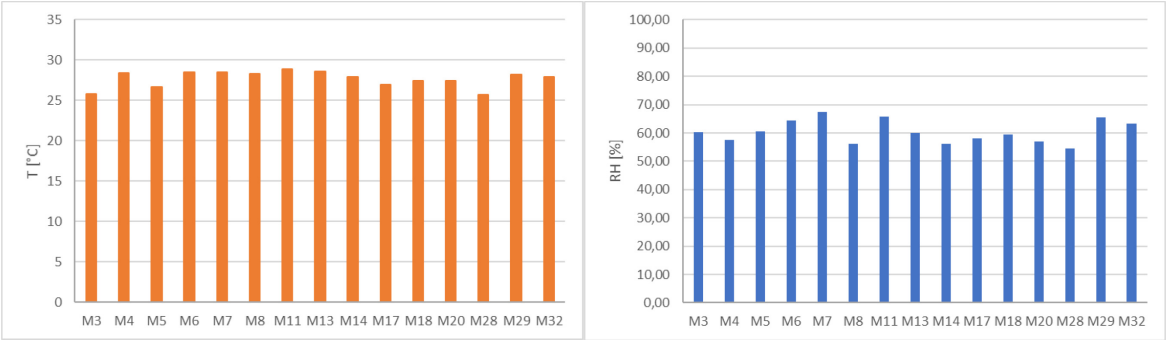

Fig. 4 Temperature T (left) and relative humidity RH (right) in the bed cave during the measurements of the water vapor resistance R_e using sweating, thermal manikin Sherlock

There are no apparent correlations between water vapor resistance R_e measured with the sweating, thermal Manikin Sherlock and the climate in the bed cave.

3.2 Subject Trial

During the monitored sleeping experiments the test subjects produced a small amount of sweat between 275 g and 490 g (table 5). Most of the produced sweat P evaporates, i.e. 95.54% (M32) - 97.27% (M14) (ratio evaporated sweat E/produced sweat P) were transported through the duvet and released into the environment. In the duvets themselves, 1.31 g (M5), 1.62 g (M14) and 3.91 g (M32) remain over the entire monitored sleeping experiment (table 5). This means that only very small amounts of sweat remain in the duvets. The results show clearly that while sleeping under the duvet M32, which has climatic zones, the subjects produces less sweat. Simultaneous duvet M32 absorbs the highest amount of sweat.

The results of the individual monitored sleeping experiments were evaluated. The data was analyzed subject-specific and product-specific. The mean values across all subjects were calculated. Due to the large number of data, the following results are limited to mean values of the recorded objective data (skin temperature, temperature in the microclimate, humidity in the microclimate) for all duvets on lower back right position.

Table 5. Produced and evaporated sweat amount during subject trial.

Clothing	**Amount of sweat [g]**		
	M5	**M14**	**M32**
Subject	490.00	461.11	275.00
Underpants	1.17	0.89	1.18
Pajama shirt	1.80	4.76	2.44
Pajama trousers	7.59	2.59	1.24
Duvet	1.31	1.62	3.91
Cushion	0.98	2.07	2.23
Bed sheet	0.70	0.68	1.26
Produced Sweat P [g]	490.00	461.11	275.00
Evaporated sweat E [g]	476.46	448.50	262.74
E/P [%]	97.24	97.27	95.54

Figure 5 shows the relative humidity (right) in the microclimate above the skin of the subject on lower back right position. All three duvets M5 (grey curve), M14 (orange curve) and M32 (blue curve) show the same curve progression with minor differences for the individual duvets. Towards the end of the sleep period of six hours, however, trends can be seen. M32 tends to have the lowest moisture in the microclimate above the skin, M14 the highest. This confirms the measurements with the sweating, thermal Manikin Sherlock.

Here M14 has the highest water vapor resistance R_e compared to the duvets M5 and M32. Low water vapor resistance R_e means produced sweat is transported through the duvet to the ambient. In case of higher values this transport is less efficient and the relative humidity in the microclimate above the skin rises.

By comparing the temperature in the microclimate (figure 5, right) above the skin of the subject on lower back right position of the three duvets similar curve progression can be seen, too. This is not surprising considering that these duvets have slightly differences in the thermal resistance R_c (table 4). The measurement fluctuations within curve M14 on the lower back right can be explained by averaging over all subjects. M14 has the highest thermal resistance, which means thermal insulation, of these three samples. It is therefore not surprising that the temperature in the microclimate of the bed cave is higher in the case of M14 than in the other duvets. Duvet M14 has the higher R_e-value compared to M5 and M32, but the relative humidity in the microclimate is almost the same for these three duvets during the subject trail. Furthermore, the subject produced 461.11 g of sweat in case of M14, which is greater than M32 and a little bit lower than M5. That implies that M14 puffers more sweat than M5 and M32.

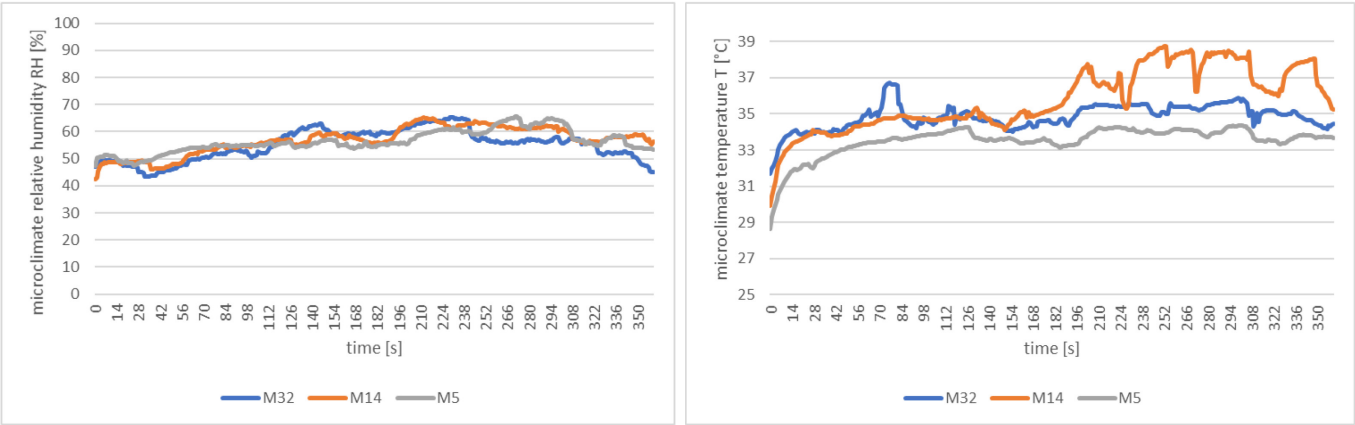

Fig. 5 Relative humidity RH (left) and Temperature T (right) in the microclimate above the skin on lower back right position during monitored sleeping experiment with subjects.

Figure 6 shows the skin temperature on lower back right position during the monitored sleeping experiment. The values show, as before the temperature in the microclimate, that the three duvets slightly differ in their thermal resistance. It can be said that the lowest skin temperatures occur while sleeping under the duvet M32. Compared to M5 and M14, this duvet also has the lowest thermal resistance (Table 4).

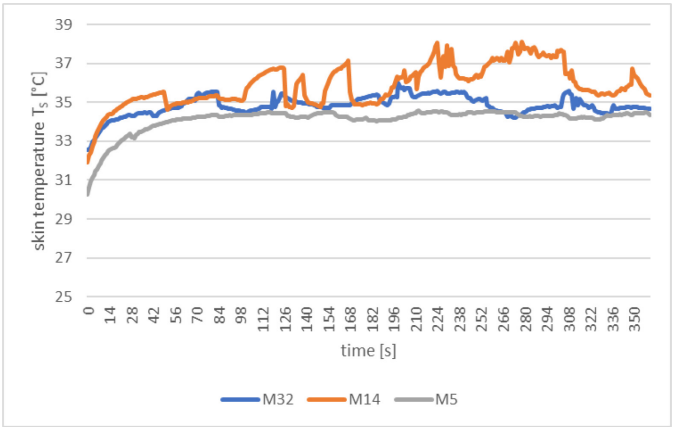

Fig. 6 Skin temperature T_s on lower back right position during monitored sleeping experiment with subjects.

After each individual sleeping experiments, the subjects filled out a detailed standardized questionnaire for the duvets M5, M14 and M32. This questionnaire includes questions about the feeling and comfort of the duvets, as well as the overall comfort. These detailed questions are relevant for the overall

assessment, to be able to classify the thermophysiological properties of duvets and the measurements with the sweating, thermal manikin Sherlock.

The examined duvets differ in terms of their stitching: M5 square, M14 body fit and M32 cross- with air chambers (table 1). The subjects did not notice any of these stitching negatively. They were consistently rated with grade 2 (good).

The evaluation of the temperature shows only slight differences between the samples. Duvets M5 and M32 are classified as comfortable (grade 2, good), M14 as comfortable-warm (grade 2.7, satisfactory) and thus as a little bit warmer and uncomfortable. This reflects the measurement data of the skin temperature on the lower back right (figure 6).

The moisture sensation of the three duvets differ slightly, too. While duvet M5 is described as dry, M14 and M32 is classified as slightly damp. The perception of moisture by the subjects is still described as good (grade 2). In addition, no humidity accumulation is felt in all duvets.

Overall, the thermophysiological comfort of duvet M5 is rated with a grade of 1.7, followed by M32 with 2.2 and M14 with 2.6. This shows clearly that there are only slight differences between the individual perception of these three duvets.

4 Conclusions

Within the German funded IGF research project AiF 19522 N “Bed Cave and Comfort”, a new system for characterizing the thermophysiological comfort of duvets should be developed, which can objectively assess the heat and moisture management of duvets considering the shape and size of the bed cave. For this purpose, a suitable measuring method was developed to characterize the thermal resistance R_c (thermal insulation) and the water vapor resistance R_e (breathability) with the sweating, thermal manikin Sherlock. It became apparent that in manikin measurements by considering the bed cave a higher information content for characterizing the clothing-physiological comfort of duvets is obtained. Based on sleep tests with subjects, these thermophysiological indicators as well as the measurement method for the sweating, thermal manikin Sherlock could be validated. The new measurement method with the sweating, thermal manikin Sherlock is suitable for characterization of the thermophysiological comfort of duvets. Here, classic as well as innovative duvets can be assessed regardless of the filling used, and the construction and manufacture of the duvets. Conventional clothing physiological characterizations with the Hohenstein skin model do not have to be carried out and there is no loss of information in accuracy and significance.

Acknowledgements

IGF project 19522 N was founded through the AiF within the framework of the program for promotion of cooperative industrial research (IGF) by the German Federal Ministry for Economic Affairs and Energy based on a resolution by the German Bundestag.

References

[1] J. Zulley, *Barmer GEK Deutsche Akademie für Gesundheit und Schlaf (DAGS)*, 5. Auflage, Juli 2011
[2] J.A. Hobson, *Sleep.* Scientific American Library, A Division of HPHLP" New York, ISSN 1040-3213, 1989
[3] Caps R & Umbach KH., *Ermittlung der Komfortkriterien bei Körperruhe.* Schlussbericht AiF-Nr. 6419, Bönnigheim, 1988
[4] Umbach KH. *Bewertungssystem für den physiologischen Schlafkomfort von Bettdecken*. Hohensteiner Report (59):41, 2003
[5] Park, S.J. and T. Tamura, Distribution of evaporation rate on human body surface. The Annals of Physiological Anthropology Journal, 1992. Nov, 11(6): p. 593-609

COMMUNICATIONS IN
DEVELOPMENT AND ASSEMBLING OF TEXTILE PRODUCTS

IMPROVEMENT OF THE STRENGTH OF ADHESION BONDS OF TEXTILE PRODUCTS FOR THE IMPROVEMENT OF THE EFFICIENCY OF CRIMINALISTIC SUPPORT OF LAW ENFORCEMENT ACTIVITIES

Maryna Yatsenko[1], Sergey Bereznenko[1], Maria Pawłowa[2], Olena Nenia[3], Nataliia Vashchuk[3]

[1](Kyiv National University of Technologies and Design), Kyiv, Ukraine
[2](Kazimierz Pulaski University of Technology and Humanities in Radom), Radom, Poland
[3](State Research Institute of the Ministry of Internal Affairs of Ukraine), Kyiv, Ukraine
mpawlowa@poczta.onet.pl, bersenik@ukr.net

INFO

CDAPT, peer reviewed article
2020, Vol.1, Nr. 7, Paper 2020-02
DOI:10.25367/cdatp.2020.1.p48-56
Received: 08 May 2020
Accepted: 7 June 2020
Available online: 25 September 2020

ABSTRACT

Analysis of methods of chemical and physical modification and activation in the manufacture of garments made of polymeric materials is carried out. The analysis studied a wide range of possibilities for the use of nanotechnology in the garment industry and can serve as a theoretical basis for the manufacture of garments made of polymeric materials of various purposes, in particular for military and law enforcement agencies. The technology of rendering shape-resistant textiles, including clothing made of genuine leather, by use of the method of chemical modification and activation of its surface, which makes it possible to use more effectively various textile materials, in particular, leather at the cutting stage, is presented.

Keywords
textile materials, garments, genuine leather, bonding, form resistance, adhesion

1 Introduction

The development of the garment industry is nowadays strongly influenced by new technologies. The harsh conditions of the current market economy also place their requirements on textile products. Along with high demand products, the satisfaction of several requirements like strength of the seams is especially important for products used in military and law enforcement activities. Thus, the units of forensic support

of pre-trial investigation bodies of the National Police of Ukraine have an urgent need for modern samples of means of maximum preservation and protection of forensically significant information (including physical evidence) and places of finding such information from negative factors, both subjective and objective ones. Such technical means and tools include mobile tents, awnings and protective screens.

The choice of fabric plays an important role and is a decisive factor for the production of both clothing and special textile products, like in their use as power structures. By this means and a proper choice, the final product may deliver all the necessary protective, functional and operational properties.

Therefore, it goes without saying that such products must be made by materials that meet the highest performance, durability, impermeability, and breathability characteristics.

In this case, a particularly important factor for the quality of textiles are the adhesive joints of materials in their formation.

During operation, garments (including clothing) are exposed to moisture, wet-heat treatment, various deformations, which lead to premature deterioration of the appearance of the garment due to the poor quality of the adhesive bonding materials during molding. Increasement of the adhesive strength of the adhesive joints of garments in bonding with adhesive linings is one of the most important problems of the garment industry [1].

Nowadays there are no high-efficiency processes of bonding of garment parts with adhesive pads, which would allow to control the adhesive interaction and to predict its behavior during garment processing. The need for the development of such processes arises because of the tendency of constant updating of the raw material basis for the manufacture of garments (clothing genuine and artificial leather, textile materials with form resistant, abrasion-proof and other types of processing), which adhesion properties have not been studied. Therefore, the search and development of new methods and techniques for the improvement of the quality and reliability of the adhesive joints of polymeric materials in the formation and molding of parts of garments is an urgent problem.

Almost all textile materials are subject to different types of decoration, which can adversely affect the quality of the adhesive. Due to such surface modifications on the garment fibers, a small, but resistant to further technological operations drug layer is fixed. As a result, the active areas of the fibers are blocked, which adversely affects the quality of the adhesive joints during the bonding of garment parts. Due to this, the effect of very expensive finishing of textile materials (for example, hydrophobization, modification of the properties of textile materials – reducing shrinkage, increasing of the invariability of fabrics in both dry and wet conditions, etc.) should sometimes be partially removed during garment production in order to make it possible to perform necessary operations in the later garment manufacturing stage. [1, 2].

One of the ways to improve the quality of the adhesive joints of garment parts is to apply methods of physical and chemical influence on the tiled surface of textile materials that have undergone various types of finishing. Such methods can be differentiated not only by the types of finishing, but also by the preparations containing the technological solution. The purpose of such processing is to obtain the maximum positive technological effect for the preservation of the consumer properties of the clothing materials provided during the outfit. The same problem arises in the manufacture of genuine leather products, which are also sensitive to the effects of temperature [1, 3, 4].

Nowadays, modern chemicals are used in the garment industry. This include dispersions based on acrylate (athebin BFF) and polyurethane (aquapol-21) which increase shape resistance and reduce the weight of garments made from costume fabrics. The increase in form resistance is due to the formation of hydrogen and covalent bonds between molecules due to the interaction of the active centers of the fibers with the reactive groups (-NH-CO-C- and -CH_2CH (COOR) -) of the chemicals polymers. Appropriate chemical treatment allows to increase the shape resistance of the form by 15–30% (compared to the sample, duplicated adhesive gasket material without additional processing), regardlessof the materials surface density values and the type of used chemical preparation.

Analysis of the literature showed that the following polymer compositions can be used for direct stabilization: aqueous dispersions of various rubbers (chloropropene, butadiene styrene, etc.), dispersion of polyvinyl acetate, or polyvinyl chloride, polyacrylic or polyurethane adhesives, aqueous solutions, aqueous solutions polyethylene, polypropylene, or polyamides [5].

The use of chemicals for fixing the shape of garments has several advantages over traditional bonding [6–8]. It allows combining the processes of formation and fixation of the form as well as fixing the new arrangement of fibers not only by the surface, but also by thickness. This allows to regulatethe properties of the semi-finished products through changes in number, concentration, and parameters of application of the polymer composition.

For example, as a result from the reinforcement of genuine leather with adhesive gaskets, the modulus of elasticity of the samples increases by 20% and is stabilized by the polymer composition from 12 to 32% (depending on the concentration). Elasticity of the bound increases for 10% and when treated with a polymer composition based on polyvinyl acetate, it is reduced for 24% This is due to the compacting of the structure as a result of the introduction of the polymer composition.

Studies have also shown the effectiveness of using a depolymerizing drug in form of an aqueous solution of ethyl alcohol (concentration of 10 g/l) at the stage of preparation of textile material for bonding (depolarization of antistatic coating). Ethyl alcoholis a solvent for adhesive polyamide components, which promotes more effective penetration of the adhesive into the structure of the material (solvation effect). Due to this treatment, the bundle effort increases by 24–40% and the stiffness increases by 26–64% [7].

The details of garments made of textile materials have to undergo the double bonding effect. It influences the increase of the indices of delamination effort and stiffness for bending. Therefore the significant academic interest consists in the search of chemical means of the influence on adhesive properties of contacting surfaces of the packing materials “skin –adhesive cushioning material". In this regard, it is advisable to search for environments for local processing of individual sections of garment parts. The advice follows up on the basis of which it is possible to equalize the rigidity indices of parts made from different topographic areas (collar, floor, chapra). In addition, it should be considered in mind that the choice of chemicals should prevent the destruction of protein (collagen), which is the basis of natural skin. Such a substance may be an alcohol that does not dissolve the protein but alters the conformational structure of the molecule by displacing water. Water is strongly bound to the active groups of collagen by molecular interaction forces (mainly hydrogen bonds). Water interacts with ionized groups –OH. The amount of H_2O bound depends on the collagen processing technology. Collagen’s behavior through the dehydration with alcohol can cause an increase of the tightness of genuine leather.

2. Method

Sometimes, to obtain adhesive compounds with high strength and shape resistance, the bonding of textile materials is carried out by use of steam chemical active media – a combination of processes of heating, pressure and chemical modification of textile materials and glue by introducing chemical agents into the zone of adhesive contact by means of a steam medium to increase the adhesive activity of components, modifications of their surfaces. Chemical compounds (up to 6 components) may be included into the composition of the vapor chemical active media. The presence of chemical activators in the adhesive contact zone (urea – 5% and sodium bisulfate – 12%) allows reducing the bonding temperature from 180 ºC to 120 ºC, upon receipt of the normalized index of the delamination force. When using a three-component composition (butadiene styrene latex SKS-65GP – 35%, sodium salt – 20%, coagulate – 15%), the stratification force increases by 2.0–3.0 times, the stiffness – 1.5–2.0 times [9].

The structural unit of collagen is tropocollagen (monomer, 1.5 × 280 nm triple helix segment). The monomers, when cross-linked, form collagen. Hydrophobic radicals are inside the protein molecule of collagen, and the hydrophilic are oriented toward the solvent. Denaturation breaks these bonds and spins. This leads to the displacement of water, changes in the conformational structure of the molecule. Intramolecular cross-links can be between spiral chains of three-helical particles, inter-molecular cross-

links can be between three-helical particles. Mucopolysaccharides in the structure of collagen stabilize the fibrils, regulate the fibril formation, limiting the thickening of the fibrils, and prevent their sticking. Polar polysaccharide sites bind to ethanol. Ethyl alcohol may bind to phosphate groups of phospholipids and carboxyl groups of oil chains. Ethanol molecules displace "bound" water molecules from phospholipids, thereby disrupting their structure [3, 4].

An important factor of the implementation of skin transformation processes at the stage of manufacture of garments, including the processes of bonding, is the temperature of welding of collagen, which is 60–65ºC for cattle skins. Welding temperature limits vary depending on the type of tanning (the fat tanning skin has a welding temperature of 65°C, vegetable – 70–85°C, chromium – up to 130°C, formaldehyde – 90°C).

In this regard, the abovementioned factor should be considered when choosing a genuine leather garment manufacturing technology. This may be managed by the appropriate selection of adhesive liners, improvement of the processes of bonding, including the skin removal itself, beyond the direct influence of temperature, determining the rational parameters of bonding and as stated above, the use of chemicals.

3 Research results

The object of the study was the process of bonding and evaluation of viscoelastic properties of genuine leather and packages based on chemical modification and activation methods. Subjects of the study: two types of natural garments (upholstery (C1, C2) and velor (V1, V2)) of the chrome tanning method and two adhesive pads of Hänsel firm (art.1101 / 2ZM4 – with low melting point of adhesive point and art. 2102 / 105MS6 used for costume bonding).

Low temperature gasket adhesive materials of various origin were used to form duplicate packages based on genuine leather velour. Initially, a number of preliminary studies were carried out, which consisted of bonding of prototypes on a stationary press and subsequent determination of the quality of the formed package on the basis of indicators of rigidity and delamination effort, as well as visual assessment of the skin surface. After testing three low-temperature adhesive pads designed to duplicate leather and fur, none of them met the quality requirements. For this type of skin adhesive pad material – art. 2102 / 105MS6 "Hänsel" was selected (most often used in bonding of so-called "complex" costume fabrics – fabrics that have undergone final stages of the treatment to give the effects of increasing invariability, reducing shrinkage, etc.). Hänsel materials are of very high quality, reliability and great technological variety. This is due to the use of the latest technology and extensive experience in production of non-wovens and other nonwovens.

The use of an aqueous solution of ethyl alcohol is the first option to evaluate the ability to create form-resistant garments, including clothing made of genuine leather. The basis of the fixing effect of alcohol is the effect on the degree of protein hydration. As a result of water loss, protein molecules decrease in size and coagulation of the plasma component occurs. In the process of fixing alcohol shows the following features:

– reduction of dielectric constant of proteins with corresponding strengthening of mutual attraction between molecules;

– the emergence of new stereochemical bonds as a result of the convergence of previously distant groups of protein molecules;

– no effect on active protein groups.

Application of the ethanol to the top layer of the wrong side of the skin was performed by a spray (2 ml per 10 cm^2) in a special chamber, without passing to the front.

Batch bonding was performed on a semi-automatic laboratory facility developed by us for bonding of parts from thermosensitive materials within the framework of the experimental design matrix (Box B2 design). The advantages of the developed installation include the reduction of the effect of temperature on genuine

leather, which reduces the likelihood of its structural changes. Under these conditions it is possible to expand the range of adhesive liners with a higher melting point of the adhesive point.

The creation of an original laboratory installation designed for the bonding of heat-sensitive materials (natural and artificial leather) with adhesive gaskets by non-contact method of heating the adhesive coating directly, followed by the connection with heat-sensitive material with the help of the pressure shafts. The general view and schematic diagram of the installation is shown on Fig.1.

Samples for research are made in the longitudinal direction of genuine leather and adhesive materials in the form of strips: length l = 160 ± 1 mm, width b = 30 ± 1 mm. Before the test, the samples are kept in normal atmospheric conditions in accordance with ISO 2419 (T = 20 ± 1 ºC, φ = 65 ± 5%).

a b

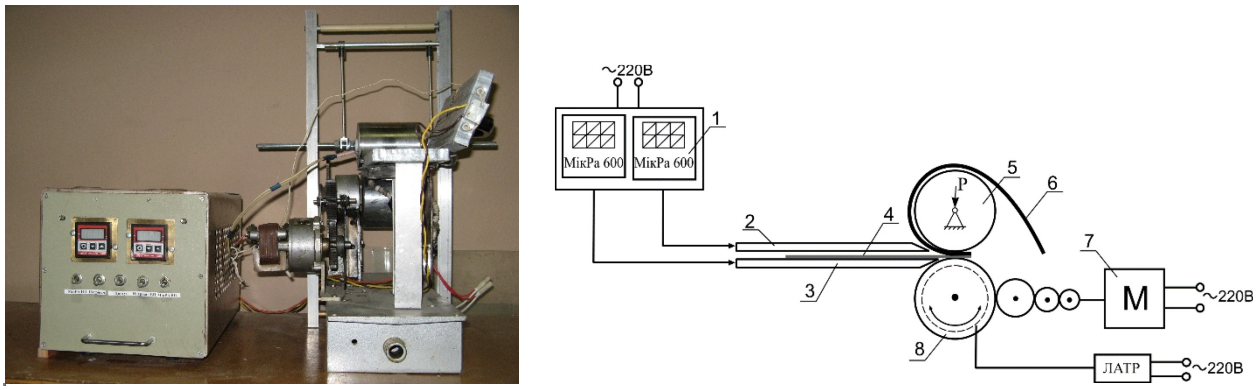

Fig.1. General view (a) and schematic diagram (b) of the laboratory installation for bonding of parts made of thermosensitive materials: 1 - temperature controller MikRa 600 upper (2) and lower (3) flat heater; 4 - sample of adhesive gasket material; 5 - upper calender; 6 – leather sample; 7 - engine; 8 - lower calender with heating.

The principle of operation of the installation. Connect the device to a power source. Switch on the MicRa 600 temperature controller 1. Set the temperature of the upper and lower flat heaters 2, 3 (the rate of temperature rise of the heaters is 6 ºC/min). Switch on the heating of the lower Heated roller 8 (Heated roller temperature rise rate 20 ºC/min). Allow time to heat the lower Heated roller and heaters to the needed temperature. Place a sample of adhesive gasket material on the lower flat heater 3, and the leather sample is positioned on the surface of the upper Heated roller 5. Close the upper flat heater. Withstand time according to the value of the melting point of the adhesive coating of the gasket material. Start the engine that will actuate the lower 8 and upper 5 rollers (rollers speed 0.02 m/s). After the bonding process, turn off the engine. The pressure in the working area is set by the load of the upper calender. At the end it is necessary to disconnect the installation from the power supply.

Taking into account previous search studies, as well as the recommendations of manufacturers, the value of input factors for bonding is presented in Table 1.

Table 1. Input Factors for Bonding

Natural garments		**velor (V1, V2)**			**upholstery (C1, C2)**		
Adhesive gasket material		**art. 2102/105MC6**			**art.1101/2ZM4**		
The levels of variation		+1	0	-1	+1	0	-1
Temperature of the lower Heated roller of T_{LC}, ºC	X1	160	150	140	120	100	80
Bonding time t, c	X2	20	15	10	20	15	10
The temperature of the flat heaters, T_{FH}= const, ºC		130			90		
Pressure P = const, MPa		0,02			0,02		

Example of mathematical processing of the planning matrix of the experiment (Boxing plan B2) PP = f (T, t) for bonding of the package V1 + art. 2102 / 105MS is given in table. 2.

Table 2. The results of mathematical processing for the package V1 + art. 2102 / 105MS

Variance of reproducibility:	*0,022*
The dispersion of the mean according to parallel observations:	*0,007*
Estimated Kohren criterion:	*0,362*
Tabular value of Kohren's criterion:	*0,516*

Regression equation coefficients:

coefficient	coded value	accuracy	natural significance	significance
X0	*2,10850*	*0,20182*	*-40,60708*	**Significant**
X1	*0,43333*	*0,07369*	*0,51883*	**Significant**
X2	*0,45000*	*0,07369*	*-0,00094*	**Significant**
$X1^2$	*-0,15850*	*0,15633*	*-0,00159*	**Significant**
X1X2	*0,00850*	*0,09026*	*0,00000*	**Irrelevant**
$X2^2$	*0,09150*	*0,15633*	*0,00143*	**Significant**

Planning matrix and experiment results:

NN	X1	X2	Y1	Y2	Y3	YMIN	YMAX	YSR	YRAS	DISP
1	1	1	2,900	3,200	3,000	2,656	3,410	3,033	2,925	0,023
2	-1	1	1,900	2,100	2,100	1,750	2,316	2,033	2,058	0,013
3	1	-1	2,200	1,900	2,000	1,656	2,410	2,033	2,025	0,023
4	-1	-1	0,900	1,200	1,100	0,690	1,444	1,067	1,158	0,023
5	1	0	2,300	2,300	2,200	2,131	2,403	2,267	2,383	0,003
6	-1	0	1,700	1,600	1,600	1,497	1,769	1,633	1,517	0,003
7	0	1	2,800	2,300	2,600	1,944	3,190	2,567	2,650	0,063
8	0	-1	1,700	2,000	1,800	1,456	2,210	1,833	1,750	0,023

Table value of the Fischer criterion (F_{tab}):	*3,2389*
Estimated value of the Fischer criterion (F_{est}):	*2,81949*
The model is adequate.	

Mathematical processing of the obtained data allowed us to obtain two-factor second-order mathematical models that adequately characterize the process under study according to Fisher's criterion (according to which, the calculated values (F_{est}) of this criterion should be less than the tabular (F_{tab}) F_{est} = 0.71–2.77 < F_{tab} = 3.63):

•*V1* + art. *2102/105MC:*
$Y=2,11+0,43X1+0,45X2-0,16X1^2+0,09X2^2$;
•*V1* + C_2H_5OH + art. *2102/105MC6:*
$Y=2,59+0,43X1+0,54X2-0,12X1^2-0,07X2^2$;
•*V2*+ art.*2102/105MC6:*
$Y=1,21+0,37X1+0,13X2+0,21X1^2+0,04X2^2$;

•*V2*+ C_2H_5OH + art.*2102/105MC6:*
$Y=2,99+0,91X1+0,16X2-0,06X1^2+0,04X2^2$;

•*C1* + art.*1101/2ZM4:*
$Y=1,51+0,45X1+0,34X2+0,06X1^2+0,04X2^2$;
•*C1* + C_2H_5OH + art.*1101/2ZM4:*
$Y=1,48+0,46X1+0,35X2+0,08X1^2+0,07X2^2$;
•*C2* + art.*1101/2ZM4:*
$Y=1,46+0,53X1+0,38X2+0,46X1^2+0,24X1X2-0,31X2^2$;
•*C2* + C_2H_5OH + art.*1101/2ZM4:*
$Y=2,18+0,53X1+0,16X2+0,19X1^2+0,10X1X2-0,01X2^2$.

According to mathematical models, geometric surfaces of the dependence of the response function on factors X1 and X2 in three-dimensional space were constructed. The graphical dependencies of the stratification force on the temperature and the time of bonding (Fig. 2), allow determining the range of rational parameters at which the achievement of the recommended level of bonding quality ($P_p \geq 2$ N/cm) is guaranteed.

a

V1 + art. *2102/105MC*

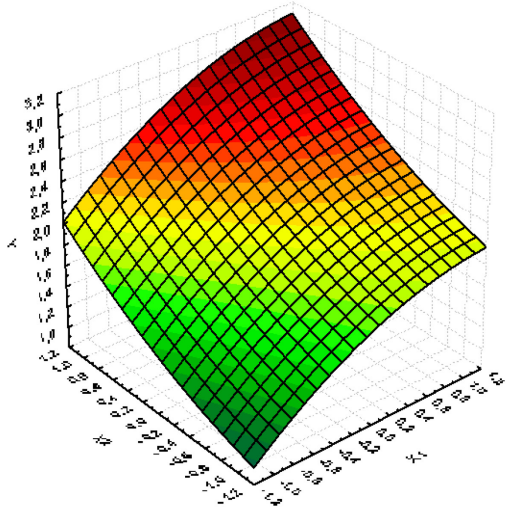

V2+ art.*2102/105MC6*

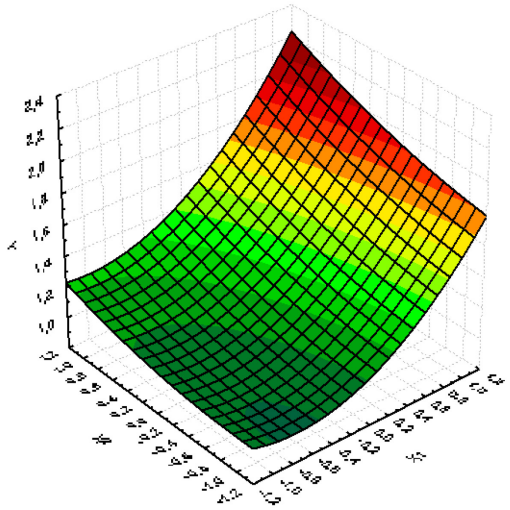

b

V1 + C_2H_5OH + art. *2102/105MC6*

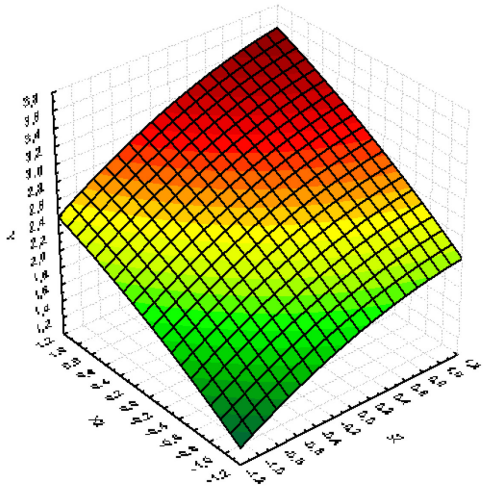

V2 + C_2H_5OH + art. *2102/105MC6*

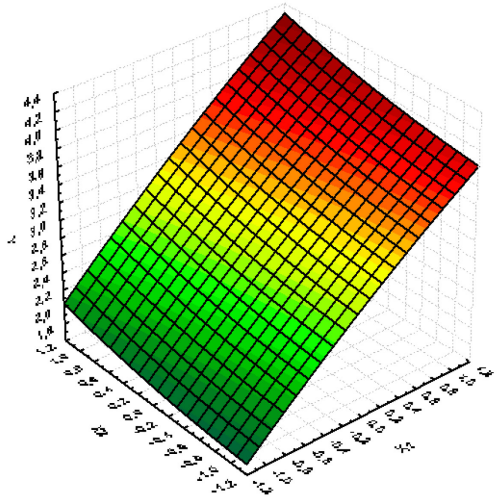

Fig. 2 Dependence of Response Function on Factors X1 and X2 for Packages Based on Genuine Leather velor (V1, V2) Before (a) and After Surface Treatment C_2H_5OH (b).

Previous studies have investigated differences in the properties of individual areas of genuine leather, which creates some complexity in the technology of manufacturing garments both at the stages of cutting individual parts, and when applying thread connections. It is established that when duplicating some types of leather with adhesive gaskets, there are certain difficulties in ensuring the normative indexes of the delamination effort. In this regard, the technology of increasing the adhesive properties of individual parts of garment parts by treating the surface of the skin with substances with amphiphilic properties (ethyl alcohol), which allow due to partial leaching of the fat component and changes occurring on the skin

surface (impact on collagen fiber) to obtain more rational (in terms of energy consumption) bonding parameters and to provide the prerequisites for creating packages with different zonal stiffness indicators (Table 3).

Table 3. Rational Options for Packet Bonding Based on Genuine Leather

Components of packages	**Bonding options**			
	without pre-treatment of the genuine leather surface		**the surface of genuine leather is pre-treated with ethanol**	
	T_{LC}, ºC	*t*, c	T_{LC}, ºC	*t*, c
C1 + art.1101/2ZM4	110	15	100	10
C2 + art.1101/2ZM4	110	15	100	10
V1 + art.2102/105MC6	150	15	130	15
V2 + art. 2102/105MC6	150	15	130	15

The effect evaluation is based on the bending stiffness and delamination efforts, such as the processing of genuine leather. It is established that due to such processing, the indices of delamination force increase by 20–35% and the indices of bending stiffness in the longitudinal direction, when placing the skin face up and face down, increase respectively by 1.5–2.2 times and by 1.4–1.6 times.

Appropriate local surface treatment of the leather gives the opportunity to simultaneously obtain the following effects: changing of the elastic properties (in particular, stiffness) and increasement of the adhesive properties of the surface of the genuine leather, while maintenance and improvement of the performance properties provided by the manufacturer.

4 Conclusions

It is established that in the manufacture of garments made of polymeric materials, which have undergone many stages of processing at the stages of production and furnishing of textile and leather materials, it is necessary to take into account the change of primary properties, including especially the adhesion of the surface.

A wide range of methods and means for activating the surface of materials have been identified that significantly affect the quality of garment performance, including changes in viscoelastic and performance properties. In this regard, it is advisable to carry out further research in the area of forming the sewing products due to the biased activation of the surface and bonding of their details. This should consider the topographical features of garments, including genuine leather, and the possibility of provision of a high-quality adhesive connection, taking into account the temperature indices of collagen welding.

Further improvement of the adhesive technology in the production of garments can be achieved due to the use of polymeric adhesives with high cohesive strength and adhesion to polymeric materials of various purposes, as well as to the development of more rational technological solutions in the production of garments that meet the economical and ecological modern challenges. Addressing this issue will not only improve the quality and competitiveness of domestic garments, but also reduce the cost of imported materials and garments, including these for the needs of power structures.

References

[1] Glubish P.A. Chemical technology of textile materials, finishing. 2005. Kiev.
[2] Artemenko T.P.; Bereznenko S.M.; Yatsenko M.V. Assessment of the influence of nanomodified leather materials on the functional state of human organs and systems; Bulletin of the Kiev National University of Technology and Design, 2015, Volume 1 (79). pp. 216-221.
[3] Kostritsky V.V.; Artemenko L.F.; Skiba M.E.; Skiba G.V. General ideas about the structure of the skin - the basis for the development of its structural and mechanical model. Structural-fibrous structure of the skin; Bulletin of the Kiev National University of Technology and Design, 2008, Volume 5 (43). pp. 13-21.
[4] Orgel J.; Irving T.; Miller A.; Wess T. Microfibrillar structure of type I collagen in situ PNAS, 2006, Vol. 103, Volume 24, pp. 9001–9005.

[5] Nutfullaeva L.N.; Tashpulatov S.Sh.; Cherunova I.V. The use of polymer compositions to increase the form stability of clothing parts; Modern High Technology, 2014, Volume 5, pp. 24-26.
[6] Saraeva T. I.; Nizamova G. A. Main characteristics and properties of the innovation of adhesive composite cushioning materials used in the manufacture of clothing; Bulletin of Kazan Technological University, 2012, T.15, Volume 7, pp. 336-338.
[7] Komarova A.A.; Veselov V.V. The use of modern chemicals for form-stable processing of garments; Textile Technology, 2009, Volume 1 (313), pp. 89-91.
[8] Polyakova N. P.; Smirnova N. A.; Zamyshlyaeva V.V.; Khammatova V.V. Experimental substantiation of the choice of hot-melt adhesive cushioning materials for clothing costume fabrics; Bulletin University of Technology, 2016, T.19, Volume 20, pp. 96-98.
[9] Kuzmichev V.E.; Gerasimov N.A. Theory and practice of gluing parts of clothing: textbook, 2005, Moscow.

COMMUNICATIONS IN
DEVELOPMENT AND ASSEMBLING OF TEXTILE PRODUCTS

Exploring weft knit fabric defects based on their presence and quality impact: A case study

A. K. M. Mobarok Hossain[1] and Md Imranul Islam[2,*]

[1]*Ahsanullah University of Science and Technology, Dhaka, Bangladesh*
[2]*Fashion Institute of Technology, New York, USA*
[(*)] Corresponding author *E-mail address:* mdimranul_islam@fitnyc.edu

INFO

CDAPT, ISSN: 2701-939X
Peer reviewed article
2020, Vol. 1, No. 1, pp. 57-64
DOI:10.25367/cdatp.2020.1.p57-64
Received: 09 May 2020
Accepted: 28 July 2020
Available online: 20 November 2020

ABSTRACT

While addressing grey fabric quality in a renowned circular weft knitting mill of Bangladesh, the authors experienced some questionable approach practiced by knitters. The subjective nature of defect detection by knitters/inspectors often causes wrong emphasizing on frequently occurring defect(s) instead of focusing on influential defect(s) and subsequently, employing wrong quality control approach to minimize the grey fabric defects. Knit fabric defects should be assessed by type, fault coverage, gravity and the frequency of occurrence instead of focusing only on frequency of occurrence in the fabric. In this study, grey weft-knitted fabric quality is investigated influential defects based on how these defects influenced fabric roll acceptance and rejection decision. Quality data of single jersey, fleece and 1X1 rib were gathered and analyzed from an established knitting factory in Bangladesh over three months duration. A fabric inspection machine and a 4-point inspection method were employed in this study. Gout was found as the most frequently occurring defect for each fabric type but not influential for rib fabric. For a significant amount of knitted fabrics, totaling of 55,524.91 m^2 inspected fabric, the most occurring defects were ranked as gout, press-off, hole, miss knit, stain, and tucking and influential defects (based on inspection points) were ranked as gout, press-off, hole, stain, miss knit, and tucking (highest to lowest). In the inspection report, the knitter/inspector mistakenly categorized gout as the most occurring as well as the most influential defect for 1X1 rib fabrics and suggested remedies accordingly.

Keywords
Knit, defect, quality, 4-point system, weft, fabric, influential

1 Introduction

In this age of commercialization, the success of any businesses is highly contingent upon the acceptance of their services and products by their target customers. In addition, globalization causes the fashion business, identical to all other businesses, entering into a fierce competition and all parties involved in the global textile and apparel (TA) market are seeking to display their products before customers at the lowest price, but still high in quality. The concept of quality is so pervasive in the TA industry that it has to maintain throughout the entire supply chain. The early detection of any quality deterioration issue will enhance the chance to rectify that defect in a timely and cost-effective manner. For an example, if a hole in the grey knitted fabric, because of faulty machine set up, identified at the beginning of knitting process, it will increase the likelihood of not carrying more holes to the finished fabric's spreading and cutting stage where having more hole could cause rejecting the entire fabric roll. Though quality control and assurance (QCA) is not free, overlooking any lack of quality from any stage of the supply chain causes that product reaching to the customer and eventually rejected by the customer has far more negative consequences and expensive than the initial QCA cost. The existence of defect(s) would reduce the expected performance of the knitted fabric. If a knitwear made out of defective fabric and having defect(s) appeared on a prominent position of that article would readily be seen and rejected by a prospective customer. In the textile industry, the grey fabric quality is often relaxed and hence, overlooked. It is because some of the defects identified in the grey fabric might disappear in the finished fabric stage after the dyeing and finishing process. This is true when both fabric manufacturing and dyeing mills are synced in terms of quality assessment and they are following right approach to fix any quality defect; if not, the cost of the defect incur exponentially until the product is rejected by the ultimate consumer.

While addressing grey fabric quality in a renowned circular weft knitting factory of Bangladesh, the authors experienced some questionable approach practiced by knitters/inspector. Though a number of smart technologies (e.g., image analysis, neural network algorithm or fuzzy logic, artificial intelligence [AI]) are available for the knit fabric inspection, human-centered inspection is still the most reliable and widely practiced method. However, a number of research argued the possibility of implementing AI in the TA industry because it might improve production efficiency and augment the capabilities of their human employees [1]. The very interlooping structure of knitted fabric along with yarn hairiness makes it difficult to use smart technologies for knit fabric than that of woven fabric [2]. The subjective nature of defect detection by knitters often causes wrong emphasizing on frequently occurring defect(s) instead of focusing on influential defect(s) and subsequently, employing wrong quality control approach to minimize the grey fabric defects. Almost all of the previous studies on knitted fabric defects control were based on cumulative defect numbers [3] [4] [5] [6] rather than emphasizing on original quality impacted by the defects (i.e., how these defects influenced fabric roll rejection or acceptance decision). In addition, these studies did not incorporate any standardize fabric inspection method to evaluate fabric quality through defect points. In the actual manufacturing business, knitted fabric quality acceptance is determined by some predetermined point limits agreed upon between the manufacturer and the buyer. Considering the defect size and gravity, if any defect is responsible for the maximum point in the quality inspection report based on the agreed point system, it should be identified as the most influential defect. Different fabric inspection methods (e.g., 4-point system, 10-point system, Graniteville "78" system, Dallas system, and Textile Distributors Institute system) are practiced throughout the world to determine the acceptability of fabrics from a quality standpoint. However, the 4-point system based on ASTM D5430-13 (2017) [7] is widely recognized for knitted fabric inspection [8]. Besides, the 4-point is system is approved by The American Society for Quality Control (ASQC), Textile and Needle Trades Division, The American Apparel Manufacturers Association (AAMA) and is used by the United States Government for all of their piece goods purchased [9]. This study is particularly aimed to evaluate the significance of knitted fabric defects based on their contribution using the widely practiced 4-point system along with their frequency of occurrence on a particular quantity of knitted fabric produced in a renowned knitting mill of Bangladesh.

1.1 Fabric defect types

Fabric defects refer to any abnormality in the fabric that hinders its acceptability by the consumer. From the ASTM D3990-12 (2016) standard, knit fabric defects are sorted as hole, stain, press-off, snag, gout, miss knit, barré, slub, tucking, think place, thin place, bow, dropped stitch, crack mark, float, loose course, skew, snarl, split stitch, spot, and streakiness [10]. According to this ASTM D3990-12 (2016) standard, gout (see Fig. 1a) referred to “foreign matter trapped in a fabric by accident, usually lint or waste”; press-off (see Fig. 1b) referred to “a condition in which the yarn fails to knit and either the fabric falls off the needles or the design is distorted or incomplete”; hole (see Fig. 1c) referred to “an imperfection where one or more yarns are sufficiently damaged to create an aperture”; miss knit (see Fig. 1d) referred to “a deviation from the designated knitting pattern”; stain referred to “an area of discoloration that penetrates the fabric surface”; and tucking referred to “one or more unwanted tuck loops.” From the same standard, crack mark referred to “an open place causing a streak of variable length approximately parallel to the length or width”; thick place (see Fig. 1e) referred to “an unintentional change in fabric appearance characterized by a small area of more closely spaced yarns, or by a congregation of thick yarns as compared to the adjacent construction”; loose course referred to “a row of loops in the widthwise direction that is larger, looser, or longer than the stitches in the main body of the fabric”; barré (see Fig. 1f) defined as “an unintentional, repetitive visual pattern of continuous bars and stripes usually parallel to the filling of woven fabric or to the courses of circular knit fabric”; and dropped stitch referred to “an unknitted stitch.”

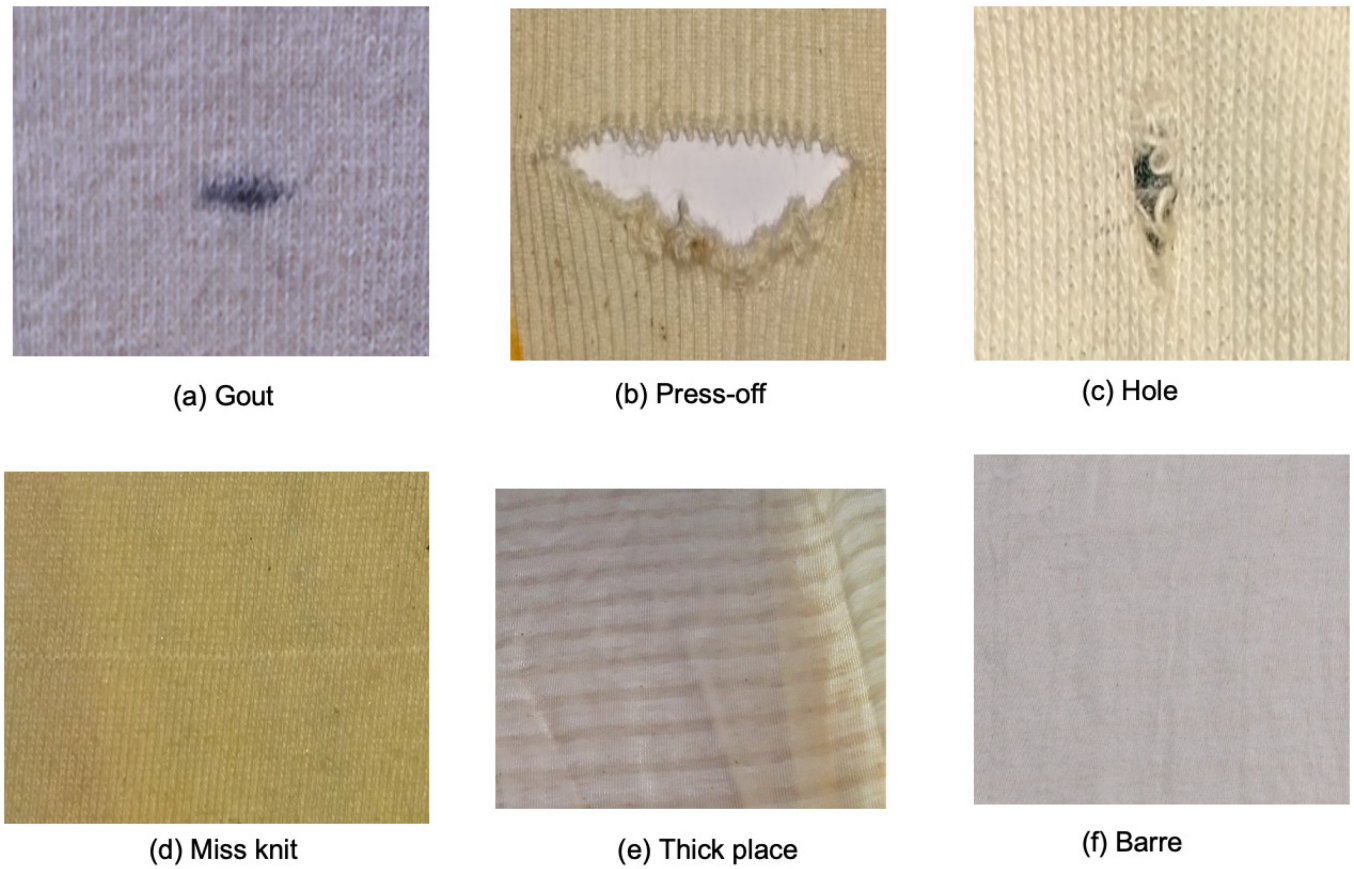

Fig. 1 Knit fabric defect types

1.2 Fabric defect causes and remedies

The sources of grey knit fabric defects could be i) faults in yarn and the yarn package, ii) yarn feeding and yarn feed regulator, iii) machine setting and pattern defects, and iv) machine maintenance [11]. From authors’ industry experience and various recognized industry standards (e.g., ASTM D3990-12 (2016), [10], ISO 8499-03 [12] and MIL-STD-1491 [13]), the causes and remedies of various defects on

grey knit fabric are discussed in this section. The presence of dead fibers and other foreign materials (e.g., dyed fibers, husk, synthetic fibers) and clinging of dyed and other types of fibers (flying from the adjacent knitting machines) that embedded in the grey fabric are causes for gout defect. Using yarns free from dead fibers and other foreign materials for knitting and segregate knitting machines with plastic curtains or nets to prevent the fibers flying from the neighboring machines are few remedies for this problem. The grounds for press-off defect are yarn end breakage on feeders and yarn's failure to feed into needle hooks due to faulty feeder position. Adjusting proper yarn tension and feeder position in relation to needle sizes along with using needle detectors would be the solution for this press-off defect. The origins for hole problem are high yarn tension, yarn overfeed or underfeed, high fabric take down force, and obstructions in the yarn passage. The sources for miss knit defect are faulty positive feed system and wrong feeder setting. The reasons for stain related defect are fiber and fluffs accumulation in the needle tricks which remain soaked with oil and excessing oiling in the needle need. Having weaker fabric take-up force, setting dial in higher place, having tighter loop, and setting course density incorrectly act as triggers for tucking defect. Most of these causes are related to the knitting machine operation and therefore, optimum and correct machine set-up is required to reduce grey fabric defects.

In the industry, the grey knit fabric defects should be assessed by type, fault coverage, gravity and the frequency of occurrence instead of focusing only on frequency of occurrence in the fabric. For an instance, the gout is found as a frequently occurring defect in the inspected knit fabric rolls. Based on the quality report, the knitter employs segregating knitting machines with plastic curtains or nets to prevent the fibers flying from the neighboring machines- a quality control approach. Apart from this gout being a frequently occurring defect, if it also exists as an influential defect (based on its gravity and point dominance in the inspection report), the action taken by the knitter is rational and justifiable. However, most of the time, the type of frequently occurring defect(s) and the influential defect(s) are not the same and it makes the quality assurance program somewhat imprudent.

1.3 Significance of this study

In comparison to the finished fabric quality, there is a paucity of studies on grey knit fabric quality. However, previous studies analogously stressed only on the frequently occurring defects while addressing grey knitted fabric quality [3] [4] [5] [6]. In the study of Sadi et al., they identified five frequently occurring defects (e.g., hole, contamination, dirty spot, oil spot and lycra out), which were accounted for 90.10% of the total defects [6]. In another study, four critical fabric defects (e.g., needle line, hole, yarn variation, and lycra jump) were determined based on their frequency of occurring and these defects were accounted for 80% causes of quality defects [3]. Similarly, other studies focused on classifying defects based on their frequency of occurring [4] [5]. Moreover, these studies used local or, factory terminology when described defects rather than using their standard name (ASTM D3990). To determine the dominant or influential defects from the fabric inspection, this study accentuates using the maximum points occupying defects rather than using their frequency of occurring only. For an example, 1000 gout defects with one point each will yield 1000 points, whereas 300 holes with four points each will yield 1200 points. Based on the previous studies, gout would be identified as dominant defect, whereas in actual situation, hole would be an influential reason for rejecting fabric before gout. In this study, grey weft-knitted fabric quality is investigated using the maximum points occupying or influential defects instead of frequently occurring defects approach.

2 Materials and methods

Quality data of plain single jersey (100% Cotton, 34/1 Ne yarn count, 140 GSM), fleece (100% Cotton, 26/1 Ne yarn count, 300 GSM) and 1X1 rib (100% Cotton, 30/1 Ne yarn count, 200 GSM) were gathered and analyzed from an established knitting factory in Bangladesh over three months duration using 24gg and 18gg for single jersey and double jersey circular knitting machine respectively. A fabric inspection machine (accuracy of checking selvedge: $\pm$5 mm and accuracy of counting length: $\leq$ 0.50%) and standard fabric inspection method (4-point system) based on ASTM D5430-13 (2017) were employed in this study. The nature of defects, number of defects and points associated with the defects were tabulated and analyzed according to the fabric type to determine their frequencies of occurrence and

influence on the fabric quality report. The Table 1 shows point values of fabric defects according to the 4-point system.

Table 1. Allotted points for fabric defects based on 4-point system

Length of defect in fabric	Demerit points	Holes and Opening	Demerit points
Up to 3 inch	1	Any hole except a pin hole	4
Over 3 inch up to 6 inch	2		
Over 6 inch up to 9 inch	3		
Over 9 inch	4		

The total penalty point is calculated by using Equation (1) for 100 yard^2 fabric. Typically, the acceptable points per 100 yard^2 inspected fabric is mostly dependent on the agreement between buyer and seller. However, this study employed grade *A, B, and Reject* for up to 20, 20-30, above 30 points per 100 yard^2 respectively.

$$\text{Points per 100 yard}^2 = \frac{\text{Total point} \times 36 \times 100}{\text{Total roll length in yards} \times \text{cuttable width in inch}} \quad (1)$$

3 Results and discussion

Total areas of inspected fabrics were 18405.10 m^2, 27308.67 m^2, and 9811.14 m^2 for single jersey, fleece, and rib fabric respectively. Fabric defects (see in Table 2) were gathered and analyzed according to fabric type and classified according to their presence and dominance. For single jersey fabric, gout was the most occurring defect (accounted for around 2/5th of total observed defects) followed by miss knit, press-off, and hole. Likewise, for fleece fabric, gout was the most occurring defect (accounted for around 3/5th of total observed defects) followed by press-off and hole. However, the presence of other defects (e.g. tucking, barré, dropped stitch) was quite rare in fleece fabric. For the 1X1 rib fabric, both gout and stain were the most occurring defect (jointly contributed for more than 1/2th of total observed defects) followed by hole and press-off (jointly contributed for around 2/5th of total observed defects).

Table 2. Allotted points for fabric defects based on 4-point system

Fabrics	Defect frequency and points	Gout	Press -off	Hole	Miss knit	Stain	Tuck ing	Crack mark	Loose course	Barré	Dropped stitch	Thick places
Single Jersey	Frequency of defect	124	49	38	56	29	8	7	6	5		
	Defect points/100 sq. yard	1.35	1.07	0.83	1.22	0.32	0.04	0.15	0.13	0.11		
Fleece	Frequency of defect	492	119	117		68	2	10		3	2	
	Defect points/100 sq. yard	3.60	1.74	1.71		0.50	0.02	0.15		0.04	0.03	
1X1 Rib	Frequency of defect	90	61	62	10	88	7		4		6	1
	Defect points/100 sq. yard	1.84	2.49	2.53	0.41	1.79	0.14		0.16		0.25	0.02

Overall, gout was found as the most frequently occurring defect for all fabric types. However, based on gout's points dominance in the inspection report, it was found as the most influential defect for both fleece and single jersey fabric, but not for the 1X1 rib fabric (see Fig. 2). Hole was found as the most influential, yet second most occurring defect for rib fabric. In the inspection report, the knitter/inspector mistakenly categorized gout as the most occurring as well as the most influential defect for 1X1 rib fabric and suggested remedies accordingly. For the grand total of 55,524.91 m^2 inspected fabric, the most occurring defects were ranked as gout, press-off, hole, miss knit, stain, and tucking (highest to lowest). This finding supports the previous study conducted by Hossain, Moin and Mahabubuzzaman [4] and hole was identified as one of the frequently occurring defects [3,6]. Considering the points occupied by these above-mentioned defects (i.e., influential defects), they were ranked as gout, press-off, hole, stain, miss knit, and tucking (highest to lowest).

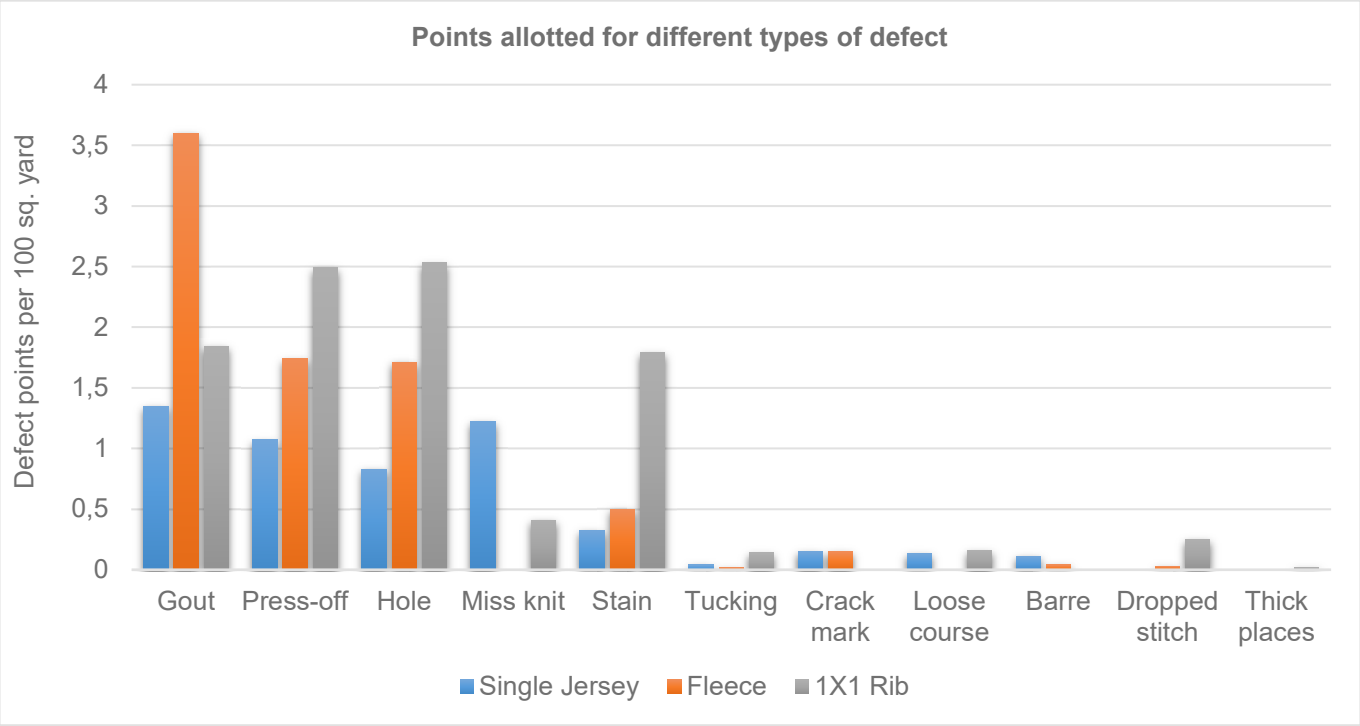

Fig. 2 Defect points allotted for different types of defect

Based upon the principle of frequently occurring defects, similar to previous studies, the gout defect would deserve the knitters' or industry practitioners' the utmost attention to contain it, followed by stain, press-off and hole for 1X1 Rib fabric. In addition, gout, stain, press-off, and hole defects are accounted for 27%, 27%, 19% and 19% of total defects respectively based on their frequency of occurring for the same fabric (Fig. 3, inner pie chart). However, this study made a case to see these defects in terms of their ultimate contribution to the fabric roll rejection or acceptance decision based on their points allocation in the fabric inspection report. In the outer pie chart of Fig. 3, gout, stain, press-off, and hole defects are accounted for 19%, 19%, 26%, and 26% of total defect points respectively in the inspection report. The fabric inspector practices defect points as a guideline to accept or reject the fabric roll instead of cumulative defect numbers. Therefore, unlike previous studies, this study identified the importance of shifting knitters' or industry practitioners' attention from cumulative defect numbers to maximum point allocating defects for knit fabric and address corrective actions accordingly. In summary, categorizing influential defects, grounded on the highest point allocation, would ensure the right approach for quality assurance for the grey knit fabric.

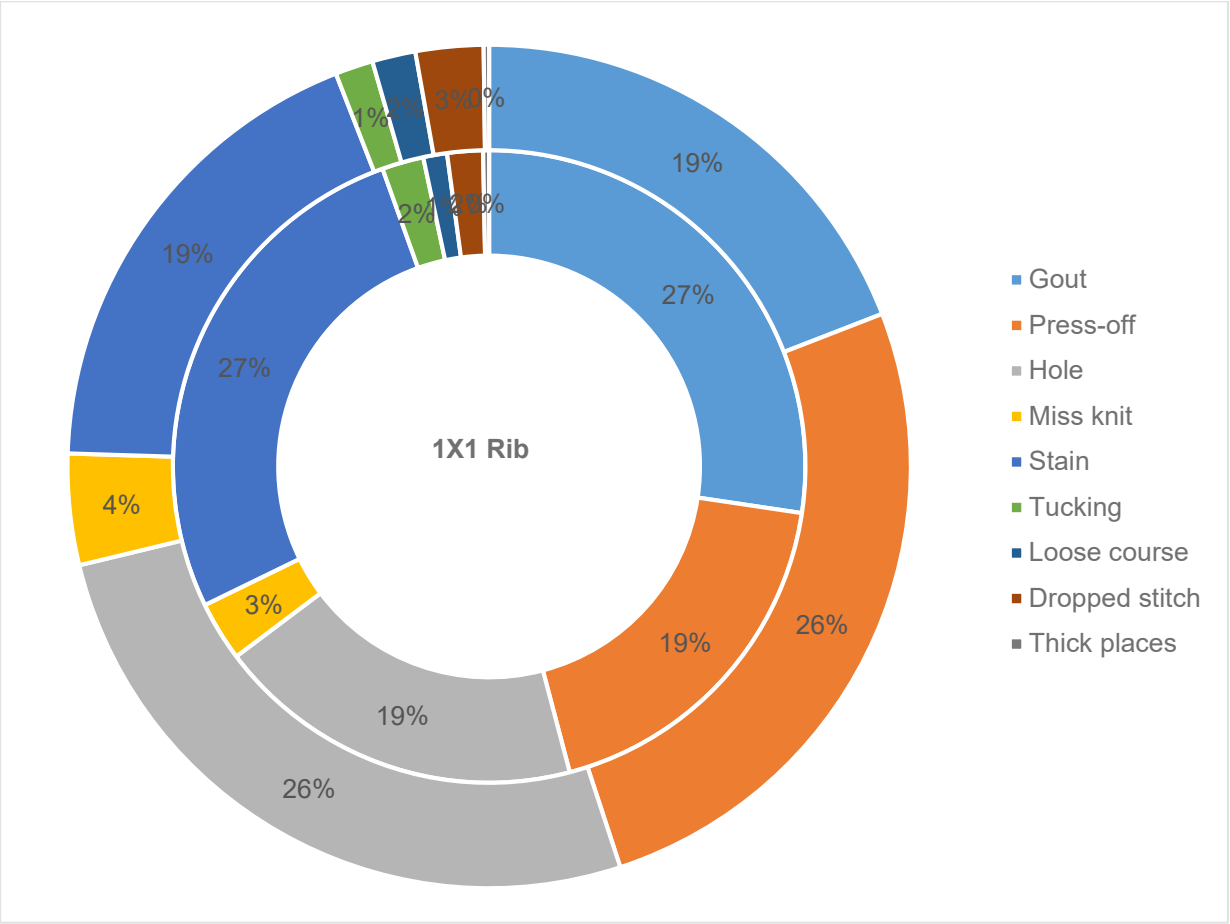

Fig. 3 Frequency of defects (inner circle) vs. defect points/100 yard² (outer circle) for 1X1 Rib fabric

4 Conclusions

Defects detection in the grey fabric state is very crucial as it gives the scope of rectifying the faults at the early stage of manufacturing process. However, some defects like spot, needle line (vertical crack mark) are noticeable in the grey fabric state could be invisible after dyeing. Alternatively, some defects (e.g., barrè) are imperceptible in the grey fabric state could be discernable after fabric coloration. The best approach would be maintaining a database of defects over a couple of years and coordinate the outcome with the dyeing department to determine which influential defects should address in the grey state through a quality assurance program. In this study, it was not possible to justify the presence and impact of observed different defects on finished fabric quality. This study was conducted in a particular factory in Bangladesh and therefore, the researchers were unable to justify the outcome of this research. The sources of knitted fabric defects are mostly— yarn fault, knitting fault, and fault occur due to the environment [11]. Therefore, grey weft knit fabric quality should be addressed and coordinated throughout the entire supply chain. Many recognized literatures and standards such ASTM D3990-12 (2016) [10], ISO 8499-03 [12] and MIL-STD-1491 [13] captured knit fabric defects/faults/flaws quite elaborately. However, a more in-depth future study is warranted to identify underlying potential root causes and eliminate grey fabric defects permanently. In this study, it is evident that knitter/inspector wrongly categorized gout as influential and the most occurring defect for all fabrics. The findings, therefore, indicate the action plans should be taken on priority basis for an effective quality assurance program in the knitting floor.

References

[1] Bharadwaj, R. (2019, November 21). Artificial intelligence in the textile industry – Current and future applications. Retrieved from https://emerj.com/ai-sector-overviews/artificial-intelligence-in-the-textile-industry-current-and-future-applications/

[2] Ben Abdessalem, S., Elmarzougui, S., Mokhtar, S., & Heni, R. (2008). Parameters influencing plain knitted fabric spirality. *Indian Textile Journal*, *4*, 29-34.

[3] Gebru, K. (2014). *Identifying defect causes of weft greige knitted fabric: The case of MAA-garment & textiles Factory* (Master's thesis, Mekelle University).

[4] Hossain, A., Moin, C., & Mahabubuzzaman, A. (2011). Determining the most frequent defects for circular weft knitting fabric machines: A case study. *Journal of Innovation & Development Strategy, 5*(2), 10-17.

[5] Taher, A., Rahman, M., Jahangir, A., Mia, S., & Ashaduzzaman, M. (2016). Study on different types of knitting faults, causes and remedies of knit fabrics. *International Journal of Textile Science, 5*(6), 119-13.

[6] Sadi, M. S., Nahar, N., Shakhawat, H. M., & Sajib, S. H. (2018). Amendment of Finished Knitted Fabric Quality by Reducing the Intensity of Defects and Improvement Techniques. *American Journal of Materials Science*, *8*(1), 6-14.

[7] American Society for Testing and Materials (2000). ASTM D5430-13 (2017): Standard test methods for visually inspecting and grading fabrics. ASTM International, USA.

[8] AQF Operations Team (2012, January 20). 4 point system for QC on fabric. [Blog post]. Retrieved from https://blog.asiaqualityfocus.com/qc-fabric/

[9] Clothing Industry. (2017, December 23). Fabric Inspection Systems for Garment Industry [Blog post]. Retrieved from https://clothingindustry.blogspot.com/2017/12/fabric-inspection-systems.html

[10] American Society for Testing and Materials (2016). ASTM D3990-12 (2016): Standard terminology relating to fabric defects. ASTM International, USA.

[11] Iyer, C., Mammel, B., & Schäch, W. (1995). *Circular knitting: Technology process,structures yarns, quality*. Meisenbach Bamberg, Germany.

[12] International Organization for Standardization (ISO) Technical Committee (2003). ISO/TC 38/SC 20 (2003) ISO 8499:2003: Knitted fabrics — Description of defects — Vocabulary. ISO, Switzerland

[13] U.S. Department of Defense (1973). United States Military Standard-1491 (MIL-STD-1491): Glossary of knitting imperfections. U.S. Department of Defense, USA.

COMMUNICATIONS IN
DEVELOPMENT AND ASSEMBLING OF TEXTILE PRODUCTS

Water vapor resistance measured on sweating thermal manikin and Permetest skin model in the vertical orientation

Frederick Fung[1], Chuansi Gao[2], Lubos Hes[1], Vladimir Bajzik[1,*]

[1] Department of Evaluation, Faculty of Textile Engineering, Technical University of Liberec, Czech Republic
[2] Thermal Environment Laboratory, Division of Ergonomics and Aerosol Technology, Department of Design Sciences, Faculty of Engineering, Lund University, Sweden

*Corresponding author *E-mail address:* tassfashion@gmail.com

INFO

CDAPT, ISSN 2701-939X
Peer reviewed article
2020, Vol. 1, No. 1, pp. 65-73
DOI:10.25367/cdatp.2020.1.p65-73
Received: 11 May 2020
Accepted: 28 July 2020
Available online: 20 November 2020

ABSTRACT

This paper is a comparison of water vapor resistance (R_{et}) measured using the Permetest skin model and Tore sweating thermal manikin, i.e. 2D versus 3D methods; and to study the relationship between them. Three materials and five air gap distances were used for the measurement between these two apparatuses, the test conditions in the climatic chambers were set up according to the ISO standard of each measurement method. Results of the correlation coefficient of three materials showed that they all had a strong increasing trend between the Permetest skin model and the sweating thermal manikin. From the regression analysis, the P-value of all three materials showed that $P < 0.05$ and 100% cotton $R^2=0.83$, 50% cotton 50% polyester $R^2 = 0.91$, 100% polyester $R^2=0.99$. However, R_{et} resulting values from each device slowed down after 12 mm air gap distance.

Keywords
Sweating thermal manikin,
Permetest skin model,
water vapor resistance,
vertical orientation,
air gap distance

1 Introduction

Water vapor resistance (R_{et}) is one of the important parameters in clothing comfort [1-3]; the sweating thermal manikin and the Permetest skin model are apparatuses used by researchers and scientists to test on garments, textile for the value of R_{et} [4-6].

The sweating thermal manikin [7,8] is an anatomically correct, human-like robot that the whole body is divided into segments; each segment of the thermal manikin is a heat zone where the body shell surface temperature can be controlled and adjusted using a computer program to simulate human body heat for thermal comfort of clothing tests (Fig. 1). Because of the human form, thermal manikin can measure convective, radiative and conductive heat losses in all directions over the whole surface or a defined, local surface area [9]. From one-segment of copper manikin, which was invented and used by the U.S. military for researching on thermal heat transfer through protective clothing ensembles in 1941 [10], to multi segments made of plastic or metal, thermal manikin has been developed and been re-invented in many different ways [11-15]; for examples, from dry to wet (sweating) thermal manikins, female and baby manikins, head, hand and foot manikins, breathable manikin for medical research purposes, fabric manikin - Walter for giving R_{ct}/R_{et} results in the same test, and even inflatable manikin [16]. In sweating thermal manikin, small holes are embedded in particular segments on the body that can secrete water to simulate the sweating glands on the human body and some models can perform simple movements like cycling and walking activities. When testing for evaporative resistance (R_{et}), the manikin will be put on a tight fabric skin which is moisture permeable to evenly spread out moisture, and clothing simply hangs on top of the skin, results are directly recorded in the computer program. Though thermal manikin is considering one of the most accurate apparatus for testing thermal and evaporative resistance of clothing system, it still has rooms for improvements. For example, researchers are still debating heat loss or mass loss method should be used when testing for R_{et} [17]; it is difficult to detect and to control the skin surface temperatures [18,19], etc.

The Permetest is one of the smallest skin models among others; like Alambeta and Thermo Labo [20,21]. The concept of the Permetest is derived from the Hohenstein skin model – sweating guarded hot plate (SGHP) – which is to measure evaporative resistance of fabric by generating a unidirectional heat flux through the sample, then the evaporative heat loss is recorded in the steady state [22-24]. However, maintaining the hot plate perfectly flat with even and constant heat; and preventing heat loss by insulation still have a discrepancy [25-29].

The Permetest skin model (developed by Hes) works on the principle of heat power sensing by maintaining constant heat supply to the measuring head is measured with and without fabric sample (Figure 2). When testing R_{et}, sample textile/clothing (without cutting) is put on the small circular hotplate which is covered by a thin layer of vapor permeable membrane function as the wet skin inside the wind channel for testing (Fig. 3a-e). The measuring head where the supplied water gets evaporated is measured; the partial saturated pressure of the measuring head with and without sample, and the partial pressure of the ambient atmosphere are also measured under the isothermal condition. A lot of articles have already published regarding these two apparatuses testing on different garments and materials like protective clothing, knitted fabrics, testing garments in multi-layers; mass, thickness, dry and wet state of materials; footwear materials and even using manikin and Permetest to test on different parameters of the same material [30-35]. These experiments showed that physical and mechanical properties like drapability, air permeability, porosity, thickness and so on of materials/clothing influence the results of R_{et}. For example, over- or underestimation of heat loss caused by condensation when low permeability clothing is tested in low ambient temperature [36-38]. However, this paper is focused on finding out the correlation between the Permetest skin model and the thermal manikin these two apparatuses. Knowing the correlation of these two apparatuses is useful to predict the R_{et} when there is no access to the manikin, and also save time and labor cost. The only limitations of the research are 1) the maximum air gap thickness is 16 mm, a limit of the Permetest; 2) only three materials were tested; 3) after 12 mm air gap distance, R_{et} started to slow down or stabilized.

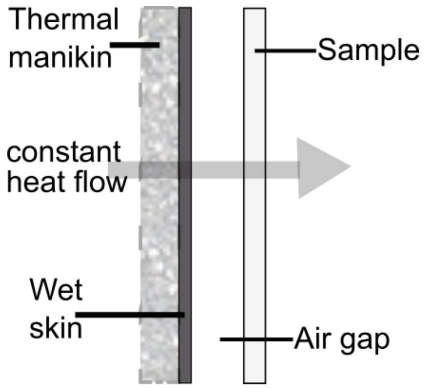

Fig. 1 Principle of thermal manikin

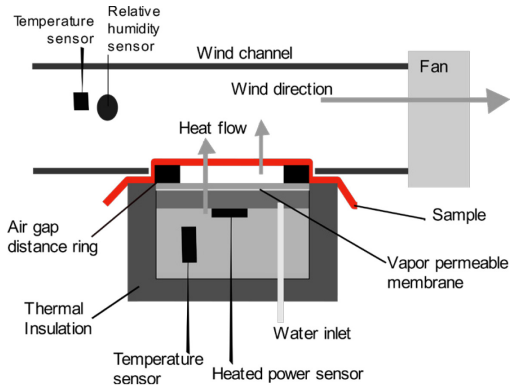

Fig. 2 Principle of Permetest skin model

2 Method

Two apparatuses were used for the experiment, Permetest skin model and the sweating thermal manikin. Tested samples were woven materials shown in Table 1. Samples were washed to minimize the finishing on the materials, hang dry then iron flat before used for tests. Five air gaps between 0-16 mm were applied during tests which were 0, 4, 8, 12 and 16 mm. Each material was tested three times on each apparatus with the combinations of five air gap distances

Table 1. Properties of materials

Material	**100% Cotton**	**50/50% Cotton/Polyester Blended**	**100% Polyester**
Type	Plain	Plain	Plain
Weight (g/m²)	156	159	159
Thickness (mm)	0.30	0.38	0.43
Fabric Density Warp/Weft (per cm)	26/22	26/26	24/16
Air Permeability (l/m²/s)	234	272	579
Absorption Rate (%/s) Top/Bottom	13.33/35.50	11.81/39.24	7.81/20.07
Porosity (%)	66	71	73
Drapability (%)	34	39	43

2.1 Permetest skin model

Materials were used directly without cutting. Air gap distance was applied by using 100 percent foamed polyethylene in 2, 4 and 5 mm thickness rings and their combinations (Fig.3a-e). To balance the thickness of the air gap distance created by the stack of rings and to maintain the smooth air current flew inside the wind channel, two types of rings were cut: outer rings were put around the base of the hotplate for counter thickness; inner rings were placed inside the wind channel on the hotplate to create the air gap distance. The outer ring was 12cm in diameter on the outer circle and 10cm on the inner circle, width 2cm. The inner ring was 8cm in diameter on the outer circle and 6cm on the inner circle, width 2cm. Each material was tested three times under 0, 4, 8, 12, 16 mm air gap distance in a vertical orientation to simulate the vertical air gaps on the manikin and in an isothermal condition. As required in the ISO 11092 [39], the climatic chamber was set up at 50-55% in relative humidity, wind speed at 1m/s and air temperature at 22-24 °C.

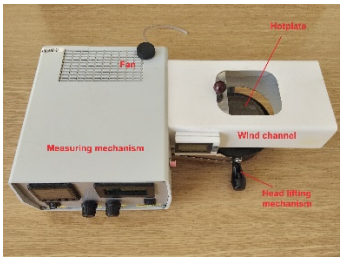

Fig. 3 (a) Permetest skin model in the horizontal orientation

(b) Permetest skin model in the vertical orientation

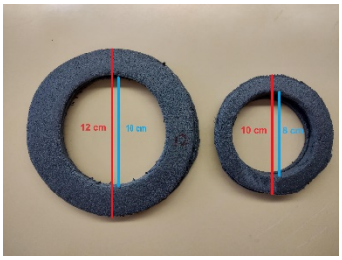

(c) Sizes of outer and inner rings

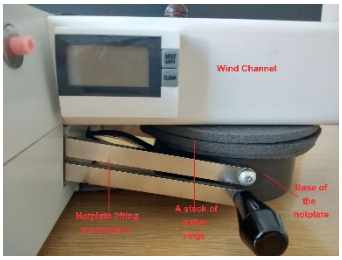

(d) Showing outer rings stacked on the base of the hotplate

(e) Showing inner rings placed inside the wind channel on the hotplate

Each determination of evaporation resistance R_{et} of a sample consists of two steps: first test without sample, second test with air gap distance ring of thickness h covered by a sample. When the heat flow q_{eto} reaches the steady state, the result of the first step is given by the Eq. (1), where R_{eto} presents resistance of the boundary layer above the measuring surface of the instrument:

$$q_{eto} = (P_s - P_o)/R_{eto} \quad (1)$$

Here, P_s means partial pressure of the saturated water vapour and P_o is the partial pressure of the water vapour in the measuring channel of the testing instrument. The second step characterises the heat flow passing through the measuring head of the instrument covered by the tested sample:

$$q_{et} = (P_s - P_o)/ (R_{eto} + R_{et}) \quad (2)$$

for the case without the distance ring in Eq. (2) or with distance ring in Eq. (3)

$$q_{etg} = (P_s - P_o)/ (R_{eto} + R_{et} + R_{eg}) \quad (3)$$

which creates the additional air gap resistance $R_{eg.}$ R_{eg} = h/D, where D is the coefficient of diffusion of water vapour in air, which can be found in tables. The required evaporation resistance of the sample R_{et} yields solution of Eq. 1 and Eq. 2. The required total evaporation resistance of the sample R_{et} + air gap resistance R_{eg} yields solution of Eq. 1 and Eq. 3. When from the achieved value the evaporation resistance of the sample R_{et} is deduced, we obtain evaporation resistance R_{eg} of the air gap.

2.2 Sweating thermal manikin

Tore is the thermal manikin used in the experiments. A close-fitted shirt (approximately 0 mm air gap, Fig. 4 a-f) was made by the molding method [40]. Based on this shirt, 4, 8, 12, 16 mm air gap distance was added into the shirt pattern circumference as wearing allowance. All shirts were sewn by a fine 100% polyester thread (Polysheen® No. 40) with a fine machine sewing needle (Schmetz 70/10). The sewn seams were pressed open under a press-cloth with high heat to melt/expand the polyester thread to minimize the size of needle holes to reduce heat loss. A total of fifteen combinations of shirts of three materials with 0, 4, 8, 12, 16 mm built-in air gap distance were made. The air gap distance around the

torso when the shirt was put on the manikin might not be the same as desired, for example; on the shoulder areas might have 0 mm air gap distance. Each of the 15 shirts combinations was tested three times for evaporation resistance on a heated thermal manikin with pre-wetted skin in an isothermal condition. ISO 15831 was followed. The climatic chamber was set up at 50% in relative humidity, wind speed at 0.145 m/s and air temperature at 34 °C.

Fig. 4 (a) Tore – sweating thermal manikin

(b) The molding method -- duct tape was applied on top of the plastic shrink wrap which was tightly wrapped around the torso of the manikin for protection and easy unmolding

(c) Unmolded front and back pieces and were divided into small segments according to the contour lines on the manikin's torso

(d) Unmolded arm piece from shoulder to wrist and cut into small segments

(e) Arm piece was converted into two-dimensional sleeve patterns

(f) The finished shirt was completed with bodice and sleeves and was closed in the center back

For each 40 minutes observation, 20 minutes of steady state was taken for calculating the result as in Eq. (4), where P_{aS} is the manikin skin water vapor pressure (only torso and arms); P_{aA} is the ambient air water vapor pressure; HL is the heat loses of the torso and arms only.

$$R_{et} = P_{aS} - P_{aA} / HL \quad (4)$$

3 Results

Resulting data in Table 2 were analyzed by three methods: a) Correlation coefficient in Table 3; b) Linear regression (Fig. 5a-c); c) 2-way ANOVA.

Table 2. R_{et} results from the Permetest skin model and the thermal manikin

Mean values of evaporative resistance of materials (Pa*m²/W)						
Air gap distance	100% CO		50/50% CO/PES		100% PES	
	Permetest	Manikin	Permetest	Manikin	Permetest	Manikin
0 mm	3.50	4.90	3.70	5.87	1.40	1.73
4 mm	5.30	4.90	6.10	6.20	4.60	4.27
8 mm	10.70	10.27	11.50	10	9	6.47
12 mm	19.40	10.27	22.20	10.87	16.70	10.23
16 mm	21.90	11.83	26.70	13.03	19.60	12.13

Results from the Permetest skin model and the thermal manikin showed that when the air gap distance increases, the evaporative resistance increases and the increasement slows down after 12 mm air gap distance in both apparatuses. An interesting thermal manikin R_{et} results from 100% cotton, it showed that 0 and 4 mm; 8 and 12 mm air gap distances had the same mean values. The original data showed that results from these four air gap distances were different but the values were very close. However, these results may also cause by the thickness, drapability, porosity and evaporation of the fabric itself, further investigation needed.

a) Correlation coefficient of Permetest skin model and the thermal manikin

Table 3. Values of correlation coefficient from three materials

Correlation Coefficient	**100% Cotton**		**50/50% Cotton/Polyester**		**100% Polyester**	
	Permetest	Manikin	Permetest	Manikin	Permetest	Manikin
Permetest	1		1		1	
Manikin	0.91	1	0.95	1	0.997	1

Results from all three materials showed that their correlation coefficient (r) values between the Permetest skin model and the thermal manikin had a very strong positive trend. For the results from 100% polyester, the r is almost 1.

b) Linear regression between Permetest skin model and the thermal manikin

Correlation determination (R^2) of 100% cotton is 0.83, 50/50% cotton/polyester blended is 0.91, and 100% polyester is 0.99 almost 1 to 1 relationship. Results mean that each unit of Ret changes in the thermal manikin is highly related to the changing in the Permetest skin model.

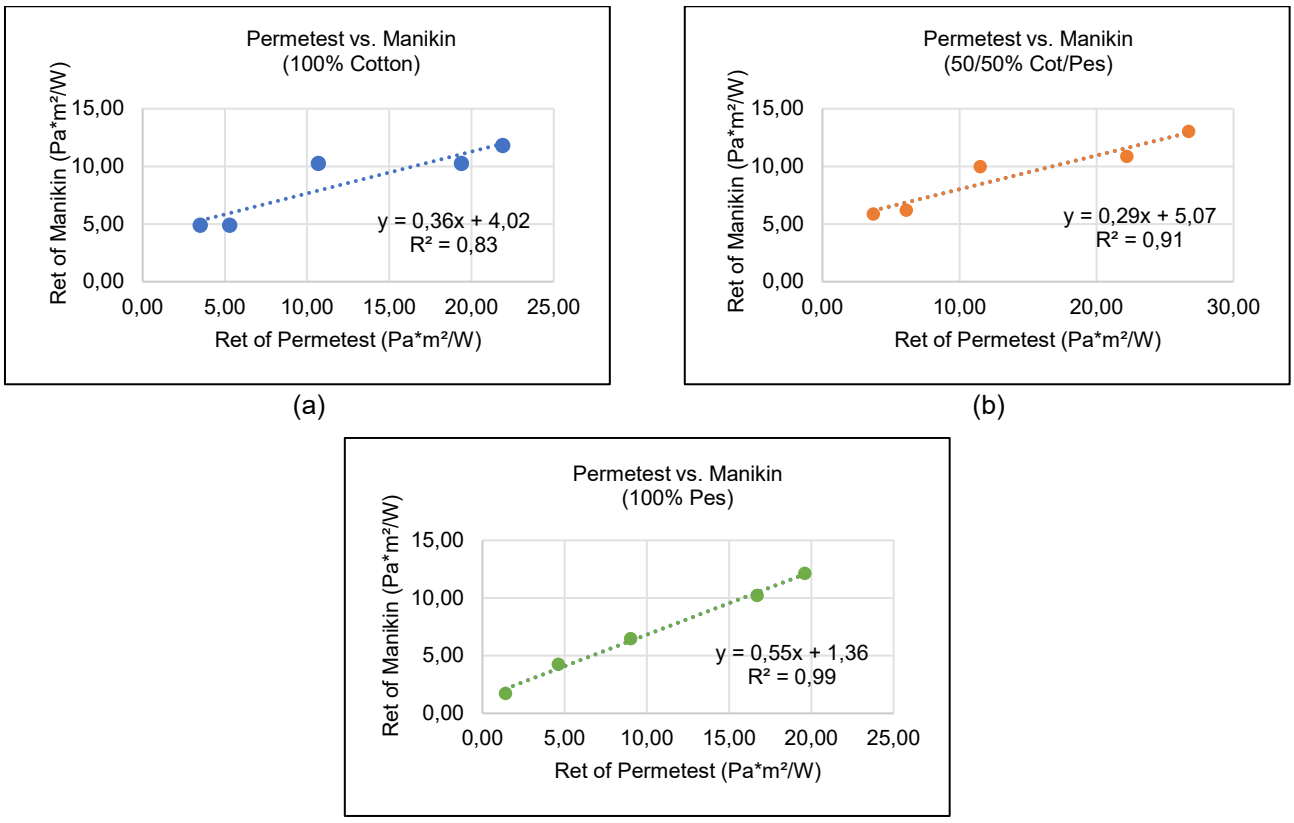

Fig. 5 Regression between Permetest and thermal manikin of 100% cotton (a), 50/50% cotton/polyester blended (b), 100% polyester (c)

c) 2-way ANOVA of Permetest skin model and the thermal manikin with 0 to 16 mm air gap distances in three materials

Results showed that P-value of three materials were: 100% cotton $P<0.05$; 50/50% cotton/polyester $P<0.05$; 100% polyester $P<0.01$ in 95% confidence level. Three materials $P<0.05$ show that there is a significant difference between the results of Permetest and the thermal manikin which is because these two apparatuses are fundamentally different when taking the R_{et} measurement as shown in Table 4.

Table 4. Differences between Tore – the thermal manikin and the Permetest skin model

	Tore – Sweating Thermal Manikin	**Permetest Skin Model**
Shape	Human form	Rectangular form
Dimension	Height 170 cm, chest 94 cm, waist 88 cm	Length 54 cm, width 23 cm, height 13 cm
Weight	Unknown	7 kg
Materials	Plastic form shell, inside supported by the metal frame for body parts and joints	Metal
Total heated measured area	1.774 m²	50.265 cm²
Measuring Method	3D – Ready-to-wear garments	2D – Flat surface of textile or garments (non-destructive)
Measuring Time	20 minutes of steady state out of 40 minutes total measuring time	1 to 5 minutes in each measurement in average
ISO Standard	15831	11092

4 Conclusions

Tore – the sweating thermal manikin and the Permetest skin model were used to examine the evaporative resistance (R_{et}) of the combinations of three materials (100% cotton, 50/50%

cotton/polyester, 100% polyester) and five air gap distances (0, 4, 8, 12, 16 mm). Each apparatus' set up environment was according to a different IOS standard but the method for testing materials was different; materials were made into shirts to be tested on the manikin and were directly tested on the Permetest without cutting. Results were analyzed by three methods: correlation coefficient, correlation determination and the P-value. The correlation coefficient results from all three materials showed a very strong positive increasing relationship between the manikin and the Permetest skin model. The R^2 of the three materials are also very strong that it indicated that the R_{et} values of the manikin are highly predicted by the Permetest skin model and vice versa. However, $P < 0.05$ in all three materials in the two-way ANOVA showed the significant difference between the two apparatuses; it was caused by the different methods of testing materials on each apparatus, 2D versus 3D. Overall, this experiment shows that values of evaporative resistance (R_{et}) can be predicted between the manikin Tore and the Permetest skin model for the 100% cotton, 100% polyester and 50/50% cotton/polyester blended within a narrow air gap from 0 to 12 mm, then the trend will become stabilized or slow down.

Acknowledgments

We would like to thank the Thermal Environment Laboratory, Division of Ergonomics and Aerosol Technology, Department of Design Sciences, Faculty of Engineering, Lund University, Sweden for offering the facilities including Tore – the sweating thermal manikin for the research, also; Mr. Amitava Halder for his assistance during the process.

References

[1] Hes, L.; de Araujo, M. Simulation of the effect of air gaps between the skin and a wet fabric on resulting cooling flow, *Textile Research Journal,* 2010, 80 (14), pp. 1488–97. DOI: 10.1177/0040517510361797.

[2] Hes, L. Optimisation of shirt fabrics' Composition from the point of view of their appearance and thermal comfort, *International Journal of Clothing Science and Technology,* 1999, 11 (2/3), 105–19. DOI: 10.1108/09556229910276250.

[3] Hes, L. Thermal Comfort: The six basic factors. Available online: https://www.hse.gov.uk/temperature/thermal/factors.htm (accessed on 14 June 2020)

[4] Holmér, I; Nilsson, H. Heated Manikins As A Tool For Evaluating Clothing, *The Annals of Occupational Hygiene*, 1995, 39 (6), pp. 809–818. DOI: 10.1093/annhyg/39.6.809.

[5] Wang, F. Measurements of clothing evaporative resistance using a sweating thermal manikin: an overview, *Industrial Health*, 2017, 55 (6), pp. 473–484. DOI: 10.2486/indhealth.2017-0052.

[6] Hes, L; Carvalho, M. Diagnostic of the composition of fabrics from their thermal permeability in wet state, *Indian Journal of Fibre and Textile Research,* 1994, 19, pp. 147-150.

[7] Manikin History | Thermetrics. Available online: https://www.thermetrics.com/solutions/manikin-history (accessed on 21 June 2020).

[8] Thermal Manikin Testing. Available online: http://www.lth.se/fileadmin/eat/Termisk_miljoe/ArbLivsRapp1997_9.PDF#page=37 (accessed 8 July 2020)

[9] Holmer, I. Thermal Manikin History and Applications'. *European Journal of Applied Physiology,* 2004, 92 (6), 614–18. DOI 10.1007/s00421-004-1135-0.

[10] USARIEM: Thermal manikin history. Available online: https://www.usariem.army.mil/index.cfm/about/divisions/bbmd/thermal_manikin (accessed on 5 July 2020)

[11] Thermetrics | Advanced Thermal Measurement Technology. Available online: https://thermetrics.com/ (accessed on 5 July 2020).

[12] Nayak, R.; and Padhye, R. *Manikins for Textile Evaluation*. Woodhead Publishing, 2017.

[13] Lei, Z. X. Review of application of thermal manikin in evaluation on thermal and moisture comfort of clothing. *Journal of Engineered Fibers and Fabrics,* 2019, 14, no. 1558925019841548. DOI: 10.1177/1558925019841548.

[14] Wang, F. A Comparative Introduction on Sweating Thermal Manikins "Newton" and "Walter", *Proc. of 7th International Thermal Manikin and Modelling Meeting,* University of Coimbra, Portugal 2008, pp. 1-7.

[15] Sun, C.; Fan, J. Comparison of Clothing Thermal Comfort Properties Measured on Female and Male Sweating Manikins. *Textile Research Journal* 2017, 87 (18), pp. 2214–2223. DOI: 10.1177/0040517516669071.

[16] Mijovic, B.; Skenderi, Z; Camara, J.; Reischl, U.; Colby, C.; Mermerian, A. Inflatable mannequin for testing thermal properties of clothing. *Proceedings of the 17th World Congress on Ergonomics.* Beijing, IEA, 2009.

[17] Wang, F.; Gao, C.; Kuklane, K.; Holmér, I. Determination of clothing evaporative resistance on a sweating thermal manikin in an isothermal condition: Heat loss method or mass loss method? *The Annals of Occupational Hygiene,* 2011, 55 (7), pp. 775–83. DOI: 10.1093/annhyg/mer034.

[18] Wang, F.-M., Gao, C.; Kuklane, K.; Holmér, I. A study on evaporative resistances of two skins designed for thermal manikin Tore under different environmental conditions. *Journal of Fiber Bioengineering and Informatics,* 2009, 1(4), pp. 301-305. DOI: 10.3993/jfbi03200908 .

[19] Wang, F.; Kuklane, K.; Gao, C.; Holmér, I. Development and validity of a universal empirical equation to predict skin surface temperature on thermal manikins'. *Journal of Thermal Biology* 2010, 35 (4), pp. 197–203. DOI: 10.1016/j.jtherbio.2010.03.004.
[20] Matusiak, M.; Sybilska, W. Thermal resistance of fabrics vs. thermal insulation of clothing made of the fabrics. *The Journal of the Textile Institute,* 2016, 107 (7), pp. 842–48. DOI: 10.1080/00405000.2015.1061789.
[21] KES-F7 Thermo Labo | KATO TECH CO., LTD. | Pioneer of texture testers and electronic measuring instruments. Available online: https://english.keskato.co.jp/archives/products/kes-f7 (accessed on 6 July 2020)
[22] Breathability in quality control at Hohenstein institute. Available online: https://www.innovationintextiles.com/breathability-in-quality-control-at-hohenstein-institute/ (accessed on 9 July 2020).
[23] Sweating Guarded Hotplate | Thermetrics. Available online: https://www.thermetrics.com/products/guarded-hotplates/sweating (accessed on 22 June 2020).
[24] Huang, J. H. Sweating Guarded Hot Plate Test Method, *Polymer Testing,* 2006, 25 (5), 709–16. DOI: 10.1016/j.polymertesting.2006.03.002.
[25] Zarr, R. R. A history of testing heat insulators at the National Institute of Standards and Technology. *Ashrae Transactions,* 2001, 107, pp. 661-671.
[26] Salmon, D. Thermal conductivity of insulations using guarded hot plates, including recent developments and sources of reference materials. *Measurement Science and Technology,* 2001, 12 (12), R89.
[27] Healy, W. M. Using finite element analysis to design a new guarded hot plate apparatus for measuring the thermal conductivity of insulating materials. Available online: https://tsapps.nist.gov/publication/get_pdf.cfm?pub_id=860852 (accessed on 17 July 2020).
[28] Scoarnec, V.; Hameury, J.; Hay, B. A new guarded hot plate designed for thermal-conductivity measurements at high temperature. *International Journal of Thermophysics,* 2015, 36 (2–3), pp. 540–56. DOI: 10.1007/s10765-014-1794-y.
[29] Reddy, K. S., Jayachandran, S. Investigations on design and construction of a square guarded hot plate (SGHP) apparatus for thermal conductivity measurement of insulation materials. *International Journal of Thermal Sciences,* 2017, 120, pp. 136–147.
[30] Oğlakcioğlu, N.; Marmarali, A. Thermal comfort properties of some knitted structures, *Fibers and Textiles in Eastern Europe*, 2007, 15 (5–6), pp. 64–65.
[31] Reiners, P.; Kyosev, K. About the thermal conductivity of multi-layer clothing, *ACC Journal, Natural Sciences and Technology*, 2013, 2013 (1), pp. 94–102.
[32] Stoffberg, M. E.; Hunter, L.; Botha, A. The effect of fabric structural parameters and fiber type on the comfort-related properties of commercial apparel fabrics, *Journal of Natural Fibers*, 2015, 12 (6), pp. 505–517. DOI: 10.1080/15440478.2014.967370.
[33] Bogusławska-Bączek, M.; Hes, L. Effective water vapour permeability of wet wool fabric and blended fabrics, *Fibres & Textiles in Eastern Europe*, 2013, 21, pp. 67–71.
[34] Akalović, J.; Skenderi, Z.; Rogale, S. F.; Zdraveva, E. Water vapor permeability of bovine leather for making professional footwear, *Leather & Footwear* 2018, 67 (49), pp. 12–17.
[35] Gericke, A.; van der Pol, J. A comparative study of regenerated bamboo, cotton and viscose rayon fabrics, Part 1: Selected comfort properties, *Journal of Family Ecology and Consumer Sciences*, 2010, 38, pp. 63-73.
[36] Havenith, G., Richards, M. Use of clothing vapor resistance values derived from manikin mass loss or isothermal heat loss may cause severe under and over estimation of heat stress, *Proc. of 7th International Thermal Manikin and Modelling Meetingm* University of Coimbra, 2008.
[37] Fukazawa, T.; Lee, G.; Matsuoka, T.; Kano, K.; Tochihara, Y. Heat and water vapour transfer of protective clothing systems in a cold environment, measured with a newly developed sweating thermal manikin, *European Journal of Applied Physiology*, 2004, 92, pp. 645–648. DOI : 10.1007/s00421-004-1124-3.
[38] Anttonen, H.; Niskanen, J.; Meinander, H.; Bartels, V.; Kuklane, K.; Reinertsen, R. E.; Varieras, S.; Sołtyński, K. Thermal manikin measurements – exact or not? *International Journal of Occupational Safety and Ergonomics* 2004, 10 (3), pp. 291–300. DOI: 10.1080/10803548.2004.11076616.
[39] Gibson, P.; Auerbach, M.; Giblo, J.; Teal, W.; Endrusick, T. Interlaboratory evaluation of a new sweating guarded hot plate test method (ISO 11092). *Journal of Thermal Insulation and Building Envelopes*, 1994, 18 (2), pp. 182–200. DOI: 10.1177/109719639401800207.
[40] Fung, F.; Krucinska, I.; Zbigniew, D.; Hes, L.; Vladimir, B. Method of pattern making for sweating thermal manikin for research experiment purposes, *Vlakna a Textil*, 2020 (1), pp. 7-11.

CDATP
COMMUNICATIONS IN
DEVELOPMENT AND ASSEMBLING OF TEXTILE PRODUCTS

TEXTILE-CIRCUIT – the opportunity of integrating functionality into a textile product

Sophia Krinner[1], Michael Kieren[1]

[1]KARL MAYER R&D GmbH, Obertshausen, Germany

INFO

CDAPT, ISSN 2701-939X
Communication
2020, Vol. 1, No. 1, pp. 74-79
DOI:10.25367/cdatp.2020.1.p74-79
Received: 30 May 2020
Accepted: 08 August 2020
Available online: 20 November 2020

ABSTRACT

With its technology KARL MAYER provides the possibility to use tailored fiber placement of functional yarns directly during the textile production process. It allows a fast production of functional fabrics with no additional steps while keeping the desired textile properties.
These functional warp knitted products can be used in a wide range of applications such as active- and sportswear, lingerie, outdoor, automotive and agricultural fabrics.

Keywords
Warp knitting,
Electronic Textiles,
Textile sensors,
Wearables,
Tailored fiber placement

1 Introduction

The idea of electronic textiles has been around for many years now and very interesting products have been launched to the market already. First products for the monitoring of vital parameters have already been developed in the nineties [1]. Those products got a lot of attention but still they could not achieve a breakthrough in the market.

We at KARL MAYER have been thinking about the reasons for this and found several obstacles that still exist for these products. Many researchers direct their activities to important topics like washability [2] and standardization of electronic textiles [3], which will improve the future products a lot. In our opinion there are still some topics missing that will be essential for a good wearer experience.

One very important topic is the price. Current smart garments tend to be expensive and are therefore not used for the daily life. The widely known jacket, which was developed by Jacquard™ by Google and Levi's® currently sells for 248 $ [4], while permitting to operate your phone when interacting with your jacket, but not adding new function to the wearers' environment. This might be fine for a jacket that will

not be needed every day, but underwear or regular clothing that you will need in a higher amount has to be affordable for everyone. While the price in case of the jacket might depend a lot on the big names of the developing companies, there are also other factors that make the products expensive.

The electrically conductive materials are more expensive than regular yarn materials. This is the one parameter we cannot change as a machinery manufacturer. What we can do is improving the textile production process. Currently a textile is produced and functionality is added later in a second step. Often these steps don't happen at the same place and are done by people with technological knowledge for this one step only. But as everyone knows, time, transport and human resources make the production more expensive and therefor also the product itself. For this reason, our approach is to reach an almost ready-made product in only one step.

Another important issue is the textile itself. All processes of functionalization have one thing in common. They add something that will change the behavior of the textile. Glued sensors will always be noticeable even if they are flexible, they will act differently than a textile. They will stick to your skin when you sweat and prevent the transport of moisture. Also the risk of delamination shortens the lifecycle of the product. Even embroidered areas will change the flexibility of a textile. Our solution is to already produce the functional textile with the properties needed and not intervene with their characteristics later on.

2 KARL MAYER's String bar technology and its original use

For this approach KARL MAYER uses their string bar technology. It is applied in a raschel machine that can do open, closed, elastic and rigid ground structures. It can also be combined with the Jacquard technology that permits designing the ground structure in terms of optical and also functional matters, meaning that you will be able to construct zones of different elasticity or air permeability.

In this ground structure you will be able to place your functional yarns. With our string bar system, you do not use ground bars full of guide needles but single guide fingers that place yarns on defined spots in the fabric. You are able to design lines but also form closed areas out of one or more functional yarns.

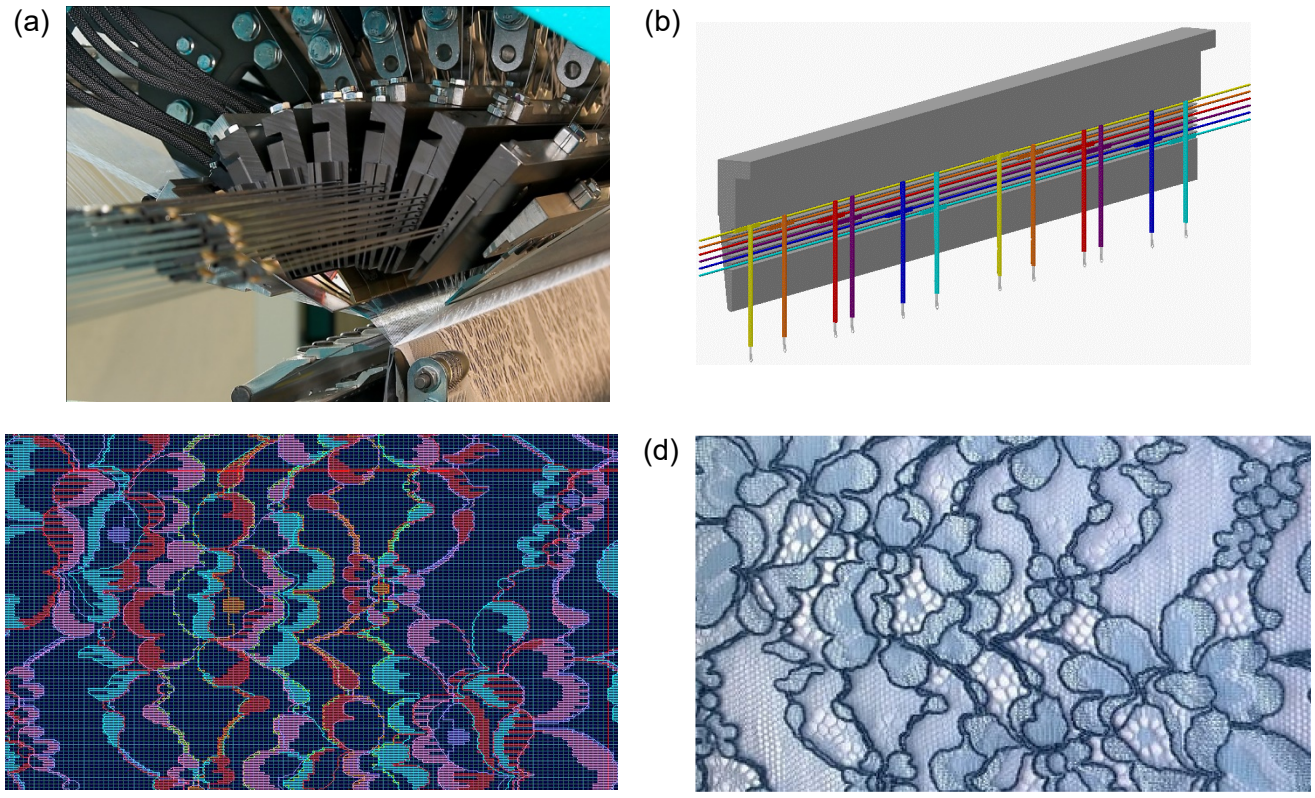

Fig. 1 (a) Knitting area of a string bar machine; (b) schematic depiction of string bars; (c) CAD-drawing of yarn-placement; (d) original fabric produced from the drafting

The yarns are guided into the textile from a creel. You can place your bobbin there and use a variety of different materials at the same time.

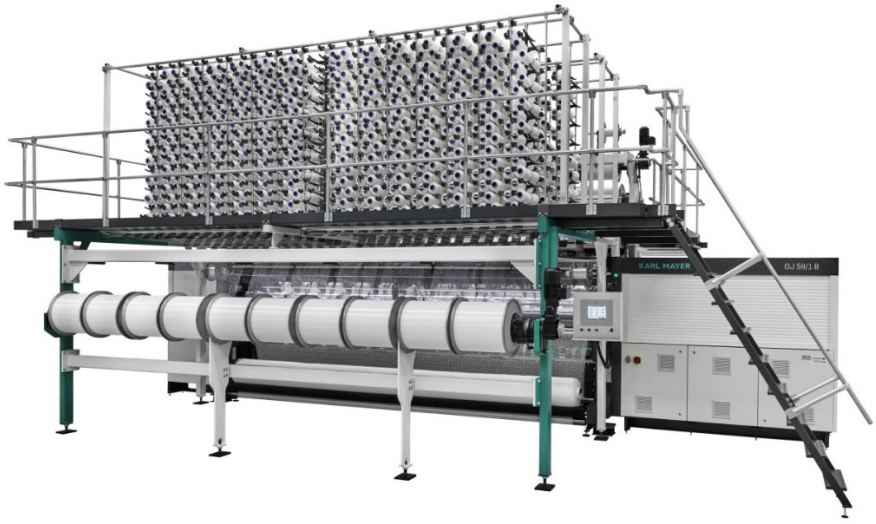

Fig. 2 (a) Example of a stringbar machine

This technology has originally been developed for the production of lace fabric and owes its great flexibility to the different designs and materials that are a crucial part of these types of fabric. It has, however, been applied to the technical field before.

Our composite machines are known for their production of strong, lightweight non-crimp fabric that can be used as prepeg structures for automotive and aircraft industries [5]. Those fabrics often consist of glass filaments and carbon fiber. Using carbon fiber in the complete fabric, however, can be very expensive given the fact that supportive carbon structures might not be necessary in the complete fabric.

This has led to the combination of or composite machines and the stringbar system. This link of technologies allows to form a base of adequate ground filaments and apply stronger, more expensive material in the shapes and amounts that are necessary already during the production of the textile, while keeping the cost at a reasonable level [6].

(a)

(b)

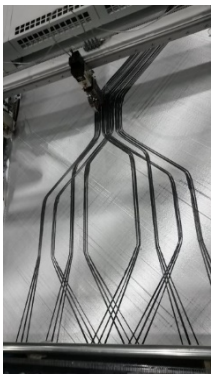

Fig. 3 (a) Example of a composite machine; (b) example of positioned carbon fibers in a non-crimp fabric

3 Applying string bar technology to electronic textiles

These advantages can also be applied to the area of electronic textiles. In our project TEXTILE-CIRCUIT we have been modifying existing KARL MAYER machines to work with different functional materials for the creation of smart textile applications.

Our successful prototypes contain a coil for inductive charging, a textile control panel and variations of a smart shirt.

For our coil we have applied insulated conductors during the warp knitting process. These form the necessary coil structure to generate an electromagnetic field. The coils are designed to match the ones that are integrated in the new generations of smart phones and are therefore able to transmit energy to them. They can also be applied for other charging systems.

Fig. 4 Fully textile inductive charging pad

For our control panel we have designed buttons that are formed by single conductive yarns. In this case we decided on non-isolated yarns to permit interaction with the skin. Each button consists of two areas that are isolated from each other but have been connected to one circuit. By touching those areas, the skin closes the circuit and a signal can be sent. All buttons are connected to a control platform that permits the transmission of different signals.

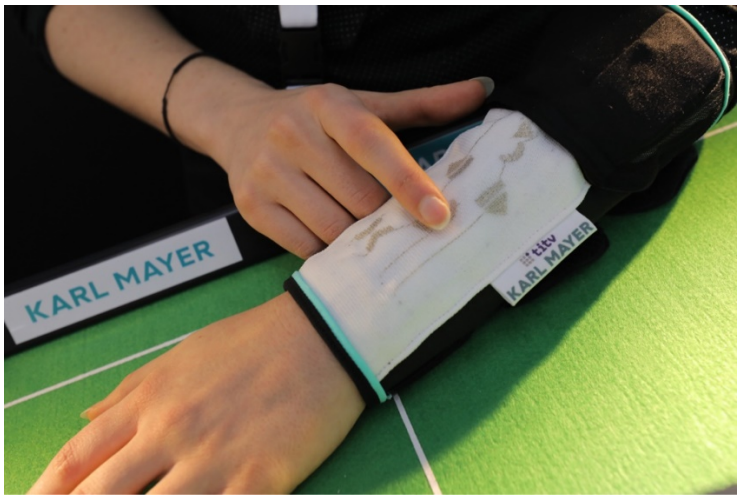

Fig. 5 Textile control panel

During our work on a smart shirt, we came up with different solutions. Our first approach was to include flat textile electrodes by forming conductive areas with non-isolated threads. Those electrodes have to have a good contact to the skin to be able to measure the heartrate of the wearer. We also decided to

integrate a humidity sensor and a temperature sensor. For our humidity sensor we decided on a resistive system. Two parallel conductors measure the electrical resistance between them and are therefore able to detect an increase of moisture with the increase of conductivity between them. Our temperature sensor is a textile thermocouple. We have integrated copper and constantan wires that detect the temperature at their meeting point inside the fabric. All data is transported into an electric box via knitted conductors. It is collected there and can be sent to any device via Bluetooth.

(a) (b)

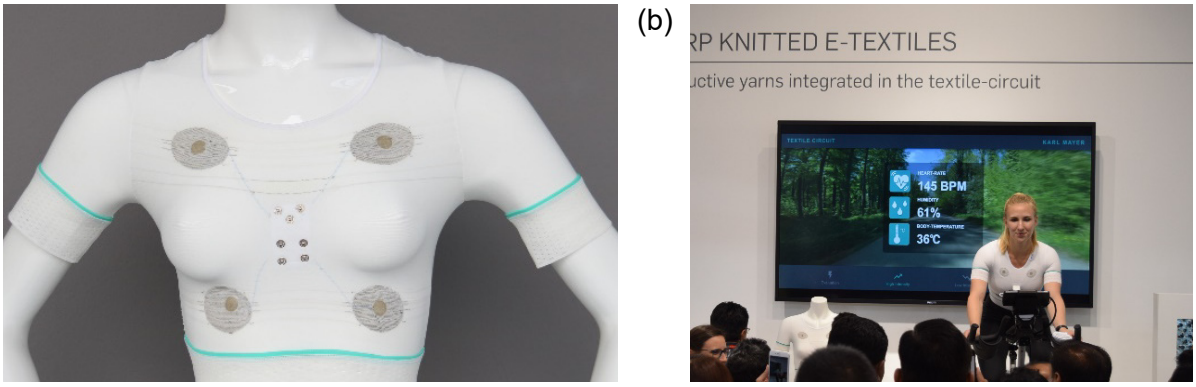

Fig. 6 (a) First smart shirt with detection of heartrate, temperature and humidity; (b) live demonstration with displayed vital signs

In our second approach we saw the need to improve the heartrate sensor. As the flat electrodes had to stay on the exact same spot for a good signal, our first shirt had to be designed very tight. To increase the comfort of the wearer we improved our electrode structure. The electrodes still have to stay at the same place for the measurement and need constant skin contact, but by forming raised electrodes we were able to decrease the pressure on the body during the measurement. Another benefit is that the electrodes are only visible at one side of the fabric, which makes it an ordinary shirt from the outside.

Fig. 7 Improved smart shirt with new sensing system

4 Materials and challenges

During our trials for different applications, we had the opportunity to work with many different materials that are already available in the market. Although not every yarn can be currently used with our technology, we were able to find a good spectrum to cover different functionalities.

The products necessary can basically been divided into two groups, non-insulated and insulated materials. For the first group there are in principle two limitations that concern surface and strength of the yarns. Regarding surface it is important to have a highly even product, which eliminates almost all staple fiber products. Those will be mostly destroyed due to friction during the knitting process. In terms of strength, it is very important that the materials can endure bending and traction at the same time. This is especially a difficult task for metal filaments like copper. This essentially leaves us with the group of

metal coated filament yarns. Those surfaces are still being improved [7]. Yet we were already able to achieve very good results with the current materials and successfully performed basic finishing and washing processes.

The second group are the insulated materials. In this case the material itself is protected by a coating, which mostly eliminates problems with friction. The coating itself often raises other difficulties. Major problems are the increased diameter and decreased flexibility of the material. During the production process all materials have to be guided in small guide fingers and also move in the gap between the knitting needles. The finer a fabric has to be, e.g. for applications in clothing, the smaller those gaps get. Materials with high diameters cannot be used in such cases. They will also be a source of irritation in the fabric later. Low flexibility of the material will even increase the problems during the knitting process. The yarn might be thin enough, but if it cannot be bend in small angles, it will not stay in the right needle gap and might be destroyed during the knitting process or destroy the knitting elements itself.

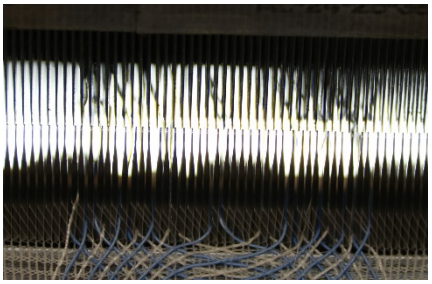

Fig. 8 Insulated yarn in the knitting area bending the needles

The challenge is to find the right combination of machine gauge and yarn count to match the product that has to be achieved and the function it will have.

5 Conclusions

Our string bar technology is a great opportunity of fast production of electronic textiles that also increases the experience of the wearer of smart garments. To bring this potential into an applicable technology for industrial productions, there are still some steps of modification on warp knitting machines needed.
Our goal is to support the development of electronic textiles and prepare the technology to enter production as soon as the demand for new products is growing.

6 References

[1] Quinn, B. Textile Futures: Fashion, Design and Technology, Berg, Oxford, 2010, p.12.
[2] Rotzler, S. Reliability and Washability of Textile-Based Circuit Boards; IPC E-Textiles Europe; Munich, Germany, 12-11-2019.
[3] Ullrich, K. Smart Textiles, auf die man sich verlassen kann – Vorstellung des Smart-Textiles-Prüflabor des TITV; Symposium Smart Textiles, SmartTex Netzwerk, Weimar; Deutschland, 29.01.2019.
[4] Levi's® Sherpa Trucker Jacket With Jacquard™ By Google. Available online: https://www.levi.com/US/en_US/apparel/clothing/tops/levis-sherpa-trucker-jacket-with-jacquard-by-google/p/773710001 (accessed on 09.07.2020).
[5] Herrmann, A. S., Eberth, U. Technische Textilien für Luftfahrt- und Fahrzeuganwendungen. In: Knecht, P. (Editor), Technische Textilien, Deutscher Fachverlag, 2006.
[6] Markgraf S.; Heinecke, T.; Nendel, S.; Kirchberg, A. KonText – Großserientaugliche Kett- und Schussfadenversatz-Technologie; 16. Chemnitzer Textiltechniktagung; Chemnitz, Germany, 29-05-2018.
[7] Cramer, J.; Neudeck, A.; Möhring, U. Mit Elektrochemie zu waschbeständigen metallisierten Garnen, Galvanotechnik 3/2019, pp. 451-456, Eugen G. Lenze Verlag.

COMMUNICATIONS IN
DEVELOPMENT AND ASSEMBLING OF TEXTILE PRODUCTS

Impact of fabric parameters and properties on a 2D cutting and stitching line

Magdalena Owczarek[1,*]

[1]Institute of Architecture of Textiles, Faculty of Material Technologies and Textile Design, Lodz University of Technology*), Lodz, Poland*
**E-mail address:* magdalena.owczarek@p.lodz.pl

INFO

CDAPT, ISSN 2701-939X
Peer reviewed article
2020, Vol. 1, No. 1, pp. 80-87
DOI:10.25367/cdatp.2020.1.p80-87
Received: 14 July 2020
Accepted: 8 August 2020
Available online: 20 November 2020

ABSTRACT

The paper presents the influence of fabric parameters and properties on the circle shape precision confectioning in the 2D plane. The properties of textiles affect the fit of the entire product, which is often subject to the subjective assessment of a technologist. In the case of cutting lines made in the two-dimensional area, it seems that there should be no problem with its implementation. Unfortunately, in the clothing, furniture, and automotive industries there are difficulties in combining the same and different textile and non-textile materials (leather). There is no objective method of predicting the precision of circle cutting shape, for different types and properties of fabrics. The work analyzes the shape of a circle cutting and stitching line in a two-dimensional area, taking into account selected properties of textiles (surface weight, elongation, relative bending stiffness). It turns out that the different properties of textiles cause, to a greater or lesser extent, the accuracy of a given circle shape. The fabric with the three-component composition of raw materials and the highest surface mass, as well as the smallest stiffness and high elongation obtained the highest precision of the circle shape reproduction. The least precision, i.e. the ability to maintain a given circle shape, was obtained in viscose fabric with low surface mass, high stiffness, and the highest relative elongation. Correlation analysis showed a significant relationship between shape and surface mass and the number of warp threads.

Keywords
pattern making,
cutting,
stitching lines,
textiles parameters and properties

1 Introduction

The properties of textiles determine the creation of clothing patterns, but also decorative and technical products. Textile properties have an impact on the possibilities of shaping and matching a more or less complicated garment design and estimating the value of construction and technological additions. Estimating the value of additions and the shape of the cutting line is always subject to the subjective assessment of the designer/technologist [1].

The aim of the work cycle and research is to determine objectively quantitative relationships in the field of the impact of parameters and properties of textiles on the clothing patterns. In the first stage of research work, the influence of parameters and properties of knitted fabrics on the structure as well as the product's drapability and fitting were determined [2-4]. Particular attention was paid to the raw material, internal mesh geometry, and structural parameters, which have a decisive influence on the elongation properties and the pressure on the body. It has been shown that individual parameters, properties of a flat textile product, and especially the weakest parameter determine the product's drapability, fitting, and durability.

In the case of fabrics [5,6], important parameters are weight, thickness, stretching, elongation, bending stiffness, shrinkage, draping, and structural parameters of the weave and raw material. Also important are internal thread friction, deformation angles that affect stability, and the ability to shape the spatial form on the body of the human body in real life or during 3D visualization. Parameters contained in KES and FAST systems can be equally useful when forecasting the shape of clothing construction forms [7].

Individual structural parameters of textiles have a huge impact on the deformation and shaping of a given form in 3D space [8]. The shape of forms is also important in building spatial forms [9, 10].

In the case of a cutting line, e.g. a circle made in a two-dimensional area, it seems that there should be no problem with its implementation. Unfortunately, in the clothing, furniture, and automotive industries there are difficulties in combining the same and different textile and non-textile materials (leather). There is no objective method of checking and predicting the precision of obtaining the oval shape of the cutting line, e.g. in the shape of a circle, as well as confectioning accessories for different types of textiles with different properties. In this work, the shape of the structural cutting line of a circle in a two-dimensional area was analyzed, taking into account selected properties of textiles (surface mass, elongation, and bending stiffness). The various properties of textiles will, to a greater or lesser extent, make the shape of the circle evaluated.

This work presents the influence of fabric parameters and properties on the precision of a shape in the process of confectioning oval lines, e.g. a circle shape in a 2D plane. The purpose of these tests is to determine the ability to maintain a given oval shape of the cutting line at the given values of additives for various properties of textiles.

2 Methods

Five samples of plain weave fabric (Fig. 1) differentiated by parameters and properties were used in the experiment. These are fabrics for various purposes, from viscose lining 1_P, to viscose fabric for blouses 2_P, to clothing fabrics 3_P - 5_P with a higher surface mass and more stable than lining and blouse fabrics. This diversity in terms of one weave will show differences in the behavior of the shape of the circle sewn in from the same fabric.

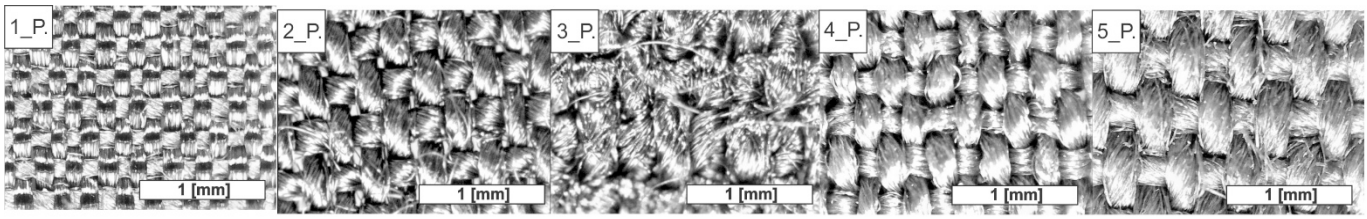

Fig. 1 Fabric samples for the experiment.

Fabrics are differentiated by the following parameters: raw material, surface mass, weft, and warp density. Their properties of bending stiffness by the loop method and relative elongation under normal conditions at 20 °C, humidity 65% [11] were also examined (Table 1).

The bending stiffness of the loop method determines the falling value of the strip of fabric tied into a loop. So, if the belt falls more, it has a higher value in mm, that is, the fabric has less rigidity.

Table 1. Fabric parameters and properties

	parameters						**properties**	
fabrics	**raw material**	**type of weave**	**type of material**	**Mp (g/m^2)**	**D_wp (threads/dm)**	**D_wf (threads/dm)**	**C (mm)**	**E (%)**
1_P	viscose	plain	lining	78	800	450	15.40	19.50
2_P	viscose	plain	blouse	116	450	300	15.90	23.00
3_P	PET+ C+E	plain	clothing	222	350	250	18.10	20.00
4_P	PET + E	plain	clothing	196	500	350	18.10	19.50
5_P	PET+C	plain	clothing	176	410	250	16.50	10.50

D_wp (threads/dm) warp density

D_wf (threads/dm) weft density

Mp (g/m^2) surface mass

C (mm) bending stiffness by the loop method

E (%) relative elongation

In the first stage, a circle template was prepared with the location of the sewing and cutting line. Sewing allowance values for a 90 mm diameter circle are 5 mm (Fig. 2).

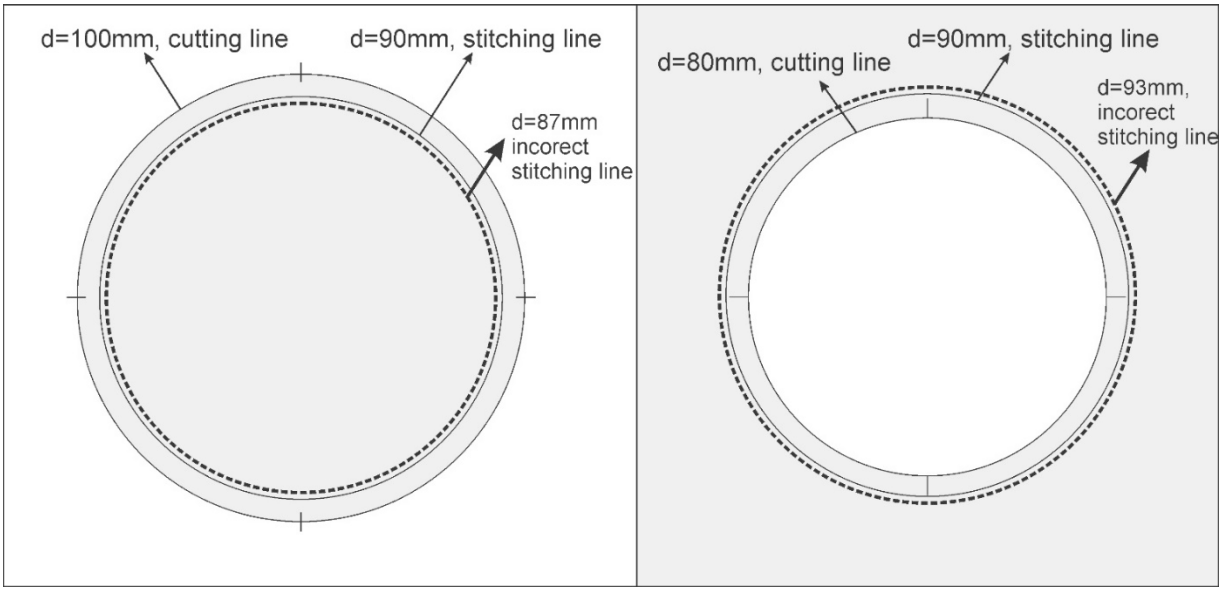

Fig. 2 Pattern of the cutting and stitching lines.

Stitching tests were carried out by the designated sewing lines (Fig. 3a) and with the incorrect setting of the sewing lines (Fig. 3b). The example below shows how the accuracy and the effect of sewing the circle deteriorates. Inaccurate stitching in the sewing line already causes a large distortion of shape and fit. Wrinkles and stretches are visible (Fig. 3). The difference of 3 mm in the position of the stitching line (Fig. 2) means that part of the circle template has a diameter d = 87 mm, L = 524.38 mm, while part of the plane template has a diameter d = 93 mm, L = 584.04 mm. This is a 59.66 mm difference in

matching the circuits. That is why it is so important to accurately identify the stitching lines in this type of shape on a 2D surface.

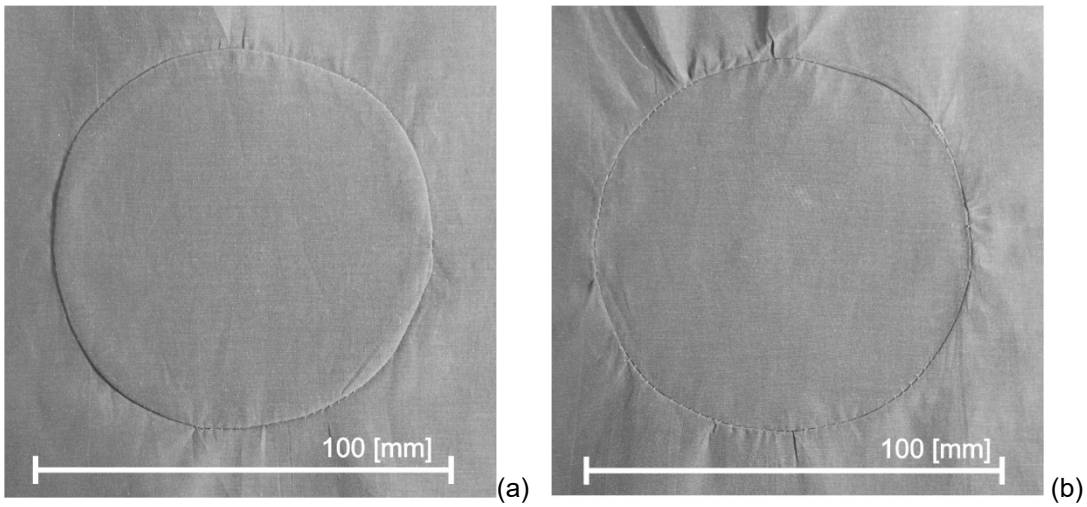

(a) (b)

Fig. 3 Samples with changing of cutting and stitching lines.

3 Test/Data

For five samples of plain weave, a circle stitching line was made according to the template (Fig. 2). Then the photos of the samples taken were taken with a Nikon Z6 camera with a 24-70 mm lens of 4528 x 3016 in the form of .NEF. The contour of the stitching line was determined on each image of the performed experimental test (Fig. 4).

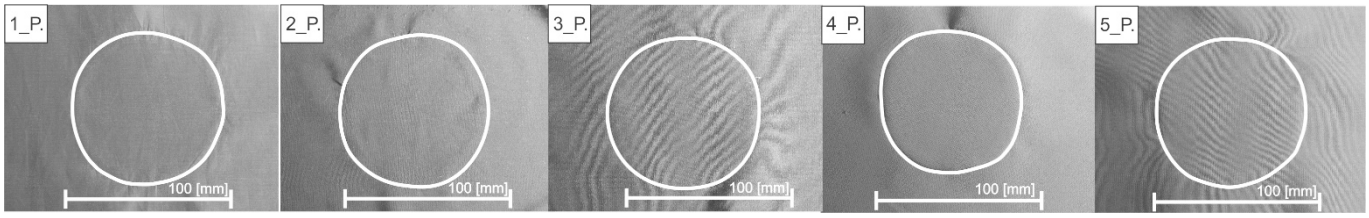

Fig. 4 Fabric samples with stitching lines.

The raw camera images were prepared for processing in the form of a bitmap with a size of 1024 x 1024 pixels. The area marked with the stitching contour line was subjected to computer image analysis in the author's MagFABRIC program (Fig. 5).

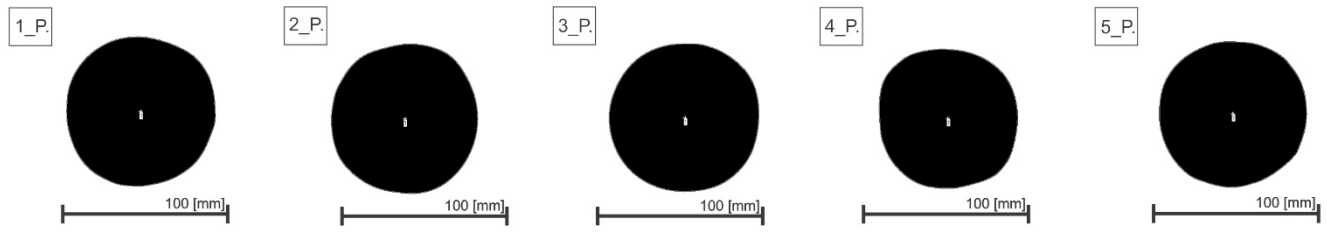

Fig. 5 Image analysis of the stitching lines in the MagFABRIC.

The shape of the stitching line in the experimental tests differs from the ideal shape of the circle. The differences in circumference and shape for all experimental trials are shown in (Fig. 6a). To quantify these differences, a morphometric stitching line analysis was performed in computer image analysis. All experimental trials were described with size and shape parameters. These parameters include circle

surface area A (mm^2), minimum and maximum circle diameters Dmin, Dmax (mm), circle circumference L (mm) and circle shape parameters dForm (%) (1), AspectR (2) and FormF (3) (Fig. 6b).

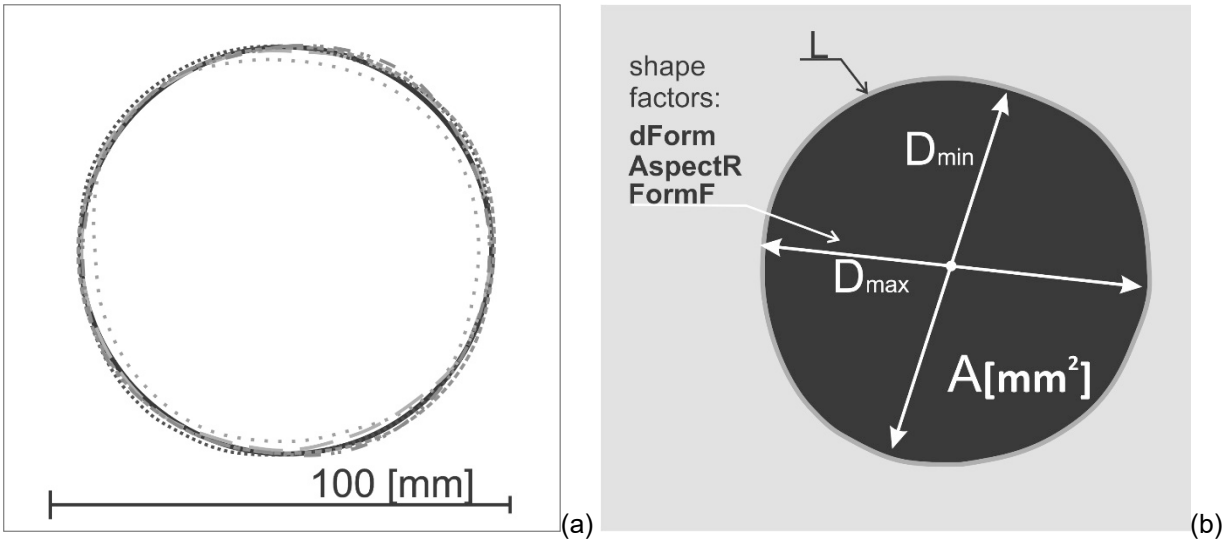

Fig. 6 Morphometrical analysis of the stitching lines: (a) The stitching lines in the fabrics samples, (b) the morphometric parameters of the stitching line.

The circle shape parameters describe three different shape factors that determine the following variation in the shape of the circle field:

- **dForm (%)** – degree of circle shape deformation:

$$dForm = \frac{Dmax - Dmin}{Dmax} * 100; \quad (1)$$

- **AspectR** – degree of ellipticity:

$$AspecR = \frac{D_{MIN}}{D_{Max}}; \quad (2)$$

where: Dmin, Dmax (mm) – min. and max. field diameters

- **FormF** – edge development:

$$FormF = \frac{4\Pi \cdot A}{L^2}; \quad (3)$$

where: A (mm^2) – surface area, L (mm) – field circumference – contour.

4 Results

The values of the parameters of the morphometric analysis of the size and shape of the circles from the experimental fabric samples are summarized in the following table (Table 2). The experimental tests were combined with a standard sample – the ideal 0_S circle.

From Table 2 and Fig. 7, the thesis is confirmed that the differentiation in the shape of a circle of stitching lines in research samples depends on the parameters and properties of textiles. The 3_P fabric obtained the highest precision of the circle shape mapping by the lowest value of the deformation coefficient dForm = 4.28% and the closest value to 1.00 in the case of the ellipticity coefficient AspectR = 0.96, which indicates a similar shape to the circle. The smallest precision, i.e. the ability to keep the given shape of the circle, was obtained by the 2_P viscose fabric with the highest deformation coefficient dForm = 9.35% and the least close to 1.00 in the case of the elliptic coefficient AspectR = 0.91, which indicates the least similar shape to the circle. The coefficient of the degree of edge development for the 2_P fabric showed the highest value of FormF = 1.05 among all research tests.

Table 2. Results of image analysis of the stitching line of fabric samples.

Fabrics	A (mm^2)	L (mm)	Dmax (mm)	Dmin (mm)	dForm (%)	AspecR	FormF
0_S	6358.50	282.60	90.44	89.38	0.00	1.00	1.00
1_P	6251.30	277.67	91.30	86.96	4.75	0.95	1.02
2_P	5560.19	258.42	88.69	80.40	**9.35**	**0.91**	**1.05**
3_P	6245.61	277.54	91.06	87.16	**4.28**	**0.96**	1.02
4_P	6026.71	272.98	89.38	84.72	5.21	0.95	1.02
5_P	6165.67	275.69	91.83	86.24	6.09	0.94	1.02

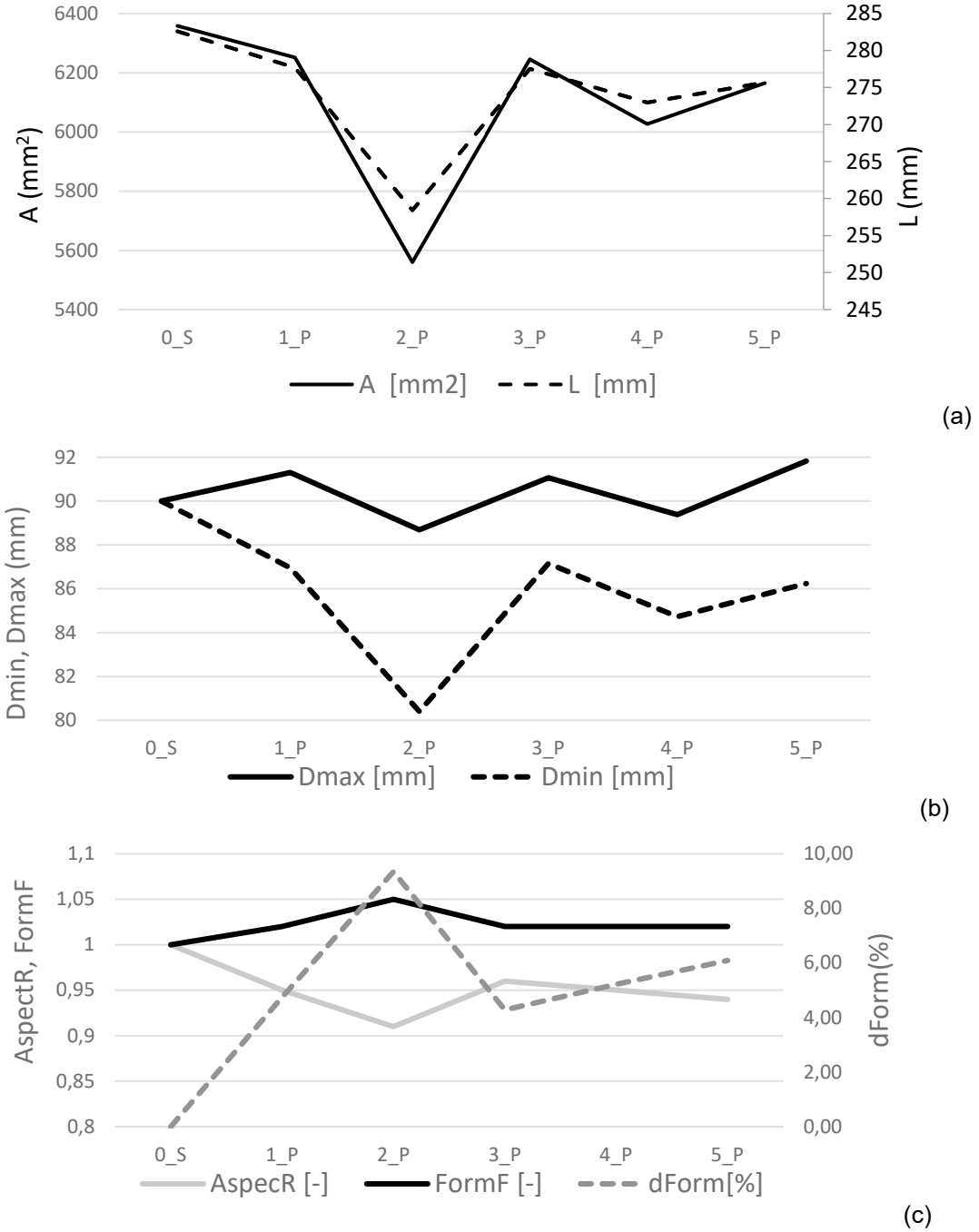

Fig. 7 Results of the stitching lines image analysis: (a) area A (mm^2) and contour L (mm), (b) minimum and maximum diameters Dmin, Dmax (mm), (c) shape factors: AspecR and FormF, dForm (%).

Taking into account the parameters and properties of fabrics, the 3_P fabric with three component raw material composition and the highest surface mass as well as the lowest stiffness and high relative elongation obtained the highest precision in mapping the shape of the circle. However, the smallest precision, i.e. the ability to maintain the given shape of the circle, was obtained by 2_P viscose fabric with a low surface mass, high stiffness, and the highest relative elongation.

A regression analysis of variable dependent shape coefficients with parameters and properties of fabrics was also carried out. Correlation analysis showed a significant dependence of shape on surface mass and warp density (Fig. 8). The strongest correlation was obtained by FormF – the degree of development of the edges (Fig. 8a). The determination coefficients R, R2, and R^2, in this case, are 0.998, which means that 99% of the overall variability of the FormF dependent variable is explained by the model. The standard error of estimation equal to 0.00129 allows for estimating the size of random deviations of the model at a low level. BETA coefficients illustrate the largest dependence of independent variables Mp and Mp^2, regardless of the unit, at levels -8.20 and 8.09, respectively. However, the t-Student p level does not exceed 0.05, therefore the variables Mp and Mp^2 are significant. Only the Dwp variable has p = 0.06, which means an insignificant relationship. The regression model is as follows (4):

$$FormF = 1.19 - 0.002 \cdot Mp + 0.00001 \cdot Mp^2 - 0.00008 \cdot Dwp \quad (4)$$

where: Mp – surface mass (g/m^2), Dwp – warp density (threads/dm)

Even greater significant correlation of surface mass and warp density was obtained by the morphometric parameter of the circumference of the circle L (mm) (Fig. 8b). The determination coefficients R, R2, and R^2, in this case, are 0.999, which means that 99% of the total variability of the dependent variable L (mm) is explained by the model. The standard error of estimation of 0.20379 allows for estimating the size of random deviations of the model at a low level. BETA coefficients illustrate the largest dependence of independent variables Mp, Mp^2, (regardless of the unit), at levels 6.29 and -6.58 and Dwp at 0.66, respectively. However, the t-Student p level does not exceed 0.05, therefore the variables Mp, Mp^2, Dwp are significant. The regression model is as follows (5):

$$L = 204.28 + 0.86 \cdot Mp - 0.003 \cdot Mp^2 + 0.03 \cdot Dwp \quad (5)$$

where: Mp – surface mass (g/m^2), Dwp – warp density (threads/dm)

Dalej...
R= ,99883783 R2= ,99767702 Popraw. R^2= ,99070807
F(3,1)=143,16 p<,06134 Błąd std. estymacji: ,00129

N=5	BETA	Błąd st. BETA	B	Błąd st. B	t(1)	poziom p
W. wolny			1,188879	,012587	94,4550	,006740
MP___G_M	-8,20764	,542407	-,001867	,000123	-15,1319	,042010
MP2	8,08781	,492081	,000006	,000000	16,4359	,038686
D_WP__TR	-,98988	,100121	-,000076	,000008	-9,8868	,064173

a)

Dalej...
R= ,99992037 R2= ,99984074 Popraw. R^2= ,99936295
F(3,1)=2092,6 p<,01607 Błąd std. estymacji: ,20379

N=5	BETA	Błąd st. BETA	B	Błąd st. B	t(1)	poziom p
W. wolny			204,2754	1,983422	102,9914	,006181
MP	6,29919	,142024	,8625	,019445	44,3531	,014351
MP2	-6,58226	,128846	-,0030	,000059	-51,0861	,012460
D_WP	,65934	,026216	,0303	,001207	25,1505	,025299

b)

Fig. 8 Results the best regression analysis (in Statistica) between fabric parameters and: (a) shape FormF stitching line; (b) size contour L (mm) stitching line.

5 Conclusions

It turns out that the different properties of textiles cause, to a greater or lesser degree, the precision of the given circle shape. The fabric with the three-component raw material composition and the highest

surface mass as well as the smallest stiffness and high stretchability obtained the highest precision of the circle shape mapping. The smallest precision, i.e. the ability to maintain the given shape of the circle, was obtained by the viscose fabric with a low surface mass, high stiffness, and the highest relative elongation. Correlation analysis showed a significant relationship between shape and surface mass and warp density. The experiment is a preliminary study in the consideration of only one group of plain weave fabrics. It confirms the thesis of the relationship between the shapes obtained, e.g. a circle in a 2D plane, and fabric parameters. This allows you to predict the behavior of fabrics with a specific surface mass in this type of shape. A broader treatment of the issue in the aspect of including a larger group of different fabric weaves will allow us to determine the possibilities in a wider scope. The second aspect extending the scope of research are sewing parameters (sewing speed, type of transport, lubrication, presser foot pressure, thread tension, sewing step) and the type of sewing needle (number, tip) and thread structure (staple fibers, type of core) and sewing thread properties (composition, linear density, twist, twist unevenness), which can have a significant effect on the precision of the shape when cutting and sewing in the two-dimensional area.

Funding

This research received no specific grant from any funding agency in the public, commercial, or non-profit sectors.

References

[1] Owczarek, M.; Nawrot, A.; Lukawska, M.; Wereszka, A.; Grzejszczak, L,; Mastalerz, P. Nonstandard Constructional Solutions in Contemporary Clothing Design. *Autex Research Journal,* 2016, 16 (4), pp. 250–255, DOI: https://doi.org/10.1515/aut-2016-0035.

[2] Owczarek, M.; Poliński, Z. Basic properties of the flat textiles in the clothing construction with negative allowance. *Proc. of 9th Joint International Conference Clotech'2010,* May 27–28 2010, Radom; ISBN 978-83-7351-377-8, pp. 20-27.

[3] Polinski, Z.; Owczarek, M. Model considerations of flat textile properties in clothing construction with negative allowance. *Proc. of 9th Joint International Conference Clotech'2010,* May 27–28 2010, Radom; ISBN 978-83-7351-377-8, pp. 13 -19.

[4] Owczarek, M.; Poliński, Z. Properties of flat textiles in clothing design with negative allowance. *Conference Knitt Tech'2010,* Rydzyna, ISBN 978-83911012-9-2.

[5] Owczarek, M.; Glinkowska, A. Textiles parameters in clothing constructing. *Innovations in clothing technology & measurement techniques,* 10th Joint International Conference Clotech'2012, September 20–21, 2012, Warszawa, ISBN 978-83-7283-492-8, pp. 66-75.

[6] Ancutienė, K.; Sinkevičiūtė, D. The influence of textile materials mechanical properties upon virtual garment fit, *Materials Science (Medžiagotyra),* 2011, 17 (2), pp. 160-167.

[7] Chajczyk, M.; Owczarek, M. Comparison of parameters related to KES and FAST textiles systems in terms of usefulness in clothes construction. In: Frydrych, I.; Bartkowiak, G.; Pawlowa, M. (Ed.) *Innovations in clothing 3D design, products, fashion, technologies, and testing of clothing materials.* ISBN: 978-83-7283-8, 2017, pp. 130-136.

[8] Owczarek, M. Susceptibility of the fabric deformation in the design and construction of clothing. *Innovative materials & technologies in made-up textile articles, protective clothing and footwear*, *Chapter I: Clothing Design And Technology,* ISBN 978-83-7283-6666-3, 2015, pp. 66-74.

[9] Owczarek, M.; Chajczyk, M. The comparison of female close fitting bodice patterns of different authors, *Innovative materials & technologies in made-up textile articles, protective clothing and footwear*, *Chapter I: Clothing Design And Technology*, ISBN 978-83-7283-6666-3, 2015, pp.75-80.

[10] Owczarek, M.; Chajczyk, M. Morphometry of clothes construction forms with the application of computer image analysis. *Innovations in clothing 3D design, products, fashion, technologies, and testing of clothing materials.* ISBN: 978-83-7283-8, 2017, pp. 17-30.

[11] Konecki, W. (red.) Metrologia surowców i wyrobów włókienniczych, Wyd. PŁ Łódź 1996, ISBN 83-86453-49-4.